DOCTORAL THESES IN FOOD SCIENCES AT THE UNIVERSITY OF TURKU

Mass Spectrometric Methodologies for Analysis of Triacylglycerol and Phospholipid Regioisomers in Natural Fats and Oils

MIKAEL FABRITIUS

Food Chemistry and Food Development
Department of Life Technologies

DOCTORAL THESES IN FOOD SCIENCES AT THE UNIVERSITY OF TURKU
Food Development (tech)

Mass spectrometric methodologies for analysis of triacylglycerol and phospholipid regioisomers in natural fats and oils

MIKAEL FABRITIUS

Food Sciences
Department of Life Technologies

TURKU, FINLAND – 2023

Food Sciences
Department of Life Technologies
University of Turku, Finland

Supervised by
Professor Baoru Yang, Ph.D.
Food Sciences
University of Turku, Finland

Jukka-Pekka Suomela, Ph.D.
Food Sciences
University of Turku, Finland

Marko Tarvainen, Ph.D.
Berner Ltd, Finland

Reviewed by
Maria Fedorova, Ph.D.
Center of Membrane Biochemistry and Lipid Research
Technische Universität Dresden
Dresden, Germany

Professor Ingela Lanekoff, Ph.D.
Department of Chemistry
Uppsala University
Uppsala, Sweden

Opponent
Professor Michal Holčapek, Ph.D.
Faculty of Chemical Technology
University of Pardubice
Pardubice, Czechia

Research director
Professor Baoru Yang, Ph.D.
Department of Life Technologies
University of Turku
Turku, Finland

The originality of this dissertation has been checked in accordance with the University of Turku quality assurance system using the Turnitin OriginalityCheck service.

ISBN 978-951-29-9315-4 (print)
ISBN 978-951-29-9316-1 (pdf)
ISSN 2323-9395 (print)
ISSN 2323-9409 (pdf)
Painosalama, Turku, Finland 2023

TABLE OF CONTENTS

ABSTRACT i

SUOMENKIELINEN ABSTRAKTI iii

LIST OF ABBREVIATIONS v

LIST OF ORIGINAL PUBLICATIONS vii

1 INTRODUCTION 1

2 REVIEW OF THE LITERATURE 4

2.1 Separation of TG *sn*-positional isomers 4

2.1.1 Reversed phase chromatography 4

2.1.2 Silver ion chromatography 8

2.1.3 Chiral phase chromatography 12

2.1.4 Supercritical fluid chromatography 18

2.1.5 Two-dimensional chromatography 19

2.1.6 Ion mobility 23

2.2 Identification of TG regioisomers by MS methodologies 24

2.2.1 Collision-induced dissociation 24

2.2.1.1 Mechanistic studies on fragmentation of TG regioisomers 24

2.2.1.2 Analysis of TG regioisomers using CID 31

2.2.2 In-source fragmentation 39

2.2.3 Electron impact excitation of ions from organics 40

2.2.4 Ozone-induced dissociation 41

2.2.5 Algorithmic interpretation of MS^n fragment data 41

2.3 Separation of PL *sn*-positional isomers 45

2.3.1 Chromatographic separation 45

2.3.2 Ion mobility 47

2.4 Identification of PL regioisomers by MS methodologies 49

2.4.1 Collision-induced dissociation 49

2.4.2 Ozone-induced dissociation 59

2.4.3 Other dissociation techniques 60

2.5 Concluding remarks 61

3 AIMS OF THE STUDY 63

4 MATERIALS AND METHODS 64

4.1 Materials 64

4.1.1 Reference standards 64

4.1.2 Sample materials 68

4.2 Methods 70

4.2.1 Lipid extraction 70

4.2.2 FA composition analysis 70

4.2.3 Lipid fractionation 71

4.2.4 TG molecular species and regioisomer analysis (Direct inlet MS^2 method) 71

4.2.4.1 TG molecular weight distribution analysis 72

4.2.4.2 TG regioisomer analysis 72

4.2.4.3 *MSPECTRA* software 73

4.2.5 TG regioisomer analysis (UHPLC-MS^2 method) 74

4.2.5.1 TG regioisomer analysis 74

4.2.5.2 *TAG analyzer* software 75

4.2.6 PL molecular species and regioisomer analysis 79

4.2.6.1 Hydrophilic interaction liquid chromatography 79

4.2.6.2 Direct infusion 79

4.2.6.3 Reversed phase chromatography 80

4.2.6.4 MS^2 analysis 80

4.2.6.5 PL molecular weight distribution 80

4.2.6.6 PL regioisomer calculations with calibration curves 81

4.2.6.7 Algorithmic calculation of PL regioisomers 81

5 RESULTS AND DISCUSSION 83

5.1.1 FA composition 83

5.1.2 TG molecular weight distribution 84

5.1.3 TG regioisomer calculations 91

5.1.3.1 *MSPECTRA* software 91

5.1.3.2 *TAG analyzer* software 96

5.1.3.3 Comparison of the TG regioisomer calculation methods 101
5.1.4 Correction factors for PL molecular weight distribution . 107
5.1.5 PL regioisomer calculations 107
5.1.5.1 Manual calculation of PL standards using the calibration curves 107
5.1.5.2 Calculation software 114
5.1.5.3 Analysis of bovine milk PC regioisomers 115
5.1.6 General discussion 117
5.1.6.1 TG regioisomer analysis methods 117
5.1.6.2 PL regioisomer analysis methods 118

6 SUMMARY AND CONCLUSION 120

ACKNOWLEDGEMENTS 121

REFERENCES 122

APPENDIX: ORIGINAL PUBLICATIONS 133

ABSTRACT

Analysis of triacylglycerol (TG) and phospholipid (PL) regioisomers is a challenging task. The liquid chromatographic-mass spectrometric (LC-MS) analysis methods can be divided into two distinct categories: a) direct separation by chromatography or other means such as ion mobility, and b) quantification of regioisomer ratios by structurally informative fragment ions with mass spectrometric methods. Challenges arise from the large number of isobaric lipid species in natural samples, often overlapping chromatographically and sharing structurally informative fragment ions.

Due to long retention times and difficult separation, researchers are moving away from direct chromatographic separation of isomers, using mass spectrometry instead. Many established analytical methods are targeting specific isomers of interest, and high-throughput untargeted analysis remains challenging, even though advancements have been made in the recent years. Fragmentation of glycerolipids is influenced by acyl chain lengths and numbers of double bonds of the attached fatty acids, and while certain fragmentation mechanisms offer better *sn*-specificity than others, the lack of available regiopure standards is still an obstacle for many researchers.

In the thesis work, new tandem mass spectrometric (MS^2) methods for investigating TG and PL regioisomer compositions in natural samples were developed. Two different instrumental methods and algorithmic calculation models were developed and validated for analysis of TG regioisomers. A direct inlet negative ion chemical ionization method along with an updated version of the *MSPECTRA* calculation software offers a rapid protocol for investigating TG regioisomers in complex samples such as human milk. While the absolute accuracy of the regioisomer ratio calculations is affected by the nature of the FAs in the TGs, the method is very useful for studying regioisomeric differences between samples.

A new fragmentation model for analysis of TG regioisomers utilizing positive electrospray ionization (ESI+) LC-MS^2 method was developed in addition to the direct inlet method. The model was created using calibration curves established with a wide range of regiopure TG standards, allowing prediction of fragmentation patterns for TG species without authentic standards. While the triple quadrupole MS instrument used for establishing the model is better suited for targeted approaches, the analysis can later be transferred to an untargeted platform utilizing data-dependent acquisition.

Both calculation programs utilize optimization functions, attempting to find concentrations of regioisomers that produce the experimentally observed fragment ion spectra. This approach mitigates the effects of interfering isobaric

fragments resulting from different isomeric TG species and the entire fragment spectra of multiple TG molecular species is handled simultaneously instead of each individually.

The analysis of PL regioisomers was divided into two parts. In the first part, a hydrophilic interaction liquid chromatography (HILIC) method combined with a data-dependent MS^2 acquisition was used to study the fragmentation behavior of different PL classes. Calibration curves were created with PL reference standards, enabling regioisomeric analysis of specific PL molecular species. For second part of the PL regioisomer analysis, the HILIC separation method was replaced by reversed phase chromatography, resulting in more reliable and efficient separation of PL molecular species within classes. An automated data preprocessing algorithm and a fragmentation model for untargeted PC regioisomer identification was created.

Together, the developed LC-MS^2 methods and calculation software and fragmentation models for TG and PL regioisomer analysis form a strong basis for further development and implementation to lipidomics platforms, enabling more detailed structural analysis in a rapidly growing area of research.

SUOMENKIELINEN ABSTRAKTI

Triasyyliglyserolien (TG) ja fosfolipidien (PL) regioisomeerien tutkimus on haastava tehtävä. Nestekromatografia-massaspektrometriset menetelmät (LC-MS) voidaan jakaa kahteen ryhmään: a) suora erottuminen kromatografialla tai muilla keinoilla, kuten esimerkiksi ioniliikkuvuuden avulla, ja b) regioisomeerien pitoisuuksien laskeminen rakenteellisesti informatiivisten fragmentti-ionien avulla käyttäen massaspektrometrisiä menetelmiä. Haastavuutta lisää luonnollisissa näytteissä esiintyvien, kromatografisesti huonosti erottuvien, ja samoja rakenteellisesti informatiivisia fragmentteja sisältävien isomeeristen lipidiyhdisteiden suuri määrä.

Pitkien retentioaikojen ja vaikean erottelun vuoksi monet tutkijat ovat siirtymässä pois kromatografiseen erotteluun perustuvista regioisomeerien analyysimenetelmistä massaspektrometrisiaan. Monilla vakiintuneilla menetelmillä voidaan tutkia yksittäisiä kiinnostavia isomeerejä, mutta laajempien ja kohdentamattomien menetelmien käyttö on haastavaa, vaikka edistystä on tapahtunut viime vuosien aikana. Glyserolipidien fragmentoitumiseen vaikuttaa esimerkiksi rasvahappojen hiiliketjujen pituus ja kaksoissidosten määrä. Vaikka tietyillä massaspektrometrisillä menetelmillä fragmentaatio on regiospesifisempää kuin toisilla, puhtaiden regioisomeeristen standardien puute on haaste monille tutkijoille.

Väitöskirjatyössä kehitettiin uusia tandem-massaspektrometrisiä (MS^2) analyysimenetelmiä TG- ja PL-regioisomeerien tutkimiseen. TG regioisomeereille kehitettiin ja validoitiin kaksi erilaista menetelmää ja laskentamallia. Suorasyöttöön ja kemialliseen ionisaatioon perustuva menetelmä päivitetyn *MSPECTRA*-laskentaohjelmiston kanssa tarjoaa nopean protokollan TG-regioisomeerien analysointiin myös monimutkaisissa näytteissä, kuten äidinmaidossa. Vaikka laskennassa regioisomeerien suhteiden absoluuttiseen tarkkuuteen vaikuttaa rasvahappojen ominaisuudet, menetelmä on erittäin hyödyllinen näytteiden eroavaisuuksien tutkimisessa.

Suorasyöttömenetelmän rinnalla kehitettiin myös toinen laskentamalli TG-regioisomeereille hyödyntäen ESI-LC-MS^2 menetelmää ja puhtailla standardeilla määritettyjä kalibraatiosuoria. Laskentamallin avulla voidaan ennustaa, miten TG fragmentoituu perustuen sen rasvahappojen kaksoissidosten määrään ja hiiliketjujen pituuksiin. Laskentamalli mahdollistaa menetelmän käyttämisen myös kohdentamattomassa analytiikassa, jolloin kaikille tutkittaville yhdisteille ei tarvita kalibraatiosuoria.

Molemmat TG-regioisomeerien laskentamallit hyödyntävät optimointialgoritmejä, joiden avulla pyritään määrittämään ne regioisomeerien pitoisuudet, jotka tuottavat alkuperäistä, kokeellisesti havaittua fragmenttispektriä vastaavan

synteettisen spektrin. Tällä periaatteella pystytään minimoimaan eri TG-isomeereistä johtuvien isobaaristen fragmenttien aiheuttamat vääristymät, kun spektriä käsitellään kokonaisuutena, eikä yksittäisinä ja erillisinä laskutoimituksina.

PL-regioisomeerien tutkimus jaettiin kahteen osaan. Ensimmäisessä osassa tutkittiin eri PL-luokkien fragmentoitumista käyttäen hydrofiilisen vuorovaikutuksen nestekromatografiaa (HILIC) ja MS^2-menetelmää. Kalibraatiosuorat luotiin käyttäen puhtaita PL-standardeja, mikä mahdollisti tiettyjen PL-regioisomeerien määrityksen. Tutkimuksen toisessa osassa HILIC-menetelmä korvattiin käänteisfaasikromatografialla, mikä johti yksittäisten yhdisteiden luotettavampaan ja tehokkaampaan erotteluun luokkien sisällä. Kohdentamatonta analyysiä varten luotiin automaattinen tunnistusalgoritmi eri PL-yhdisteille sekä laskentamalli regioisomeerien pitoisuuksien määritystä varten.

Yhdessä nämä kehitetyt ESI-LC-MS^2-menetelmät ja laskentamallit muodostavat vahvan perustan TG- ja PL-regioisomeerien kohdentamatonta lipidomiikkatutkimusta varten, mahdollistaen nykyisiä menetelmiä tarkemman rakenteellisen analyysin nopeasti kasvavalla ja kehittyvällä tieteenalalla.

LIST OF ABBREVIATIONS

ACN	Acyl carbon number
ACN:DB	Acyl carbon number : double bond number
Ag-HPLC	Silver ion chromatography
APCI	Atmospheric pressure chemical ionization
APPI	Atmospheric pressure photoionization
CCS	Collisional cross section
CI	Chemical ionization
CID	Collision-induced dissociation
DB	Double bond
DESI	Desorption electrospray ionization
DDA	Data-dependent acquisition
DG	Diacylglycerol
DMS	Differential mobility spectrometry
DTIMS	Drift tube ion mobility spectrometry
ECN	Equivalent carbon number
EID	Electron-induced dissociation
EIEIO	Electron impact excitation of ions from organics
ESI	Electrospray ionization
FA	Fatty acid
HCD	Higher-energy collisional dissociation
HESI	Heated electrospray ionization
HILIC	Hydrophilic interaction liquid chromatography
IMS	Ion mobility spectrometry
LC	Liquid chromatography
LCOOV	Leave-one-out cross-validation
MAE	Mean absolute error
MALDI	Matrix-assisted laser desorption/ionization
MS	Mass spectrometry
MS^2	Tandem mass spectrometry
MS^n	Sequential fragmentation with *n* product ion stages
nanoESI	Nanoelectrospray ionization
OzID	Ozone-induced dissociation
PA	Phosphatidic acid
PB	Paterno-Buchi photochemical reaction
PC	Phosphatidylcholine
PE	Phosphatidylethanolamine
PG	Phosphatidylglycerol
PI	Phosphatidylinositol
PL	Phospholipid

PS	Phosphatidylserine
QTOF	Quadrupole time-of-flight mass spectrometer
rac	Racemic
RP	Reversed phase
SFC	Supercritical fluid chromatography
sn	Stereospecific numbering
TG	Triacylglycerol
TIMS	Trapped ion mobility spectrometry
UVPD	Ultraviolet photodissociation

Other nomenclature

Shorthand notations of fatty acids (FA), triacylglycerols (TG) and phospholipids (PL) mainly follow the updated LIPID MAPS classification (Liebisch et al., 2020). Briefly, TGs are annotated based on the level of structural information as follows: species level (total number of acyl carbons and double bonds (ACN:DB) is known, for example TG 52:2), molecular species level (FA composition is known, but structural location is unknown, TG 16:0_18:1_18:1), regioisomer level (FA composition and *sn*-2 FA are known, TG 16:0_18:1 *sn*-2_18:1) and enantiomer level (structural location of all three FAs is known, TG 16:0/18:1/18:1). Similarly, PLs are annotated at species level (PC 34:1), molecular species level (PC 16:0_18:1) and regioisomer level (PC 16:0/18:1).

In addition, FAs can be interchangeably denoted with the LIPID MAPS classification or a single letter system as follows: FA 4:0 (Bu), 6:0 (Co), 8:0 (Cy), 10:0 (Ca), 12:0 (La), 14:0 (M), 16:0 (P), 16:1 (Po), 18:0 (S), 18:1 (O), 18:2 (L). 18:3 (Ln), 20:0 (A). In certain cases different terminology for TG and DG shorthand naming is used, for example, AAB / ABA refers to regioisomers, where A and B are different FAs, only providing location of the *sn*-2 FA, whereas the *sn*-1 and *sn*-3 FAs cannot be distinguished from one another. *sn*-AAB / *sn*-BAA / *sn*-ABA means that the *sn*-position of each FA is known. AA / AB refer to DGs with known FA composition, but unknown *sn*-positions.

LIST OF ORIGINAL PUBLICATIONS

I. Fabritius, M., Linderborg, K., Tarvainen, M., Kalpio, M., Zhang, Y., & Yang, B. **(2020)**. Direct inlet negative ion chemical ionization tandem mass spectrometric analysis of triacylglycerol regioisomers in human milk and infant formulas. *Food Chemistry*, 328, 126991.

II. Sazzad, M., Fabritius, M., Boström, P., Tarvainen, M., Kalpio, M., Linderborg, K. M., Kallio, H., & Yang, B. **(2022)**. A novel UHPLC-ESI-MS/MS method and automatic calculation software for regiospecific analysis of triacylglycerols in natural fats and oils. Analytica Chimica Acta, 1210, 339887.

III. Fabritius, M., & Yang, B. **(2021)**. Direct infusion and ultra-high-performance liquid chromatography/electrospray ionization tandem mass spectrometry analysis of phospholipid regioisomers. *Rapid Communications in Mass Spectrometry*, 35(18).

IV. Fabritius, M., Boström, P., & Yang, B. (**2023**) UHPLC-ESI-MS/MS analysis of phosphatidylcholine regioisomers with a fragmentation model. *Manuscript*

1 INTRODUCTION

Triacylglycerols (TG) are the prime constituents of natural fats and oils, while phospholipids (PL) are structural components of cell membranes. TGs consist of a glycerol backbone with three fatty acids (FA) esterified to positions *sn*-1, *sn*-2 and *sn*-3 (**Figure 1**). PL structure is similar, but in addition to two FAs they also have a class-specific phosphate head group. While there is evidence on the health effects of individual FAs, the effect of their structural location in the glycerol backbone has been studied to a much lesser extent.

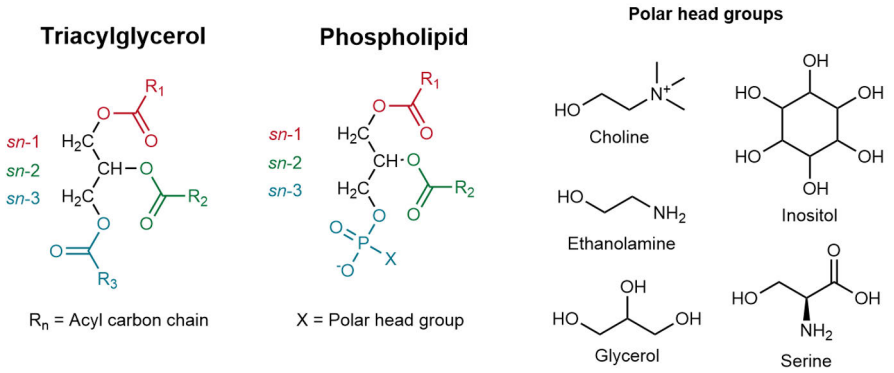

Figure 1 Structures of triacylglycerols and phospholipids

With dietary TGs it has been shown that FAs located in *sn*-2 position are more readily absorbed, influencing nutritional properties (Bar-Yoseph et al., 2013; Lasekan et al., 2017; Linderborg & Kallio, 2005; López-López et al., 2001). In infant nutrition, especially the positional distribution of palmitic acid affects lipid metabolism and has implications for absorption and digestion (Innis, 2011). Long-term feeding of TGs with different structures containing polyunsaturated FAs has been shown to impact plasma lipid concentrations in animals (Ikeda et al., 1998). Lipids with a specific structure, featuring medium-chain FAs in the *sn*-1 and *sn*-3 positions and essential FA in the *sn*-2 position, have been shown to play an important role in providing nutritional assistance to animals suffering from malabsorption issues (Straarup & Høy, 2000). In addition, TG regioisomer structure influences fat crystallization, affecting texture and melting behavior of fats (Minato et al., 1997; Watanabe et al., 2018), and adjusting the molecular structure of fat ingredients can have a noticeable effect food production and storage (Watanabe et al., 2021). Additionally, FA chain length differences and regioisomerism impact polymorphism and oxidative stability of fat (Bouzidi & Narine, 2012). Highly polyunsaturated FAs like docosahexaenoic acid are more

stable in the *sn*-2 position (Damerau et al., 2023; Wijesundera et al., 2008), and similar results have been reported for other unsaturated FAs (Dote et al., 2016).

In case of dietary PLs, the health effects have mostly been studied on class level, and the role of individual PL molecular species and especially regioisomers remains largely a question (Küllenberg et al., 2012; Skórkowska-Telichowska et al., 2016; Sun et al., 2018; C. Wang et al., 2018). More interestingly, PLs have a multitude of important biological functions, and they also have potential to be used as diagnostic markers of health and diseases.

PLs play crucial roles in various biological processes, such as providing membranes for protein synthesis and export, maintaining cholesterol balance, and managing TG storage and secretion (Lagace & Ridgway, 2013). Disruptions in PL metabolism are associated with lipid storage issues and stress responses, ultimately contributing to health conditions such as obesity, diabetes, atherosclerosis, and neurological disorders (Dai et al., 2021; Lagace & Ridgway, 2013). Lipidomics is a rapidly expanding field of research focused on the comprehensive analysis of lipids to better understand their functions and health impacts. Despite this growth, the biological significance of individual phospholipid compounds, particularly the effects of PL regioisomers, remains largely unexplored due to a lack of powerful analytical methods to determine the regioisomeric composition of natural lipids. Recently, human breast cancer and lung cancer cells were found to contain certain phosphatidylcholine regioisomers at different ratios compared to adjacent healthy tissue (Cao et al., 2020).

Comprehensive structural characterization of TGs and PLs is a challenging task primarily because there are many possible FA combinations, which can total up to hundreds of individual regioisomers in natural samples. Determining the qualitative species and molecular species structural levels of TGs or PLs is reasonably straightforward with tandem mass spectrometric (MS^2) methodologies utilizing fragment ions. Going deeper into the structural analysis of TGs and assigning the *sn*-positions of each FA and accurately determining ratios of the isomers is a much more demanding task.

Generally, analysis of TG and PL *sn*-positional isomers can be divided into two main categories: the first being direct separation either by chromatographic or ion mobility techniques. Comprehensive separation of the isomers is difficult, and most existing methods can only achieve partial or specific separation of individual compounds of interest. The second category is identification utilizing differential fragmentation efficiency of FAs from different *sn*-positions. TG and PL regioisomers can be identified with MS^n methods, but analysis of TG enantiomers is not possible because the fragmentation methods cannot distinguish *sn*-1 and *sn*-3 FAs due to identical fragmentation efficiencies. The intensities of the resulting fragment ions reflect the FA distribution in the glycerol backbone. Many isobaric TG species, including isomers, are often

chromatographically overlapping and may produce shared isobaric fragment ions, making the analysis of TG regioisomers even more challenging.

For PLs the situation is somewhat less complicated as they can only contain up to two different FAs, resulting in significantly less interfering isobaric fragments. However, adding to the complexity of analysis of PLs is the different head groups of each class, influencing the fragmentation behavior. Traditional separation methods relying on column chromatography alone for analysis of TG regioisomers are becoming increasingly less common, especially if trying to achieve comprehensive identification of a wide range of regioisomers, while many current applications are shifting towards MS^n fragmentation and identification. Separation by ion mobility is also an emerging technique for isomeric lipid analysis.

Analysis of TG and PL *sn*-positional isomers is not covered by standard lipidomics approaches (Heiles, 2021; Züllig & Köfeler, 2021), highlighting the need for further development and integration of untargeted regioisomer analysis methods for lipidomics protocols. The literature review focuses on the liquid chromatographic, mass spectrometric and liquid chromatographic-mass spectrometric methodologies for analysis of *sn*-positional isomers, including regioisomers and enantiomers of TGs and PLs, detailing the chromatographic separation, ionization, fragmentation and identification as well as the challenges related to the field. Analysis of double bond isomers is not covered in the literature review. The focus of this doctoral thesis was to develop and validate accurate, high-throughput analysis methods for TG and PL regioisomers.

2 REVIEW OF THE LITERATURE

2.1 Separation of TG *sn*-positional isomers

2.1.1 Reversed phase chromatography

Reversed phase (RP) chromatography, especially with C18 columns, is the most commonly used method for separating TGs in natural samples. The C18 column, or octadecylsilane, consists of alkyl chains of 18 carbon atoms bound to silica. The octadecyl chains are hydrophobic, making the stationary phase a common choice for analysis of lipids with hydrophobic FAs. The separation is primarily governed by the equivalent carbon number (ECN) of the TG, which is defined as ACN – (2 × DB). TGs with the same ECN typically elute in clusters, and many are at least partially overlapping with each other (Ovčačíková et al., 2016).

Comprehensive separation of TG regioisomers in sources of natural origin is difficult to achieve with C18 columns, and the role of this technique combined with MS methodologies has recently been mainly for TG species profiling and qualitative identification of molecular species based on the fragment ion spectra (M. Li et al., 2020; Zhu et al., 2021). Specific applications for separation of TG regioisomers have been developed over the years using C18 columns, including analysis of various TG reference standards with four different columns (Momchilova et al., 2006), vaccenic and oleic acid containing TGs (Leskinen, Suomela, Yang, et al., 2010) and hexadecenoic acid containing TGs (Řezanka et al., 2022). Oxidized forms of TG regioisomers have also been analyzed by coupling two Kinetex C18 columns (100 × 2.1 mm, 1.7 µm) in a series (Suomela et al., 2011). The resolution of TG regioisomer separation with C18 columns is strongly influenced by the nature of the attached FAs. Generally, TG regioisomers containing FAs with higher degree of unsaturation and longer acyl carbon chains are easier to resolve from one another, whereas TGs containing only saturated or monounsaturated FAs are more difficult to separate (Momchilova et al., 2006). It was observed that the regioisomer with an unsaturated FA in *sn*-2 and two palmitic acids in *sn*-1/3 positions eluted earlier than the *sn*-1/3 unsaturated regioisomer. The choice of column and the stationary phase also had a noticeable effect, and presence of higher number of residual silanol groups in the supporting material was attributed to increased TG regioisomer resolution (Momchilova et al., 2006).

Polymeric columns, such as Nucleodur C18 ISIS with a C18/C11-OH mixed acyl stationary phase has been particularly effective for TG regioisomer separation is some cases compared to monomeric C18 columns (**Figure 2**). Using isocratic elution with varying ratios of acetonitrile/isopropanol mobile phase, a near baseline separation for various TG regioisomer pairs was achieved

usually in less than 10 min elution with a higher 55% isopropanol concentration. Reducing the amount of isopropanol in the mobile phase further enhanced separation, but also increased retention time. The authors noted that the presence of hydroxyl groups in the stationary phase was important for the high separation efficiency and steric selectivity when analyzing TG regioisomers (Tamba Sompila et al., 2017).

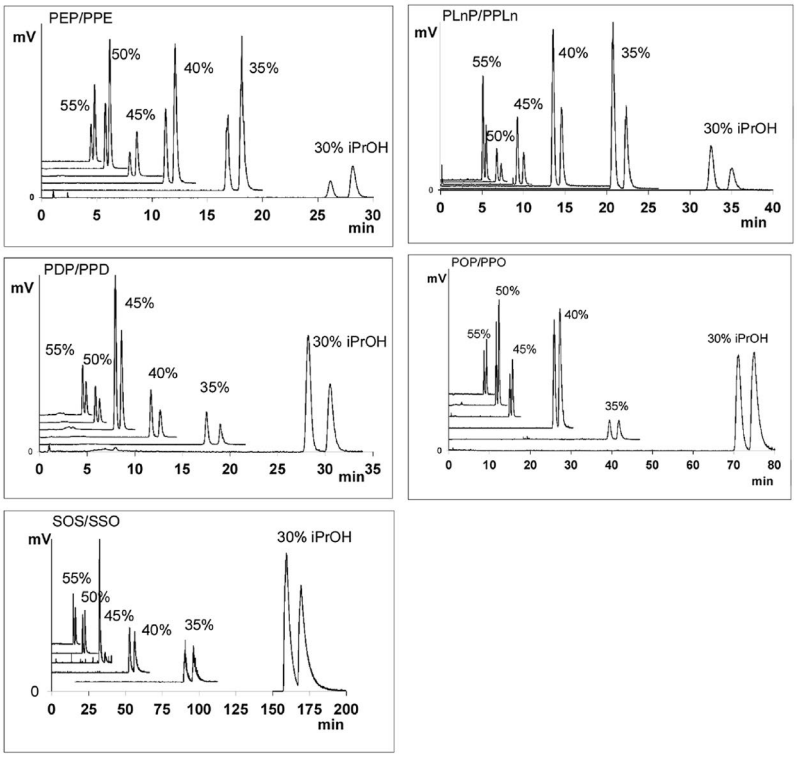

Figure 2 Effect of percentage of isopropanol in acetonitrile/isopropanol mobile phase on separation of regioisomers TG 16:0_20:5 *sn*-2_16:0 / TG 16:0_16:0 *sn*-2_20:5 (PEP/PPE), TG 16:0_22:6 *sn*-2_16:0 / TG 16:0_16:0 *sn*-2_22:6 (PDP/PPD), TG 16:0_18:3 *sn*-2_16:0 / TG 16:0_16:0 *sn*-2_18:3 (PLnP/PPLn), TG 16:0_18:1 *sn*-2_16:0 / TG 16:0_16:0 *sn*-2_18:1 (POP/PPO), TG 18:0_18:1 *sn*-2_18:0 / TG 18:0_18:0 *sn*-2_18:1 (SOS/SSO) separations. Nucleodur C18 ISIS (50 × 2 mm, 1.8 µm). Reprinted with permission from (Tamba Sompila et al., 2017), copyright 2017 Elsevier.

Two Nucleodur C18 ISIS (250 × 2.1 mm, 1.8 µm) columns were used for a more comprehensive lipid class analysis, including some TG regioisomer pairs (Causevic et al., 2021). C28 columns have also been used for TG regioisomer

separation, mainly for pairs containing two palmitic acids and one unsaturated FA. Lowering the temperature of the column to 10-15 °C was critical to achieve good chromatographic resolution for the studied TG standards. Interestingly, it was noted that separation of a regioisomer pair with two unsaturated FAs, such as TG 18:1_18:1 *sn*-2_16:0 and TG 18:1_16:0 *sn*-2_18:1 was not achieved even though they could be separated with a C18 column (Nagai et al., 2015; Nagai, Gotoh, et al., 2011). While it has some specific applications, reversed phase chromatography alone is generally not powerful enough for separation of TG regioisomers in complex samples, but it is a very useful tool for separation of TG species for further MS-based detection and identification. Methods using RP chromatography for separation of TG regioisomers are listed in **Table 1**.

Table 1 Analysis methods primarily based on separation of TG regioisomers using reversed phase chromatography.

Reference	Column	Mobile phase	Separation category	Sample material
(Řezanka et al., 2022)	3 × Luna Omega C18 (150 × 2.1 mm, 1.6 µm)	A: ACN with 5 mM ammonium acetate, B: IPA with 5 mM ammonium acetate	Reversed phase C18	Algae, fungus, yeast
(Causevic et al., 2021)	2 × Nucleodur C18 ISIS (250 × 2.1 mm, 1.8 µm)	A: 0.4 % Acetic acid in ACN, B: IPA, C: Heptane	Reversed phase C18/C11-OH	Vegetable oils
(Tamba Sompila et al., 2017)	Nucleodur C18 ISIS (50 × 2 mm, 1.8 µm)	ACN/IPA at various concentrations tested, isocratic	Reversed phase C18/C11-OH	Vegetable fats, cocoa butter
(Nagai et al., 2015)	Sunrise C28 (250 × 4.6 mm, 5 µm)	A: Acetone, B: ACN	Reversed phase C28	Milk
(Gotoh et al., 2012)	2 × Inertsil ODS-P (250 × 4.6 mm, 5 µm), Sunrise C28 (250 × 4.6 mm, 5 µm)	ACN/IPA/Hexane (3:2:1), isocratic	Reversed phase C18 and C28	Milk, cheese
(Řezanka et al., 2012)	2 × Hichrom HIRPB-250AM (250 × 2.1 mm, 5 µm)	A: ACN, B: IPA	Reversed phase C18/C8	Bacteria
(Nagai, Gotoh, et al., 2011)	Sunrise C28 (250 × 4.6 mm, 5 µm)	Acetone, isocratic	Reversed phase C28	TG standards
(Suomela et al., 2011)	2 × Kinetex C18 (100 × 2.1 mm, 1.7 µm)	A: ACN, B: Acetone/ACN (80:20)	Reversed phase C18	Oxidized TG standards
(Gotoh et al., 2011)	Preparative molecular species separation: Intersil ODS (250 × 10 mm, 10 µm). Regioisomer separation: 2 × Inertsil ODS-P (250 × 4.6 mm, 5 µm)	ACN/IPA/Hexane (3:2:1), isocratic	Reversed phase C18/C11-OH	Fish, marine mammals
(Řezanka et al., 2010)	2 × Hichrom HIRPB-250AM (250 × 2.1 mm, 5 µm)	A: ACN, B: IPA	Reversed phase C18/C8	Bacteria

2.1.2 Silver ion chromatography

Silver ion liquid chromatography (Ag-HPLC) in lipid analytics relies on the interactions of silver ions immobilized in the column stationary phase with the double bonds of the FAs. The higher number of double bonds means stronger interactions of the analyte with the stationary phase. Silver ions can be introduced to a column for example with silver nitrate solution, in which case the separation is also governed by the respective stationary phase of the column, for example reversed phase C18 (Dobson et al., 1995). However, addition of silver ions to the mobile phase is not compatible with mass spectrometry due to ion suppression and contamination of the ion source with non-volatile compounds (Holčapek & Lísa, 2017).

Instead, cation exchange columns in the stationary phase are currently the column type of choice for TG regioisomer analytics when using Ag-HPLC (Chen et al., 2020; Lísa et al., 2011; Santoro et al., 2018). No silver ions are needed in the mobile phase with cation exchange columns as they are strongly embedded in the stationary phase, resulting in minimal leakage, and making the application suitable for MS detection (Holčapek & Lísa, 2017). Self-modified cation exchange columns embedded with silver ions have been used for TG regioisomer separation (Leskinen et al., 2008, 2009; Santoro et al., 2018). ChromSpher Lipids (250 × 4.6 mm, 5 μm) has been a popular Ag-HPLC column choice for TG regioisomer separations (Chen et al., 2020; Lísa et al., 2013), sometimes two (Adlof & List, 2004) or even three (Holčapek et al., 2010; Lísa et al., 2009, 2011) of them coupled together in a series.

The effect of column temperature on retention times has been investigated using two ChromSpher Lipids (250 × 4.6 mm, 5 μm) columns, resulting in an interesting observation that higher temperatures significantly increased retention time for more unsaturated compounds, also increasing chromatographic resolution of TG regioisomers, for example regioisomers of molecular species TG 18:0_18:0_18:3 and TG 18:1_18:2_18:2 (Adlof & List, 2004). This effect is opposite to the usual temperature effect in liquid chromatography, which typically results in faster retention times at elevated temperatures. The increased temperature retention effect was less pronounced for TGs with lower degree of unsaturation, such as TG 16:0_16:0_18:1. It was noted that this effect is likely limited to hexane-based solvent systems. The authors suggested that the inverse retention behavior may have been caused by a temperature-induced change in the acetonitrile/Ag^+ complex, which is presumably exothermic. The acetonitrile/Ag^+ complex might be less stable in higher temperatures, allowing more interactions between the complex and the double bonds of the FAs, resulting in increased retention (Adlof & List, 2004). Similar effect was observed in another study, where retention times of TGs increased with higher temperature

in the hexane mobile phase, while an opposite effect was observed for the dichloromethane mobile phase (Lísa et al., 2013).

Separation of various TG regioisomers obtained by randomization of TG 18:0/18:0/18:0, TG 18:1/18:1/18:1 and TG 18:3/18:3/18:3 is presented in **Figure 3**. Adequate separation of all regioisomers was achieved using three ChromSpher Lipids (250 mm × 4.6mm, 5µm) columns (Holčapek et al., 2010). Clear separation into groups differing in the number of double bonds was observed in all mixtures of randomized TGs.

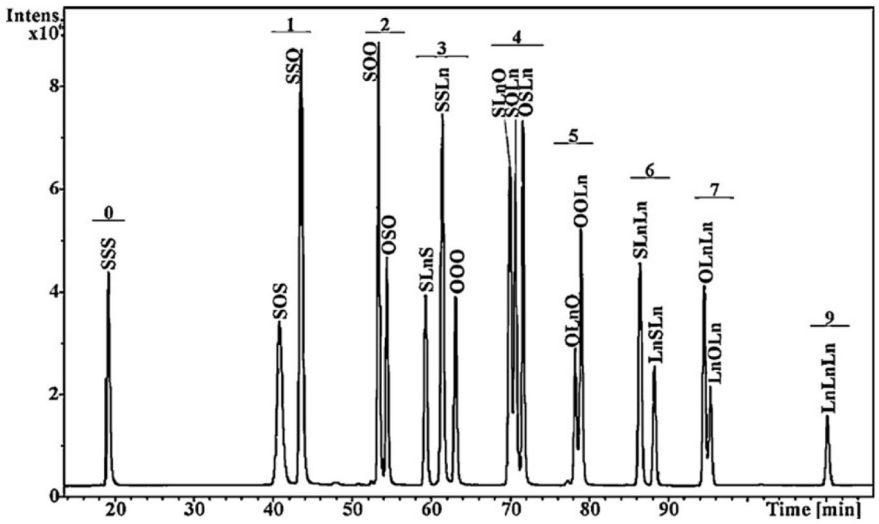

Figure 3 Silver-ion HPLC/APCI-MS chromatogram of the randomization mixture prepared from tristearin (TG 18:0/18:0/18:0), triolein (TG 18:1/18:1/18:1) and trilinolenin (TG 18:3/18:3/18:3) using three ChromSpher Lipids (250 mm × 4.6mm, 5µm) columns. Numbers correspond to the double bond number. Reprinted with permission from (Holčapek et al., 2010), copyright 2010 Elsevier.

Even with the more modern Ag-HPLC columns and methodologies, comprehensive separation of a wide range of TG regioisomers remains challenging and time consuming, and the role of this separation technique has remained as a more targeted method for specific regioisomers of interest (Chen et al., 2020; Santoro et al., 2018), as molecular species might need very different chromatographic conditions for adequate regioisomer separation based on their FA compositions and degree of unsaturation. One of the main challenges of Ag-HPLC is also poor reproducibility using conventional hexane mobile phases. Adding isopropanol to the mobile phase increased reproducibility by improving miscibility of the commonly used hexane and acetonitrile (Holčapek et al., 2010).

Additionally, the fact that the separation is governed by the number of double bonds of the FAs makes separation of TGs containing only saturated FAs unviable. Methods using silver ion chromatography for separation of TG regioisomers are listed in **Table 2**. Ag-HPLC can offer complementary separation capabilities when used together with RP chromatography in two-dimensional applications. RP separates TGs mainly according to the ECN, while retention with Ag-HPLC is mainly influenced by the number and geometry of DBs (Holčapek et al., 2009).

Table 2 Analysis methods primarily based on separation of TG regioisomers using silver ion chromatography

Reference	Column	Mobile phase	Separation category	Sample material
(Chen et al., 2020)	ChromSpher Lipids (250 × 4.6 mm, 5 µm)	A: Hexane, B: Hexane/IPA (98:2)	Embedded silver ion stationary phase	Human milk
(Santoro et al., 2018)	Luna SCX (150 × 2.0 mm, 5 µm)	Two isocratic steps: n-heptane/Ethylacetate (93:7) and (90:10)	Silver ion modification with $AgNO_3$ solution	Confectionery oils
(Lísa et al., 2013)	ChromSpher Lipids (250 × 4.6 mm, 5 µm)	(i) A: Hexane/IPA/ACN (99.8:0.1:0.1), B: Hexane/IPA/ACN (96:2:2). (ii) A: CH_2Cl_2, B: CH_2Cl_2/ACN (90:10)	Embedded silver ion stationary phase	TG standards
(Dillon et al., 2012)	Custom silver thiolate column (150 × 3 mm, 3 µm)	A: Hexane, B: Acetone	Embedded silver ion stationary phase	Vegetable oils
(Lísa et al., 2011)	3 × ChromSpher Lipids (250 × 4.6 mm, 5 µm)	A: Hexane/IPA/ACN (99.8:0.1:0.1), B: Hexane/IPA/ACN (96:2:2)	Embedded silver ion stationary phase	Animal tissue
(Holčapek et al., 2010)	3 × ChromSpher Lipids (250 × 4.6 mm, 5 µm)	A: Hexane/IPA/ACN (99.8:0.1:0.1), B: Hexane/IPA/ACN (96:2:2)	Embedded silver ion stationary phase	TG standards
(Leskinen et al., 2009)	2 × Nucleosil 100-5 SA (250 × 4.6 mm, 5 µm)	A: Acetone, B: Acetone/ACN (4:1)	Silver ion modification with $AgNO_3$ solution	Berry seed oils
(Lísa et al., 2009)	3 × ChromSpher Lipids (250 × 4.6 mm, 5 µm)	A: Hexane/IPA/ACN (99.8:0.1:0.1), B: Hexane/IPA/ACN (96:2:2)	Embedded silver ion stationary phase	Vegetable oils
(Leskinen et al., 2008)	Nucleosil 100-5 SA (250 × 4.6 mm, 5 µm)	A: Acetone, B: Acetone/ACN (4:1)	Silver ion modification with $AgNO_3$ solution	Berry seed oils
(Adlof & List, 2004)	2 × ChromSpher Lipids (250 × 4.6 mm, 5 µm)	Isocratic, Hexane:ACN (99:1)	Embedded silver ion stationary phase	TG standards

2.1.3 Chiral phase chromatography

Chiral chromatography is a powerful technique for separating *sn*-positional isomers of TGs. By employing a chiral stationary phase, this methodology allows the separation of TG isomers based on the spatial arrangements of the attached FA chains. Generally, the chiral recognition is based on the formation of diastereomeric complexes with different stability between the chiral selector in the stationary phase and the separated enantiomers (Alvarez-Rivera et al., 2020).

There are various chiral stationary phases utilizing different chiral selectors, resulting in complex retention mechanisms, which have been reviewed previously (Cavazzini et al., 2011). For TGs, chiral phase chromatography is currently the only chromatographic technique capable of separating enantiomers while also being capable of separating regioisomers. Current MS-based fragmentation methods cannot differentiate enantiomers due to identical fragmentation efficiencies of *sn*-1 and *sn*-3 FAs, making chiral phase chromatography an important technique for this type of work. Very long analysis times are typical for chiral separations of TG isomers, and sometimes a sample recycling system is used, where the sample is repeatedly cycled through the column (Nagai, Mizobe, et al., 2011) or two columns (Kalpio et al., 2015, 2021; Nagai et al., 2015) to obtain acceptable peak resolution.

The performance of different chiral columns (CHIRALPAK IA, IB, IC, AD-H, AS-H and AY-H CHIRALCEL OD-H, OJ-H, OZ-H AD-RH, AS-RH, OD-RH, and OJ-RH) using methanol or acetonitrile as the mobile phase has been evaluated for separation of TG enantiomers. Only the CHIRALCEL OD-RH (150 × 4.6 mm, 5 µm) with methanol as the mobile phase slightly separated the TG 16:0/16:0/18:1 and TG 18:1/16:0/16:0 from one another. Multiple passes in a recycling system were required for an adequate resolution between the two peaks, taking more than two hours. It seems that not only is the chiral selector important for the separation, but also how it is incorporated in the stationary phase. For example, CHIRALPAK IB and CHIRALCEL OD-RH have the same chiral selector (cellulose tris-(3,5-dimethylphenylcarbamate), but the former has it immobilized in silica gel and the latter has it coated on silica gel. Adequate separation was not achieved with CHIRALPAK IB (Nagai, Mizobe, et al., 2011).

The CHIRALCEL OD-RH (150 × 4.6 mm, 5 µm) has also been used for separation and studying the retention behavior of various pure racemic TG standards found in common fats and oils (Kalpio et al., 2015). TG enantiomers were analyzed by cycling the sample through two columns until desired chromatographic resolution was achieved or it was deemed that no separation would be achieved. Eleven of the fifteen racemic TGs were successfully separated. Separation of a series of racemic TGs containing dioleoylglycerol backbone and one saturated FA in *sn*-1/3 position (TG 18:1_18:1 *sn*-2_X, where

X = 12:0, 14:0, 16:0, 18:0, 20:0 or 22:0) was evaluated (**Figure 4)**. Retention time increased and resolution of the TG enantiomers improved as the acyl chain length of the saturated FA increased. Interestingly, no enantiomer separation was achieved for TG 18:1_18:1 *sn*-2_18:2 containing only unsaturated FAs, whereas TG 18:0_18:1 *sn*-2_18:1 was successfully separated. No fully saturated TGs were analyzed in this study due to inadequate UV detector response (Kalpio et al., 2015). The same columns and sample recycling system were later used for characterization of TG enantiomers in sea buckthorn pulp oil, where careful preparative pre-separation of TGs of interest was required for following enantiomer separations (Kalpio et al., 2021).

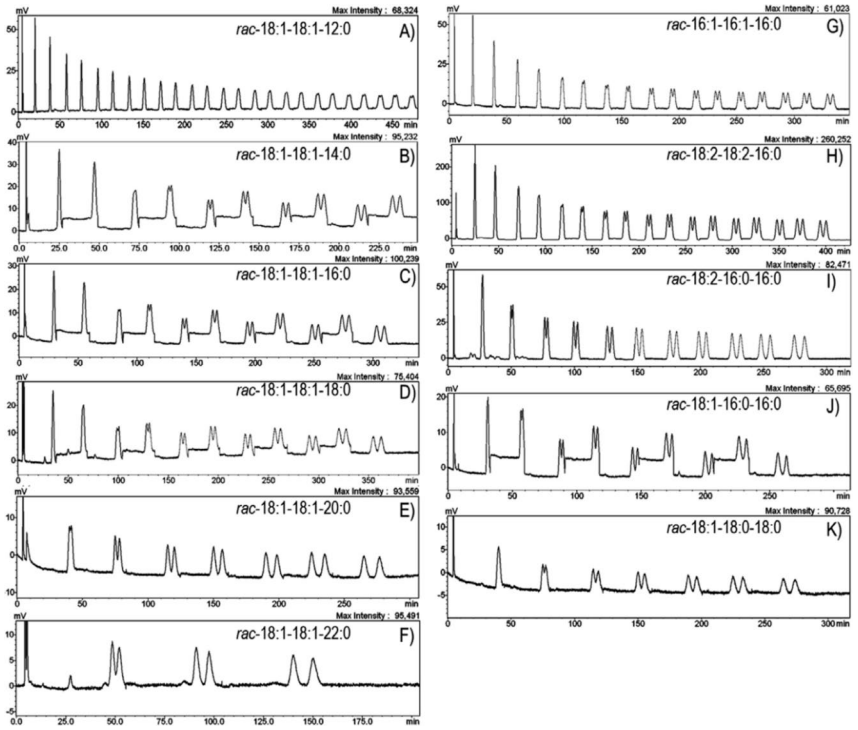

Figure 4 UV chromatograms of eleven racemic TG standards: TG 12:0_18:1 *sn*-2_18:1 **(A)**, TG 14:0_18:1 *sn*-2_18:1 **(B)**, TG 16:0_18:1 *sn*-2_18:1 **(C)**, TG 18:0_18:1 *sn*-2_18:1 **(D)**, TG 20:0_18:1 *sn*-2_18:1 **(E)**, TG 22:0_18:1 *sn*-2_18:1 **(F)**, TG 16:0_16:1 *sn*-2_16:1 **(G)**, TG 16:0_18:2 *sn*-2_18:2 **(H)**, TG 16:0_16:0 *sn*-2_18:2 **(I)**, TG 16:0_16:0 *sn*-2_18:1 **(J)** and TG 18:0_18:0 *sn*-2_18:1 **(K)** using 2 × CHIRALCEL OD-RH (150 × 4.6 mm, 5 µm) with sample recycling and methanol as the mobile phase. Reprinted with permission from (Kalpio et al., 2015), copyright 2015 Elsevier.

Previously it had been reported that both saturated and unsaturated FAs at the *sn*-1 and *sn*-3 would be required for separation, but TG enantiomers in bovine

milk fat comprising of dipalmitoylglycerol backbone and a short- or medium chain saturated FA in *sn*-1/3 position (TG 16:0_16:0_X, where X = 4:0, 6:0, 8:0, 10:0 or 12:0) have been separated using a CHIRALCEL OD-3R (150 × 4.6 mm, 3 μm) column and a sample recycling system (Nagai et al., 2015). The CHIRALCEL OD-3R has the same cellulose tris-(3,5-dimethylphenylcarbamate) coated on silica gel as the CHIRALCEL OD-RH, with the only difference being particle size. Sufficient separation for all enantiomers of interest was achieved in five passes through the column. It was noted that the probable reason for the chiral separation was because of the CH-π interaction between the saturated FA acyl chain and the chiral stationary phase (Nagai et al., 2015).

The enantiomeric composition of TGs consisting of C16 and C18 FAs in hazelnut oil and human plasma was analyzed with two Lux Cellulose-1 (250 × 4.6 mm, 3 μm) columns connected in series. This was one of the first routine chiral analysis methods for TG enantiomers in natural samples. Most TGs eluted between 80-120 min, and while the ratios of certain enantiomers were quantified, there were several cases of coelution of regioisomers or enantiomers, preventing unambiguous determination of some isomer ratios (Lísa & Holčapek, 2013). Two Lux Cellulose-1 (250 × 4.6 mm, 3 μm) in series have also been used to determine enantiomers of TG 16:0_18:1_18:2, which is the most abundant molecular species in human milk (Chen et al., 2020).

Two Astec Cyclobond I 2000 DMP (250 × 4.6 mm, 5 μm) columns in a series have been used by the same group for several studies analyzing different types of TGs of interest containing FAs such as polyunsaturated C18 FAs (Řezanka et al., 2016), C16 FAs (Řezanka et al., 2022; Řezanka & Sigler, 2014), allenic and acetylenic FAs (Palyzová & Řezanka, 2020b) and cyclofatty acids (Palyzová & Řezanka, 2020a). The chiral stationary phase of the column is 3,5-dimethyl-phenylcarbamate modified β-cyclodextrin. The mobile phase used with the Astec Cyclobond columns in these studies was mostly hexane with a small fraction of isopropanol, usually around 1 % or less at any given time during the gradient. Isopropanol was found to be important for controlling retention time, resolution, and reproducibility (Řezanka & Sigler, 2014). Enantiomers containing a more highly unsaturated FA in *sn*-1 position was found to elute earlier (Řezanka et al., 2016). As with most other chiral chromatography applications, retention times are long, and depending on the compounds of interest, acceptable separation can take anywhere from 70-90 min (Palyzová & Řezanka, 2020b, 2020a; Řezanka et al., 2022) up to several hours (Řezanka et al., 2016; Řezanka & Sigler, 2014).

The performance of more recently developed CHIRALPAK ID, IE and IF columns was evaluated for TG enantiomer and regioisomer separation. CHIRALPAK IF-3 (250 × 4.6 mm, 3 μm) column showed notably improved selectivity for TG isomers compared with the older generation CHIRALPAK OD-RH columns, enabling acceptable resolution of various TG enantiomers and

regioisomers in just one pass without sample recycling, and significantly faster (Nagai et al., 2019). For example, TG 16:0_16:0_18:1 regioisomers and enantiomers were sufficiently separated in less than 30 min with the CHIRALPAK IF-3 column, whereas with the older CHIRALPAK OD-RH it took more than two hours and sample recycling to achieve similar resolution (Kalpio et al., 2015; Nagai, Mizobe, et al., 2011). Methods using chiral chromatography for separation of TG regioisomers are listed in **Table 3**.

Overall, chiral chromatography can be a powerful, albeit often time-consuming tool for separating *sn*-positional isomers of TGs. As MS methodologies cannot distinguish FAs dissociated from *sn*-1/3 positions, chiral chromatography is also one of the rare applications that can be used to analyze TG enantiomers. While sample recycling through multiple columns is sometimes employed with chiral chromatography, this prevents the use of MS for monitoring the separation between the columns, as the detector needs to be non-destructive. UV detector is often employed for this purpose, while MS can be used at the end for regioisomer identification once desired separation is achieved.

Table 3 Analysis methods primarily based on separation of TG regioisomers using chiral phase chromatography

Reference	Column	Mobile phase	Separation category	Sample material
(Řezanka et al., 2022)	2 × Astec Cyclobond I 2000 DMP (250 × 4.6 mm, 5 µm)	A: Hexane, B: Hexane/IPA (97:3)	Chiral phase	Yeast, algae, and fungi
(Kalpio et al., 2021)	RP: Ascentis C18 (250 × 4.6 mm, 5 µm) Chiral: 2 × CHIRALCEL OD-RH (150 × 4.6 mm, 5 µm) with sample recycling	RP: A: ACN, B: Acetone Chiral: MeOH, isocratic	Reversed phase C18 for preparative TG separation and chiral phase for enantiomer/regioisomer separation	Berry seed oil
(Palyzová & Řezanka, 2020a)	2 × Astec Cyclobond I 2000 DMP (250 × 4.6 mm, 5 µm)	A: Hexane, B: Hexane/IPA (97:3)	Chiral phase	Plant seed oil
(Chen et al., 2020)	RP: Zorbax Eclipse Plus C18 (100 × 2.1 mm, 1.8 µm). Chiral: Lux Cellulose-1 (250 × 4.6 mm, 3 µm)	RP: A: ACN/MeOH/H_2O (19:19:2) with 10mM ammonium acetate and 0.1 % formic acid, B: IPA with 10mM ammonium acetate and 0.1 % formic acid Chiral: A: Hexane, B: Hexane/IPA (99:1)	Reversed phase C18 for preparative TG separation and chiral phase for enantiomer/regioisomer separation	Human milk fat
(Palyzová & Řezanka, 2020b)	2 × Astec Cyclobond I 2000 DMP (250 × 4.6 mm, 5 µm)	A: Hexane, B: Hexane/IPA (97:3)	Chiral phase	Plant seed oil
(Nagai et al., 2020)	CHIRALPAK IF-3 (250 × 2.1 mm, 3 µm)	Acetonitrile, isocratic	Chiral phase	Palm oil, lard
(Nagai et al., 2019)	CHIRALPAK IF-3 (250 × 2.1 mm, 3 µm)	Acetonitrile, isocratic	Chiral phase	TG standards

Reference	Column	Mobile phase	Separation category	Sample material
(Řezanka et al., 2016)	2 × Astec Cyclobond I 2000 DMP (250 × 4.6 mm, 5 µm)	A: Hexane, B: Hexane/IPA (99:2)	Chiral phase	Algae oil
(Nagai et al., 2015)	RP: Sunrise C28 (250 × 4.6 mm, 5 µm). Chiral: CHIRALCEL OD-3R (150 × 4.6 mm, 3 µm) with sample recycling	RP: A: Acetone/Acetonitrile (50:50), B: Acetone Chiral: MeOH, isocratic	Reversed phase C28 for preparative TG separation and chiral phase for enantiomer/regioisomer separation	Milk fat
(Kalpio et al., 2015)	2 × CHIRALCEL OD-RH (150 × 4.6 mm, 5 µm) with sample recycling	MeOH, isocratic	Chiral phase	TG standards
(Řezanka & Sigler, 2014)	2 × Astec Cyclobond I 2000 DMP (250 × 4.6 mm, 5 µm)	Chiral: A: Hexane, B: Hexane/IPA (99:2)	Chiral phase	Algae, yeast
(Lísa & Holčapek, 2013)	2 × Lux Cellulose-1 (250 × 4.6 mm, 3 µm)	A: Hexane, B: Hexane/IPA (99:1)	Chiral phase	Hazelnut oil, human plasma
(Nagai, Mizobe, et al., 2011)	RP: Inertsil ODS-P (250 × 4.6 mm, 5 µm). Chiral: CHIRALCEL OD-RH (150 × 4.6 mm, 5 µm) with sample recycling	RP: ACN/IPA/Hexane (3:2:1), isocratic Chiral: MeOH, isocratic	Reversed phase C18 for preparative TG separation and chiral phase for enantiomer/regioisomer separation	TG standards

2.1.4 Supercritical fluid chromatography

In recent years, supercritical fluid chromatography (SFC) has seen an increase in usage in the field of lipidomics (Lísa & Holčapek, 2015; Takeda et al., 2018; Wolrab et al., 2020) and TG profiling (Tu et al., 2017; Zhang et al., 2019, 2021), including some regioisomeric separation methods (Lee et al., 2014; Masuda et al., 2021). SFC employs supercritical fluid, typically carbon dioxide, as part of the mobile phase. There are several reasons why carbon dioxide is the most widely used supercritical fluid in SFC, such as miscibility with most organic solvents used in the mobile phase and the critical values of pressure and temperature being easy to reach. Some additional benefits of carbon dioxide are affordability, non-flammability and limited toxicity (West, 2018). Six TG regioisomer pairs found in palm and canola oils have been successfully separated using YMC Carotenoid C30 (250 × 4.6 mm, 4 μm) column (**Figure 5**).

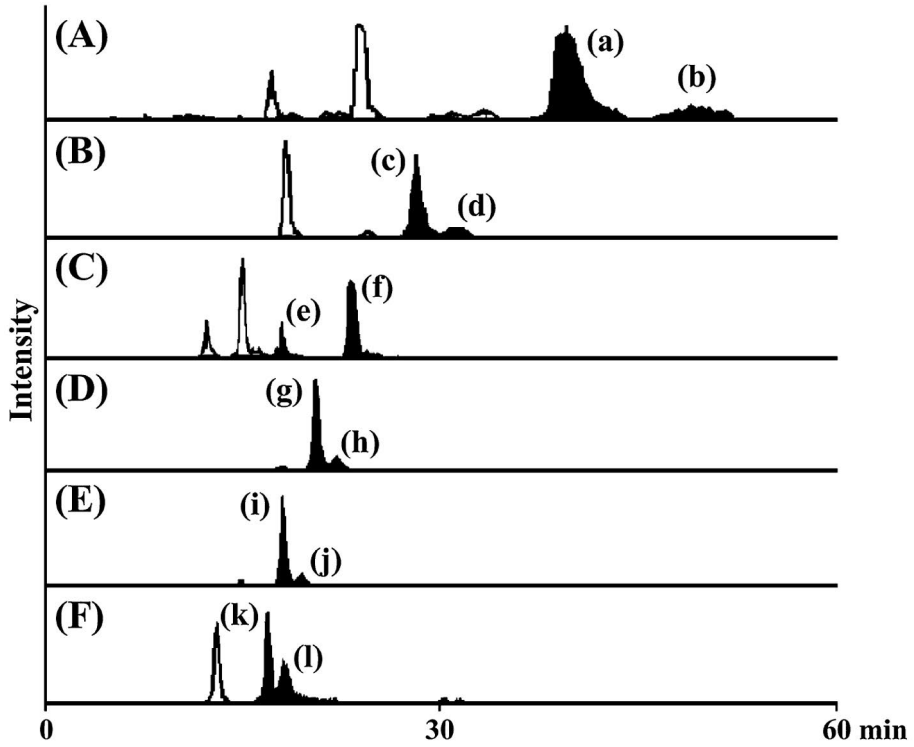

Figure 5 MRM chromatogram of six regioisomeric TG pairs **(a)** TG 18:0_18:1 *sn*-2_18:0, **(b)** TG 18:0_18:0 *sn*-2_18:1, **(c)** TG 18:0_18:1 *sn*-2_16:0, **(d)** TG 18:0_16:0 *sn*-2_18:1, **(e)** TG 18:0_18:3 *sn*-2_16:0, **(f)** TG 18:0_16:0 *sn*-2_18:3, **(g)** TG 16:0_18:1 *sn*-2_16:0, **(h)** TG 16:0_16:0 *sn*-2_18:1, **(i)** TG 16:0_18:2 *sn*-2_16:0, **(j)** TG 16:0_16:0 *sn*-2_18:2, **(k)** TG 16:0_18:3 *sn*-2_16:0, and **(l)** TG

16:0_16:0 *sn*-2_18:3 using YMC Carotenoid C30 (250 × 4.6 mm, 4 μm) column. Reprinted with permission from (Lee et al., 2014), copyright 2014 Elsevier.

Two chiral phase columns CHIRALPAK IG-U (100 × 3 mm, 1.6 μm) and CHIRALPAK IG-U (150 × 3 mm, 1.6 μm) in series were used to separate both enantiomers and regioisomers of TG 16:0_18:1_18:1 for the first time using SFC (Masuda et al., 2021). Suitability of different organic solvent modifiers such as methanol, ethanol, isopropanol and acetonitrile was screened, and a mixture of 90 % acetonitrile and 10 % methanol was selected. Near baseline separation of enantiomers TG 16:0/18:1/18:1 and TG 18:1/18:1/16:0 was achieved in 35 min. The regioisomer TG 18:1/16:0/18:1 was partially overlapping with TG 18:1/18:1/16:0, but the resolution was sufficient for quantification purposes (Masuda et al., 2021). Recently, five reversed-phase columns in a series (four Kinetex C18 (150 × 4.6 mm, 2.6 μm) and one Accucore C18 (150 × 4.6 mm, 2.6 μm)) were used for identification of TGs of a wide variety of vegetable fats and oils using SFC. While analysis of TG regioisomers was not the main objective of this study, several TG regioisomer pairs were resolved chromatographically (Gros et al., 2023). SFC for the separation of TG regioisomers remains relatively unused. Most existing applications primarily focus on high-throughput general lipidomics with MS identification. However, the rapid advancements and growing popularity of SFC instrumentation warrant a more in-depth exploration of its potential for separating TG regioisomers.

2.1.5 Two-dimensional chromatography

A two-dimensional chromatography system consists of two columns, typically with orthogonal selectivity. The peaks of interest separated in the first dimension can be further directed into the second dimension, which will separate the compounds that were co-eluting in the first dimension. Two-dimensional chromatography has been used for analysis of TG regioisomers, commonly comprising of a silver ion and a reversed phase column. There does not seem to be a clear preference on which technique to start with, as researchers are using silver ion followed by reversed phase chromatography (Arena et al., 2021; Mondello et al., 2005; Yang et al., 2012) and vice versa (Chen et al., 2019; Dugo et al., 2004; Holčapek et al., 2009).

Depending on the complexity of the sample and the compounds of interest, sometimes it might be more practical to start with silver ion chromatography to get first dimension separation based on the number of double bonds, or sometimes starting with separation by ECN using reversed phase can be useful. Two-dimensional chromatography can be done either off-line or on-line. Off-line two-dimensional chromatography means that the peaks of interest are

fractionated in the first column, collected, and then reinjected to the other column in a separate analysis.

On-line two-dimensional chromatography uses a series of valves, tubing, and careful timing to direct the compounds from the first dimension to the second within the same analysis. For two-dimensional systems using silver ion and reversed phase chromatography for TG regioisomer separation, some are off-line (Chen et al., 2019; Dugo et al., 2004; Holčapek et al., 2009) and some on-line methods (Arena et al., 2021; Mondello et al., 2005; Yang et al., 2012). There are also several examples of using a reversed phase C18 column for preparative molecular species or regioisomer separation and fraction collection, followed by chiral phase chromatography for enantiomer separation (Chen et al., 2020; Kalpio et al., 2015, 2021; Nagai, Mizobe, et al., 2011). Methods using chiral chromatography for separation of TG regioisomers are listed in **Table 4**.

While two-dimensional chromatography can offer enhanced separation of TG regioisomers compared to more conventional chromatographic applications, it also has some drawbacks. Off-line two-dimensional chromatography is cumbersome, requires precise timing for fraction collection, and is not well suited for high-throughput applications. On-line two-dimensional chromatography necessitates specialized instrumentation and generally demands more expertise compared to conventional chromatography, which can limit its widespread adoption. Furthermore, solvent compatibility between the two dimensions can pose some challenges. Great care should be used when selecting the solvent compositions and flow rates. As separation of TG regioisomers is rather delicate, excessive or too strong eluent from the first dimension may negatively impact peak shape in the second dimension, potentially decreasing the performance of the overall method.

Table 4 Analysis methods primarily based on separation of TG regioisomers using two-dimensional chromatography

Reference	Column (1D)	Mobile phase (1D)	Column (2D)	Mobile phase (2D)	2D Setup	Sample material
(Arena et al., 2021)	Custom silver thiolate column (150 × 1 mm, 5 µm)	A: Hexane/Butyronitrile (99:1), B: Hexane/Butyronitrile (90:10)	Titan C18 (50 × 4.6 mm, 1.9 µm)	A: ACN, B: IPA	Ag-HPLC / RP C18 (On-line)	Borage seed oil
(Kalpio et al., 2021)	Ascentis C18 (250 × 4.6 mm, 5 µm)	A: ACN, B: Acetone	2 × CHIRALCEL OD-RH (150 × 4.6 mm, 5 µm) with sample recycling	MeOH, isocratic	RP C18 / Chiral (Off-line)	Berry seed oil
(Chen et al., 2020)	Zorbax Eclipse Plus C18 (100 × 2.1 mm, 1.8 µm)	A: ACN/MeOH/H_2O (19:19:2), B: IPA, both with 10mM ammonium acetate and 0.1% formic acid	Lux Cellulose-1 (250 × 4.6 mm, 3 µm)	A: Hexane, B: Hexane/ IPA (99:1)	RP C18 / Chiral (Off-line)	Human milk fat
(Chen et al., 2019)	Zorbax Eclipse Plus C18 (100 × 2.1 mm, 1.8 µm)	A: ACN/MeOH/H_2O (19:19:2), B: IPA, both with 10mM ammonium acetate and 0.1% formic acid	ChromSpher Lipids (250 × 4.6 mm, 5 µm)	A: Dichloro-methane, B: Acetone	RP C18 / Ag-HPLC (Off-line)	Infant formulas
(Nagai et al., 2015)	Sunrise C28 (250 × 4.6 mm, 5 µm).	A: Acetone/ACN (50:50), B: Acetone	CHIRALCEL OD-3R (150 × 4.6 mm, 3 µm) with sample recycling	MeOH, isocratic	RP C28 / Chiral (Off-line)	Milk fat
(Yang et al., 2012)	TSK gel SP-2SW (150 × 1 mm, 5 µm)	Hexane/ACN (98:2), isocratic	Chromolith Performance RP-18e (100 × 4.6 mm, 2.7 µm)	A: ACN, B: IPA/Hexane (2:1)	Ag-HPLC / RP C18 (On-line)	Peanut oil, mouse tissue

Reference	Column (1D)	Mobile phase (1D)	Column (2D)	Mobile phase (2D)	2D Setup	Sample material
(Nagai, Mizobe, et al., 2011)	Inertsil ODS-P (250 × 4.6 mm, 5 µm).	ACN/IPA/Hexane (3:2:1), isocratic	CHIRALCEL OD-RH (150 × 4.6 mm, 5 µm) with sample recycling	MeOH, isocratic	RP C18 / Chiral (Off-line)	TG standards
(Holčapek et al., 2009)	2 × Nova-Pak C18 (300 × 3.9 and 150 × 3.9 mm, 4 µm)	A: ACN, B: IPA	3 × ChromSpher Lipids (250 × 4.6 mm, 5 µm)	A: Hexane/ IPA /ACN (99.8: 0.1:0.1), B: Hexane/ IPA/ACN (96:2:2)	RP C18 / Ag-HPLC (Off-line)	TG standards
(Mondello et al., 2005)	Nucleosil 100–5 SA (150 × 1 mm, 5 µm)	Hexane/ACN (99.5:0.5), isocratic	Chromolith Performance RP-18e (100 × 4.6 mm, 2.7 µm)	A: ACN, B: IPA	Ag-HPLC / RP C18 (On-line)	Rice oil
(Dugo et al., 2004)	Restek Ultra C18 (250 × 4.6 mm, 5 µm)	Acetone/ACN (70:30), isocratic	ChromSpher Lipids (250 × 4.6 mm, 5 µm)	Hexane/ACN (99.5:0.5)	RP C18 / Ag-HPLC (Off-line)	Rice oil

2.1.6 Ion mobility

Ion mobility as a separation technique for analysis of TGs has seen an increase in relevance over the recent years, allowing rapid separation of ions moving through inert gas buffer in an electric field. Separation with ion mobility is based on differences in the collisional cross section (CCS) of the analytes. Molecules with higher CCS values encounter higher resistance as they are moving through the gas phase. Different three-dimensional configurations of TG isomers result in slightly different CCS values, potentially enabling separation of the isomers. Current ion mobility applications capable of separating TG regioisomers are limited in numbers, but the potential exists.

To our knowledge the first study to separate TG regioisomers with ion mobility employed differential mobility spectrometry (DMS) (Šala et al., 2016). This study also investigated several factors influencing the separation, such as adduct type, chemical modifier composition, chemical modifier flow rate, separation voltage and pressure of the compensation gas. No separation was observed for the $[M+Na]^+$ or $[M+NH_4]^+$ adducts of regioisomers TG 18:0_18:1 *sn*-2_18:1 and TG 18:1_18:0 *sn*-2_18:1 with the initial settings. $[M+Ag]^+$ adducts, however, were possible to separate, and were selected for further optimization. Both chemical modifier composition and flow rate had significant effect on the ion mobility separation, and out of the tested methanol, ethanol, isopropanol, 1-propanol and 1-butanol, depending on whether resolution or sensitivity was prioritized, 1-Propanol was better for sensitivity while providing acceptable resolution, whereas 1-butanol provided better resolution at the cost of sensitivity. Higher separation voltages increased regioisomer resolution. While higher throttle gas pressure also resulted in better separation, it also significantly reduced sensitivity (Šala et al., 2016). In another study, DMS was used to test separation of various lipid isomer standards, including regioisomers TG 16:0_18:1 *sn*-2_20:0 and TG 16:0_20:0 *sn*-2_18:1, achieving partial separation (Bowman et al., 2017).

Recently, our group had the opportunity to test TG regioisomer separation of various standards with the Waters SELECT SERIES Cyclic ion mobility spectrometer (Unpublished results). The instrument has a unique feature of the possibility to recycle the ions in the circular path of the ion mobility system for improved separation. Regioisomer pairs TG 14:0_14:0 *sn*-2_18:1 / TG 14:0_18:1 *sn*-2_14:0 and TG 16:0_16:0 *sn*-2_18:1 / TG 16:0_18:1 *sn*-2_16:0 were nearly baseline separated, whereas pairs TG 18:1_18:2 *sn*-2_18:2 / TG 18:2_18:1 *sn*-2_18:2 and TG 18:1_18:1 *sn*-2_18:3 / TG 18:1_18:3 *sn*-2_18:1 were partially separated. Analyses were performed with direct infusion. Optimization of parameters was not attempted in these tests, and only $[M+NH_4]^+$ adducts were investigated (Unpublished results). An earlier study (Šala et al., 2016) suggests that further improvements to TG regioisomer separation could

have been possible after thorough method optimization. So far ion mobility techniques for separating TG regioisomers have only been demonstrated on a quite narrow range of regioisomer standards. Compared to direct separation of TG regioisomers, there is likely a greater potential for ion mobility to be coupled with liquid chromatography for further separation of co-eluting isobaric TG molecular species before MS-based identification.

2.2 Identification of TG regioisomers by MS methodologies

As opposed to other methods purely relying on separation TG isomers, MS methodologies typically utilize the differential fragmentation of FAs from *sn*-1/3 or *sn*-2 positions to determine the regioisomer ratios. The MS methodologies still often use chromatographic separation TGs to reduce the number of co-eluting TG species that might convolute the MS^n identification due to isobaric fragments from different molecular species. Some applications use direct inlet techniques without separation. Electrospray ionization (ESI) in positive polarity mode with collision-induced dissociation (CID) is currently the most commonly used MS^2 technique for analysis of TG regioisomers.

Atmospheric pressure chemical ionization (APCI) or chemical ionization (CI) are also used in some methods. Most methods rely on one fragmentation step, but depending on instrument capabilities, several studies also utilize sequential fragmentation, commonly MS^3. Because APCI produces abundant structurally informative in-source fragments, it has been used for TG regioisomer analysis without a dedicated fragmentation step. Analysis of TG regioisomer ratios using MS^n methodologies typically rely on calibration curves created with regiopure reference standards. Different TG species produce fragment ions at different abundance ratios depending on their FA composition, and if these differences are not accounted for, the results may be inaccurate.

2.2.1 Collision-induced dissociation

2.2.1.1 Mechanistic studies on fragmentation of TG regioisomers

Different TG adducts may have distinct fragmentation patterns, some of them being better suited for TG regioisomer analysis than others. For example, using ESI–CID–MS^n, different methods have used $[M+NH_4]^+$, $[M+Li]^+$, $[M+Na]^+$, $[M+Ag]^+$ or $[M+Ag+AgNO^3]^+$ ions to produce structurally informative fragment ions. Examples of typical CID fragment spectra of two TG regioisomer pairs is displayed in **Figure 6**, showing the structurally relevant DG fragment ions and their relative differences in abundance ratios that can be used to establish calibration curves for regioisomer analysis.

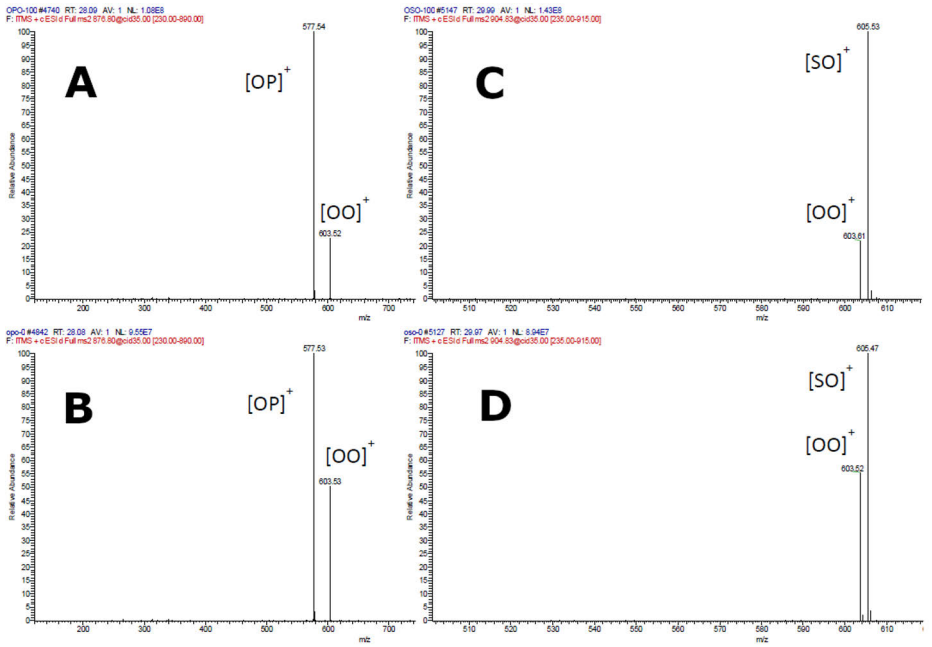

Figure 6 Fragment ion spectra of two TG regioisomer pairs: TG 18:1_16:0 *sn*-2_18:1 **(A)**, TG 16:0_18:1 *sn*-2_18:1 **(B)**, TG 18:1_18:0 *sn*-2_18:1 **(C)** and TG 18:0_18:1 *sn*-2_18:1 **(D)**. Reprinted with permission from (Liu & Rochfort, 2021), copyright 2021 MDPI.

Ammoniated $[M+NH_4]^+$ precursor ions is the most commonly used adduct type for TG regioisomer analysis, and there are several studies that have investigated the CID fragmentation patterns of $[M+NH_4]^+$ ions. A series of three studies focused on oleic acid (X. Li & Evans, 2005), palmitic acid (X. Li et al., 2006) and linoleic or arachidonic acid (Gakwaya et al., 2007) containing TGs. The first study, consisting of the series with TG 18:1/X/18:1 and TG X/18:1/X (X = saturated or monounsaturated FAs with varying chain lengths), discovered that there were linear correlations between the fractional intensities of the various DG fragments and the chain length of the X FA (X. Li & Evans, 2005), indicating that fragmentation efficiencies of various TG molecular species could be predicted based on the FA composition of the TG. In the second part of the study, a series of TG 16:0/X/16:0 and TG X/16:0/X produced similar results in terms of the chain length affecting the fractional abundance of DG-like fragments $[M+NH_4-RCO_2H-NH_3]^+$ with saturated or monounsaturated FAs accompanying the palmitic acid (X. Li et al., 2006). However, with the more unsaturated linoleate (TG 18:2/X/18:2 and TG X/18:2/X) and the arachidonate series (TG 20:4/X/20:4 and TG X/20:4/X) the effects of the chain length were less clear (Gakwaya et al., 2007). Predicting fragmentation patterns of TGs is

useful, because the amount of naturally occurring TGs is vast, and the number of commercially available regiopure TG standards is relatively low.

The fragmentation efficiencies of $[M+NH_4]^+$ adducts of various TGs were also studied after a synthesis of a wide range of regioisomer reference standards. Presence of multiple unsaturated FAs decreased the slopes of the calibration lines closer to zero, especially for TGs containing two arachidonic or docosahexaenoic acids, meaning that the fragmentation is less regiospecific. This caused uncertainties in determining the regioisomer ratios, as the fractional abundances of the structurally informative DG fragments are relatively similar with both regioisomers (Judge et al., 2017). Negative linear correlations have been observed between the number of double bonds in the *sn*-2 FA and the slope of the calibration curve (**Figure 7**) (Tarvainen et al., 2019). The correlation was much stronger when TGs were grouped into four groups having the same primary position FAs within groups. Negative linear correlation was also discovered between the ACN + 2 × DB and the intercept of the calibration curve. Combining these two observations it could be possible to create a fragmentation model (Tarvainen et al., 2019). A mechanistic study on the TG fragmentation pathways concluded that the loss of *sn*-1/3 FAs have lower activation energies than *sn*-2 FA. The loss of *sn*-2 FA is, however, entropically more favorable, and is highly influenced by the FA in that position (Renaud et al., 2013).

The double bond positions in the FAs also seem to play a role in the fragmentation process. Double bonds positioned close to the carbonyl carbon along the fatty acid chain promote the formation of the DG fragment ion corresponding to the loss of the fatty acid. For example, synthetic standards TG 16:0_18:1(9Z) *sn*-2_16:0 and TG 16:0_18:1(6Z) *sn*-2_16:0 have distinctly different fragmentation patterns (X. Li et al., 2006). This creates some additional challenges as natural mixtures might contain various FA double bond isomers in the same TG molecular species. Most current analysis methods utilizing CID and fragments of ammoniated $[M+NH_4]^+$ adducts cannot distinguish FA double bond isomers as they have the same *m/z* ratio.

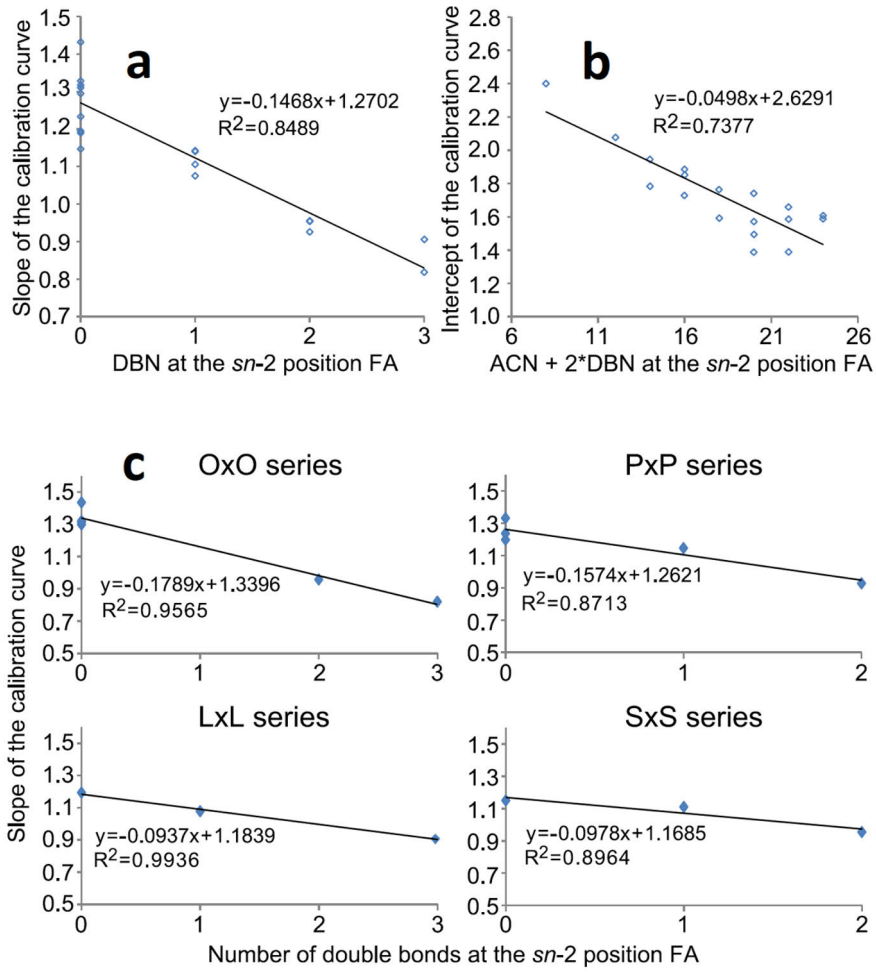

Figure 7 Negative linear correlation between the DB in the *sn*-2 FA and the slope of the calibration curve **(a)**. Negative linear correlation between the ACN + 2 × DB and the intercept of the calibration curve **(b)**. Negative linear correlations between the DB at the *sn*-2 FA and the slope of the calibration curve when the TGs are grouped in four groups having the same primary position FAs within groups **(c)**. Reprinted with permission from (Tarvainen et al., 2019), copyright 2019 American Chemical Society.

In addition to FA composition of the TG molecules, the influence of different TG adduct ion types on the fragmentation efficiencies has been studied. Positional sensitivity of CID fragments from $[M+NH_4]^+$, $[M+Li]^+$, $[M+Na]^+$ and $[M+Ag]^+$ adduct ions was investigated in a series of two studies (Gazlay & Evans, 2022; Makarov et al., 2018). An important observation was that despite $[M+NH_4]^+$ adducts being the most frequently used in many methods and the most thoroughly studied, they might not be the most suitable ones for analysis of TG

regioisomers. Fragmentation behaviors, including the relative abundances of the DG-like fragment ions from both $[M+NH_4]^+$ $[M+Ag]^+$ precursor ion adduct types were less consistent compared with fragments of $[M+Na]^+$ and $[M+Li]^+$ adducts (**Figure 8**). With $[M+NH_4]^+$ ions, some of the calibration plots had significantly higher slopes and different intercepts (Makarov et al., 2018), and as also observed in an earlier study (Gakwaya et al., 2007), the TG standards containing two arachidonic acids produced calibration plots with nearly flat slope due to low positional sensitivity of the fragmentation. The $[M+Ag]^+$ adduct series was even more erratic and random compared to the $[M+NH_4]^+$ series, suggesting that attempt to create a model for the fragmentation pattern would not be viable (Makarov et al., 2018). However, the calibration plots for $[M+Li]^+$ and especially $[M+Na]^+$ adducts were significantly more uniform with similar slopes and intercepts reasonably closely clustered together (**Figure 8c-d**). Another earlier study investigating the same four adduct types came to the same conclusion that $[M+Na]^+$ adducts are the most suitable for TG regioisomer analysis as they produced the most consistent level of positional sensitivity for the fragmentation (Ramaley et al., 2015).

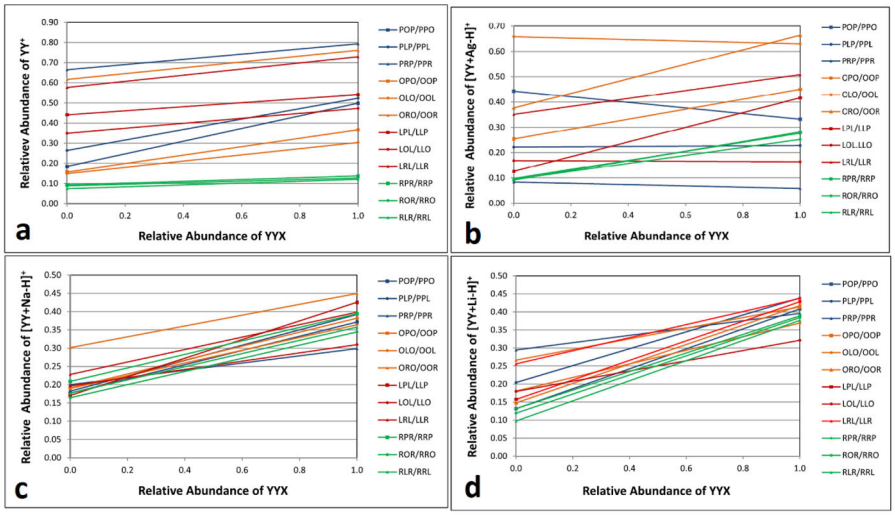

Figure 8 Calibration plots of relative abundances of DG-like fragment ions for twelve TG regioisomer pairs using ammonium ion **(a)**, silver ion **(b)**, sodium ion **(c)** or lithium ion **(d)** as the complexing reagent. Reprinted with permission from (Makarov et al., 2018), copyright 2018 John Wiley and Sons.

However, according to some previous literature, fragments of $[M+Na]^+$ adducts provided limited structural information (Segall et al., 2005). This might have been caused by differences in instrumentation or collision gas used, suggesting that testing different ion complexing agents could be worth trying

when developing a TG regioisomer analysis method for a specific laboratory system. While $[M+Li]^+$ adducts also produce consistent calibration plots, the lithium salts used in the mobile phase are known to sometimes cause precipitation of lithium salt crystals in the instrumentation (Kallio et al., 2017). Methods studying the mechanisms of TG fragmentation patterns with reference standards are listed in **Table 5**.

Table 5 Analysis methods for studying the mechanisms of TG fragmentation patterns with reference standards

Reference	LC separation / direct inlet type	MS instrument	Instrument configuration	TG adducts
(Velasco et al., 2022)	Reversed phase C18 (SFC)	Waters Synapt G2 HDMS	ESI(+)-CID-MS^2	$[M+NH_4]^+$
(Gazlay & Evans, 2022)	Direct infusion	Thermo Fisher LCQ Advantage Ion Trap	ESI(+)-CID-MS^2	$[M+NH_4]^+$, $[M+Li]^+$, $[M+Na]^+$
(Grossert et al., 2020)	Direct infusion	Waters VG Quattro Triple Quadrupole	ESI(+)-CID-MS^3	$[M+Li]^+$
(Makarov et al., 2018)	Direct infusion	Thermo Fisher LCQ Advantage Ion Trap	ESI(+)-CID-MS^2	$[M+NH_4]^+$, $[M+Li]^+$, $[M+Na]^+$, $[M+Ag]^+$
(Judge et al., 2017)	Direct infusion	Thermo Finnigan LCQ Advantage Ion Trap	ESI(+)-CID-MS^2	$[M+NH_4]^+$
(Grossert et al., 2014)	Direct infusion or flow injection	Various	ESI(+)-CID-MS^2	$[M+NH_4]^+$, $[M+Li]^+$, $[M+Na]^+$, $[M+Ag]^+$, $[M+K]^+$
(Ramaley et al., 2013)	Direct infusion	AB SCIEX 2000 QTRAP Quadrupole Linear Ion Trap	ESI(+)-CID-MS^3	$[M+Li]^+$, $[M+NH_4]^+$
(Renaud et al., 2013)	Direct infusion	Water Synapt G1	ESI(+)-CID-MS^2	$[M+NH_4]^+$
(Gakwaya et al., 2007)	Reversed phase C18	Thermo Fisher LCQ Advantage Ion Trap	ESI(+)-CID-MS^2	$[M+NH_4]^+$
(X. Li et al., 2006)	Reversed phase C18	Thermo Fisher LCQ Advantage Ion Trap	ESI(+)-CID-MS^2	$[M+NH_4]^+$
(X. Li & Evans, 2005)	Reversed phase C18	Thermo Fisher LCQ Advantage Ion Trap	ESI(+)-CID-MS^2	$[M+NH_4]^+$

2.2.1.2 Analysis of TG regioisomers using CID

Composition of human milk TGs, including tentative identifications of numerous regioisomers, has been analyzed using a non-targeted lipidomics method (George et al., 2020). While the study was able to reveal detailed TG composition and many molecular species not previously reported in human milk, the TG regioisomer identifications were simply based on identifying the least abundant DG fragment, as that is most likely the one that has lost its *sn*-2 FA. As the ratios of DG fragments represent mixtures of TGs instead of a single isomer, the identifications were only given for the highest abundance regioisomer, and no attempt was made at determining the regioisomer ratios (George et al., 2020). Similarly, in certain studies, sometimes only one regioisomer is identified based on the relative abundances of the fragment ions, and the fact that natural TGs are commonly mixtures of regioisomers is omitted (Nguyen et al., 2018; Tu et al., 2017).

While CID strongly favors dissociation of FAs from *sn*-1/3 positions, only examining the least abundant DG fragment, which presumably has lost sn-2 FA, will at best provide information on the most abundant TG regioisomer, but should not be used as the basis for excluding the presence of other isomers as seen in some previously published literature. Establishing calibration curves with regiopure reference standards for the TG regioisomers of interest is common using the fractional abundances of the DG fragment ions (Leskinen, Suomela, Yang, et al., 2010; Liu & Rochfort, 2021; Malone & Evans, 2004). Calibration curves for ABC type TGs (**Figure 9**) were reported for the first time in addition to numerous AAB/ABA type TGs (Tarvainen et al., 2019). The effects of chromatographically overlapping isobaric fragments should be considered, as the abundance ratios of structurally informative fragments can be distorted by fragments of other coeluting TGs. Either acceptable chromatographic resolution between the isobaric TG molecular species (Liu & Rochfort, 2021) must be achieved, or an alternative method, such as algorithmic interpretation of the spectra (Kurvinen et al., 2001; Sazzad et al., 2022), should be employed to mitigate the interference of the overlapping fragments is needed. In reality, algorithmic interpretation is necessary for non-targeted isomeric analysis of natural lipids, since complete separation of isobaric TG molecular species is practically not yet achievable with current methodologies. Recently, our laboratory developed an algorithmic optimization tool called *TAG Analyzer*, which utilizes a fragmentation model derived from an extensive set of standard curves. This innovative tool has demonstrated its effectiveness in determining the detailed regioisomer profile of highly complex natural fats and oils, including human milk (Sazzad et al., 2022).

Regioisomers of TGs containing vaccenic acid (FA 18:1(11Z)) and oleic acid (FA 18:1(9Z)) have been analyzed (ESI(+)-CID-MS^2, $[M+NH_4]^+$) in sea

buckthorn (*Hippophaë rhamnoides* L.), and the calibration curves for regioisomers of molecular species TG 16:1(9Z)_16:1(9Z)_FA 18:1(11Z) and TG 16:1(9Z)_16:1(9Z)_FA 18:1(9Z) were similar (Leskinen, Suomela, Yang, et al., 2010). However, minor differences were observed due to preferential loss of FA 18:1(9Z) acid compared to FA 18:1(11Z). As the MS technique used in this study was not able to distinguish the FA isomers with different double bond locations from overlapping peaks, chromatographic resolution of the two molecular species was vital (Leskinen, Suomela, Yang, et al., 2010).

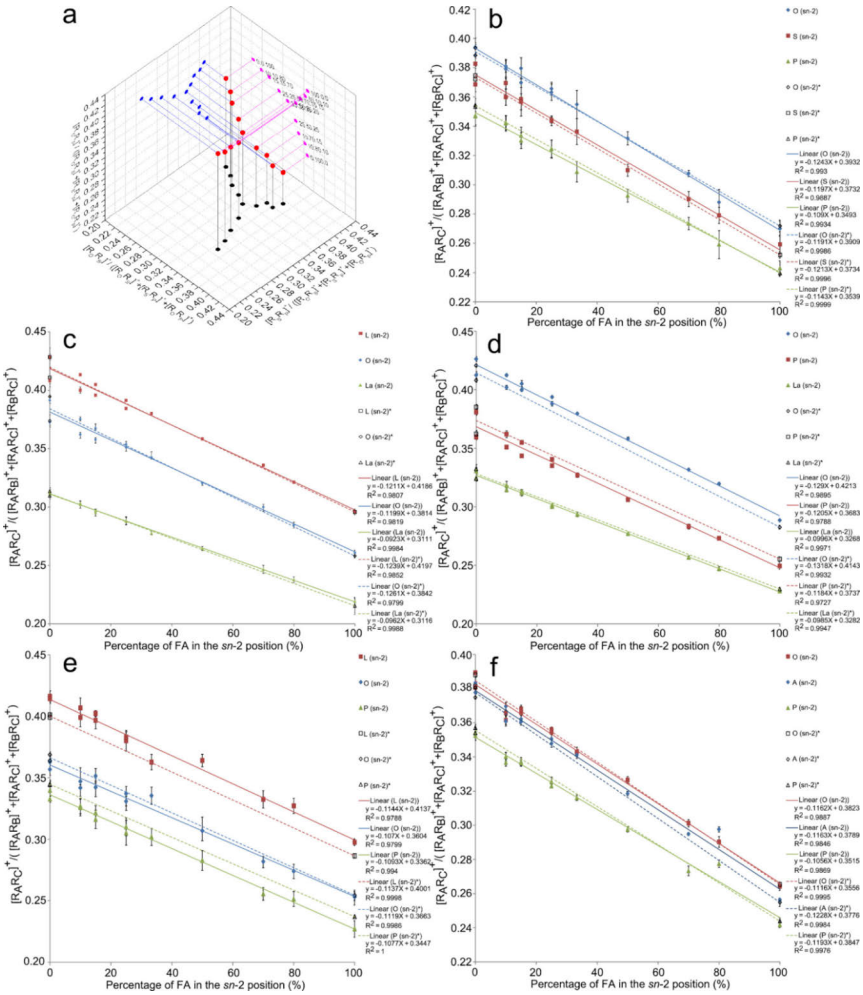

Figure 9 Three dimensional scatter plot of the product ion ratios of OSP/SOP/OPS TG mixtures at 13 different molar ratios (ratios are shown on the projection) **(a)**, and negative linear correlations of product ion ratios and the amount of FA in the *sn*-2 position in OSP/SOP/OPS **(b)**, LOLa/OLLa/LLaO **(c)**, OPLa/POLa/OLaP **(d)**, LOP/OLP/OPL **(e)**, and OAP/AOP/OPA **(f)**. Data series

marked with asterisk (*) are constructed of 100% *sn*-2 regioisomers. Reprinted with permission from (Tarvainen et al., 2019), copyright 2019 American Chemical Society.

In their work of analyzing a wide range of TG regioisomer standards, the composition of olive oil was analyzed (ESI(+)-CID-MS^2, $[M+NH_4]^+$) using the established calibration curves (Tarvainen et al., 2019). Olive oil being a relatively simple mixture of TGs, there were only few chromatographically overlapping isobaric TG molecular species with interfering fragment ions, most notably TG 18:1_18:1_18:3 and TG 18:1_18:2_18:2. The solution was to select the spectra from the leading edge of the partially resolved first peak and the tailing edge of the second peak to avoid isobaric interference of the fragment ion abundance ratios. This is not ideal solution, and the edge does not represent the entire peak, as there is usually at least some chromatographic separation of the TG regioisomers in addition to the molecular species. Regioisomers of molecular species TG 16:0_18:0_18:1, TG 18:0_18:0_18:1 and TG 18:0_18:1_18:1 were analyzed (ESI(+)-CID-MS^2, $[M+NH_4]^+$) from various sources, including vegetable oils and meat. Calibration curves were established with reference standards, and the authors also noted that analysis of 18:0_18:0_18:1 was not possible from the selected vegetable oils due to interfering DG fragments from other TG molecular species with the same molecular weight (Malone & Evans, 2004).

A reversed phase C30 column (Acclaim C30 (250 × 3 mm, 3 μm)) has been used to mitigate the effects of overlapping isobaric molecular species to analyze (HESI(+)-CID-MS^2, $[M+NH_4]^+$) specific TG regioisomers in bovine milk (Liu & Rochfort, 2021). In addition to separating TG 18:0_18:1_18:1 and 18:0_18:0_18:2, also double bond isomers of TG 18:0_18:1_18:1 were identified. While the major molecular species were separated, also other minor interfering TGs were observed. However, their contribution to the abundances were deemed minimal, and calibration curves could be used for quantifying the regioisomers of the major molecular species (Liu & Rochfort, 2021).

Sequential fragmentation with an ion trap instrument (ESI(+)-CID-MS^3, $[M+Li]^+$) has been applied for analysis of TG regioisomers in olive oil utilizing lithiated adducts. The DG-like fragment ions $[M+Li–RCOOH]^+$ from the first CID step were further fragmented, and calibration curves were established using the resulting α,β-unsaturated FA fragments. The calibration curves were not linear, and it was suspected that this was mainly caused by the sequential two fragmentation steps instead of just one (Lin & Arcinas, 2008). Non-linear calibration plots were also observed in another study using two-step fragmentation of lithiated TG adducts (ESI(+)-CID-MS^3, $[M+Li]^+$) (Ramaley et al., 2013), suggesting that the non-linearity of the TG calibration curves could

be intrinsic, only being accentuated by the MS^3 fragmentation. Most MS^2 calibration plots in the literature are using linear fitting, but this might not be ideal as the non-linearity, especially when using MS^3, could be affected by acyl chain lengths and numbers of double bonds in the attached FAs (Ramaley et al., 2013). For example, when analyzing TG regioisomers in fish oils (ESI(+)-CID-MS^3, $[M+Li]^+$), the calibration plot for TG 16:0_16:0_22:6 and TG 16:0_16:0_20:5 were non-linear (Cubero Herrera et al., 2013), suggesting that linearity or non-linearity should be experimentally verified by assessing different fittings to the calibration data. Later, the applicability of MS^3 without chromatographic separation for analysis (ESI(+)-CID-MS^3, $[M+Li]^+$) of complex TG mixtures such as fish oil was investigated (Ramaley et al., 2015). In MS^3, the peaks arising from the loss of a lactone were used for the calculations. As there is no chromatographic separation, the influence of ^{13}C isotopes needed to be considered. For example, the M+2 isotope of TG 16:1_18:0_18:1 has the same m/z as TG 16:0_18:0_18:1, as the difference of one double bond in the molecular species results in the difference of 2 Da. Using MS^3 removed the interference of isomeric TGs with one FA in common with the target analyte. In cases where the interfering isotopes had two FAs in common with the target analyte, corrections of the isotope clusters were more complicated, though possible (Ramaley et al., 2015).

Major TG regioisomers in *Mycobacterium smegmatis* biofilm were assessed (ESI(+)-CID-MS^3, $[M+Li]^+$) by the notion that the fragment ions arising from the loss of *sn*-2 FA are less abundant than those of arising from loss of sn-1/3 FAs. No attempt was made at determining the regioisomer ratios, and only the most abundant were reported (Purdy et al., 2013). Trihydroxy-FA containing TG regioisomers in castor oil have been characterized (ESI(+)-CID-MS^3, $[M+Li]^+$). Despite the additional hydroxyl groups attached to the acyl chains of the FAs, the regioisomer ratios could be determined in a similar manner as with TGs containing only regular FAs (Lin & Chen, 2010). A kinetic method utilizing lithium as a transition metal ion to form complex ions involving both an analyte TG and a reference TG has been used to analyze (ESI(+)-CID-MS^3, $[M+Li+M_{ref}]^+$) soya oil. The method utilizes competitive dissociation between the reference and the analyte TG. The ratio of the competitive fragmentation efficiencies, defined by the product ion branching ratio was related to the regioisomer composition of the investigated TGs. Linear correlation was discovered between composition of the mixture of each TG regioisomer and the logarithm of the branching ratio for competitive dissociation (Leveque et al., 2012).

While ESI is currently the dominant ionization technique for analysis of TG regioisomers, also APCI has seen some use together with CID for analysis of TG regioisomers. Selected regioisomers in human milk were analyzed on negative

polarity with ammonia as the nebulizer gas to form deprotonated molecular ions (APCI(–)-CID-MS^2, $[M–H]^–$). Calculations of regioisomer ratios were based on the relative abundances of $[M–H–100–FA]^–$ fragment ions (Linderborg et al., 2014). The method was first adapted from an old direct inlet negative ion chemical ionization method (CI(–)-CID-MS^2, $[M–H]^–$) (Kallio & Currie, 1993) to an LC-MS system (APCI(–)-CID-MS^2, $[M–H]^–$) (Leskinen, Suomela, & Kallio, 2010). TGs containing polyunsaturated FAs in tuna oil and algae oil have been analyzed (APCI(+)-CID-MS^2, $[M+H]^+$) and the major TG regioisomer within each co-eluting molecular species was reported (Baiocchi et al., 2015). MS methodologies used for TG regioisomer analysis are listed in **Table 6**.

Table 6 Mass spectrometric methodologies used for TG regioisomer analysis

Reference	LC separation / direct inlet type	MS instrument	Instrument configuration	TG adducts	Sample material
(Zhang et al., 2022)	Reversed phase C18	Waters MALDI Synapt Q-TOF	ESI(+)-CID-MS^2	$[M+NH_4]^+$	Human milk, mammal milks, fish oil
(Liu & Rochfort, 2021)	Reversed phase C30	Thermo Fisher Scientific LTQ Orbitrap	HESI(+)-CID-MS^2	$[M+NH_4]^+$	Bovine milk
(Abreu et al., 2021)	Normal phase	Thermo Fisher Scientific LTQ Orbitrap Velos Pro	APPI(+)-MS	$[M+H]^+$	Vegetable fats and oils
(Fabritius et al., 2020)	Direct exposure probe	Thermo Fisher Scientific TSQ 8000 EVO Triple Quadrupole	CI(–)-CID-MS^2	$[M–H]^-$	Infant formulas, human milk
(George et al., 2020)	Reversed phase C18	Waters Synapt G2-S IM-Q-TOF	ESI(+)-CID-MS^2	$[M+NH_4]^+$	Human milk
(Tarvainen et al., 2019)	Reversed phase C18	Waters Quattro Premier Triple Quadrupole	ESI(+)-CID-MS^2	$[M+NH_4]^+$	Olive oil
(Nguyen et al., 2018)	Reversed phase C18	Agilent 6530 QTOF	ESI(+)-CID-MS^2	$[M+NH_4]^+$	Milk thistle
(Baba et al., 2018)	Direct infusion	Custom SCIEX Q-TOF	ESI(+)-EIEIO-MS^2	$[M+Na]^+$	Animal tissue
(Kallio et al., 2017)	Reversed phase C18	Waters Quattro Premier Triple Quadrupole	ESI(+)-CID-MS^2	$[M+Li]^+$	Human milk

Reference	LC separation / direct inlet type	MS instrument	Instrument configuration	TG adducts	Sample material
(Marshall et al., 2016)	Reversed phase C18	Thermo Fisher Scientific LTQ XL Linear Ion Trap	HESI(+)-OzID-CID-MS^3	$[M+Na]^+$	*Drosophila* flies
(Baba et al., 2016)	Direct infusion	Custom SCIEX QTOF	ESI(+)-EIEIO-MS^2	$[M+Na]^+$	Vegetable oils
(Baiocchi et al., 2015)	Reversed phase C18	Thermo Fisher Scientific LTQ Orbitrap	APCI(+)-CID-MS^2	$[M+H]^+$	Tuna, algae oil
(Ramaley et al., 2015)	Direct infusion	AB SCIEX 2000 QTRAP Quadrupole Linear Ion Trap	ESI(+)-CID-MS^3	$[M+Li]^+$	Fish oil
(Linderborg et al., 2014)	Reversed phase C18	Waters Quattro Premier Triple Quadrupole	APCI(–)-CID-MS^2; ESI(+)-CID-MS^2	$[M–H]^–$; $[M+NH_4]^+$	Human milk
(Cubero Herrera et al., 2013)	Reversed phase C18	AB SCIEX 2000 QTRAP Quadrupole Linear Ion Trap	ESI(+)-CID-MS^3	$[M+Li]^+$	Fish oil
(Purdy et al., 2013)	Reversed phase C8	Thermo Fisher Scientific LTQ Orbitrap Velos	ESI(+)-CID-MS^3	$[M+Li]^+$	*Mycobacterium smegmatis*
(Leveque et al., 2012)	Reversed phase C18	Thermo Fisher LCQ Quadrupole Ion Trap	ESI(+)-CID-MS^2	$[M+Li]^+$	Soya oil
(Řezanka et al., 2011)	Reversed phase C18/C8	Thermo Finnigan MAT Quadrupole	APCI(+)-MS	$[M+H]^+$	Algae
(Lin & Chen, 2010)	Reversed phase C18	Thermo Finnigan LCQ Advantage Ion Trap	ESI(+)-CID-MS^3	$[M+Li]^+$	Castor oil

Reference	LC separation / direct inlet type	MS instrument	Instrument configuration	TG adducts	Sample material
(Leskinen, Suomela, & Kallio, 2010)	Reversed phase C18	Micromass Quattro Premier Triple Quadrupole	APCI(–)-CID-MS^2	$[M–H]^-$	Vegetable oils
(Herrera et al., 2010)	Reversed phase C18	Waters Premier Q-TOF	ESI(+)-CID-MS^2	$[M+NH_4]^+$, $[M+Li]^+$, $[M+Na]^+$, $[M+Ag]^+$	TG standards, vegetable oils
(Leskinen et al., 2010)	Reversed phase C18	Micromass Quattro Premier Triple Quadrupole	ESI(+)-CID-MS^2	$[M+NH_4]^+$	Sea buckthorn
(Lévêque et al., 2010)	Reversed phase C18	Thermo Finnigan LCQ quadrupole ion trap	ESI(+)-CID-MS^5	$[M+Ag+AgNO_3]^+$	Soya oil
(Lin & Arcinas, 2008)	Preparative reversed phase C18, Direct infusion of collected fractions	Thermo Finnigan LCQ Advantage Ion Trap	ESI(+)-CID-MS^3	$[M+Li]^+$	Olive oil
(Malone & Evans, 2004)	Reversed phase C18	Thermo Finnigan LCQ Advantage Ion Trap	ESI(+)-CID-MS^2	$[M+NH_4]^+$	Vegetable oils, animal fats
(Fauconnot et al., 2004)	Reversed phase C18	Waters Premier Triple Quadrupole	APCI(+)-MS	$[M+H]^+$	Vegetable oils, animal fats

2.2.2 In-source fragmentation

Some ionization techniques such as APCI produce abundant in-source fragmentation of TG molecular ions. This feature can be utilized for structural analysis of TGs without a dedicated fragmentation step. However, due to the lack of precursor-fragment ion relationship offered by tandem mass spectrometry, in-source fragmentation is only suitable for simple TG mixtures or using chromatographic separation of the molecular species with overlapping DG fragments. A comparison of different mass spectrometers (APCI(+)-MS, $[M+H]^+$) for investigating TG fragmentation behavior with APCI was performed with a total of 84 synthesized TG standards. The main conclusion was that while there were minor differences between the instruments, the number of double bonds and their position in the acyl chain had significantly larger influence on the DG fragment ion ratios (Holčapek et al., 2010) The results were grouped according to the degree of saturation (saturated, monounsaturated, diunsaturated and triunsaturated) of the individual FAs on the TGs, and good correlation was observed in the fragment ion ratios within the groups. The authors suggest that the data of TGs with specific unsaturation patterns could be generalized for other TGs with similar unsaturation pattern (Holčapek et al., 2010).

FA 20:4 and FA 20:5 containing TG regioisomer ratios, consisting of molecular species TG 16:0_16:0_20:4, TG 16:0_16:0_20:5, TG 16:0_20:4_20:4 and TG 16:0_20:5_20:5, in *Trachydiscus minutus* algal oil were estimated (APCI(+)-MS, $[M+H]^+$) after acceptable chromatographic separation (Řezanka et al., 2011). Some molecular species were only partially separated, but the resolution was good enough to evaluate the regioisomers based on the DG fragment abundances. No calibration curves were used, and the estimations relied on previous observations (Holčapek et al., 2010) of fragmentation behavior of various TG standards. A significant difference in DG fragment ion ratios with in-source fragmentation (APCI(+)-MS, $[M+H]^+$) and CID (APCI(+)-CID-MS^2, $[M+H]^+$) has been observed for TGs containing one shorter and less unsaturated FA together with two long chain polyunsaturated FAs (Baiocchi et al., 2015). However, the fragment abundance ratios were consistent for TGs containing FAs with similar chain lengths and numbers of double bonds, emphasizing the need for reference standards for TGs of interest when determining the regioisomer ratios, as the *sn*-2 FA cleavage might not always result in DG fragment of the lowest abundance (Baiocchi et al., 2015). Selected TG regioisomers from cocoa butter, palm oil and certain animal fats have been analyzed (APCI(+)-MS, $[M+H]^+$), but several regioisomer ratios, especially in the animal fats, could not be evaluated due to lack of reference standards or chromatographically overlapping TGs with common structurally informative fragment ions (Fauconnot et al., 2004). In addition to APCI, in-source fragmentation with atmospheric pressure photoionization (APPI) has been

utilized for structural analysis of TGs. While the study was focusing on the TG molecular species composition, determining regioisomer ratios would follow similar principles as with APCI in-source fragmentation, and the fragment ions resulting from loss of *sn*-2 FA were less abundant than those from loss of *sn*-1/3 FA (Abreu et al., 2021).

2.2.3 Electron impact excitation of ions from organics

Electron impact excitation of ions from organics (EIEIO) is a relatively unused technique for structural analysis of TGs, but in recent years it has shown potential for very in-depth characterization of TG isomers. Unlike CID, which cleaves off the acyl chains, EIEIO breaks the glycerol backbone (Baba et al., 2016), resulting in unique structurally informative fragment ions after loss of two FAs. Cleavage of the glycerol backbone produces two doublet ions (*sn*-1 and *sn*-3), both spaced 2 Da apart, and one singlet ion (*sn*-2) as indicated in **Figure 10a-c**. Especially useful for identifying TG regioisomers is the formation of *sn*-2 singlets, which are unique to the FAs attached to *sn*-2 position. The remaining *sn*-1/3 FAs can be identified from the two doublet ions, but their *sn*-positions are indistinguishable. Even though CID heavily favors cleavage of FAs from sn-1/3 positions, it always produces some fragments resulting from *sn*-2 FA cleavage, which also is influenced by the nature of the FA. However, the uniqueness of the *sn*-2 singlet from EIEIO fragmentation implies that calibration standards for determining TG regioisomer ratios are of less importance. An example of quantifying regioisomer ratios is shown in **Figure 10d**, consisting of two *sn*-2 singlets, identified as FA 18:1 and FA 18:2. Additionally, two *sn*-1/3 doublets are observed, identified as FA 18:1 and FA 18:2. Based on this information, the regioisomers are identified as TG 18:2_18:1 *sn*-2_18:1 and TG 18:1_18:2 *sn*-2_18:1, and the regioisomer ratios calculated with the fragment abundances are 58 and 42 %, respectively (Baba et al., 2016). The method (ESI(+)-EIEIO-MS^2, $[M+Na]^+$) was later expanded and used for profiling TG regioisomers in addition to several other lipid classes in porcine brain (Baba et al., 2018). The acquisition time for each EIEIO spectrum was 1 min. Direct infusion in conjunction with DMS ion mobility separation was utilized. As multiple lipid classes might contain several isobaric species, the DMS separation was used for selecting the class-specific molecular species. Conventional chromatographic separation would not be viable with such spectra acquisition times (Baba et al., 2018).

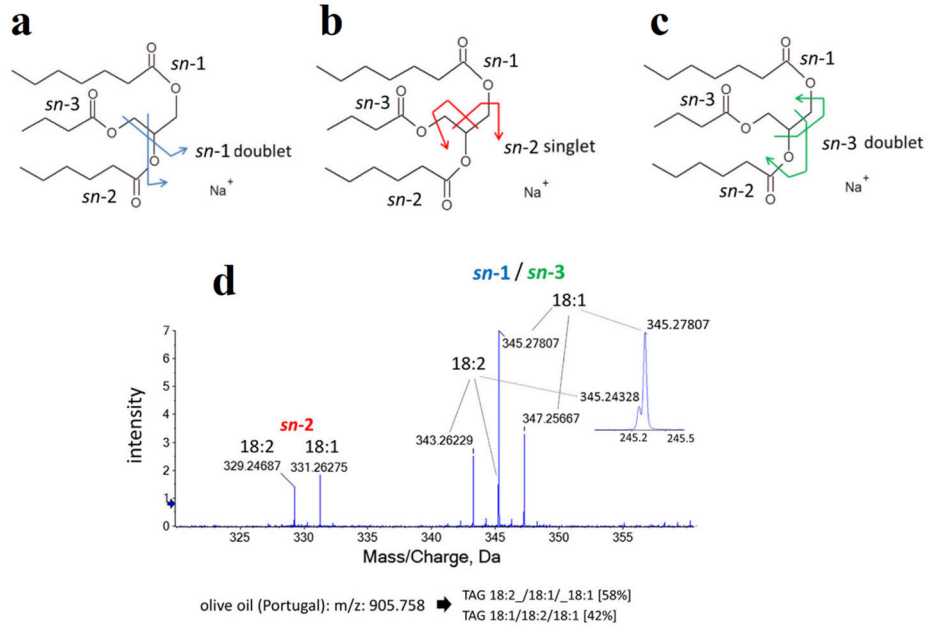

Figure 10 EIEIO cleavage sites of the diagnostic peaks shown in *sn*-1 doublet (blue) **(a)**, *sn*-2 singlet (red) **(b)** and *sn*-3 doublet (green) **(c)**. EIEIO spectrum of *m/z* 905 precursor ions in olive oil showing an example of deconvolution of TG regioisomers **(d)**. Reprinted with permission from (Baba et al., 2016), copyright 2016 American Society for Biochemistry and Molecular Biology.

2.2.4 Ozone-induced dissociation

Sequential fragmentation with CID followed by ozone-induced dissociation (OzID) has been used for analysis (HESI(+)-OzID-CID-MS^3, $[M+Na]^+$) of TG regioisomers in *Drosophila* flies (Marshall et al., 2016). The used linear ion trap instrument had been modified to seed ozone into the helium buffer gas of the ion trap. After CID of the sodiated $[M+Na]^+$ adducts, the resulting DG fragments of interest are trapped in the presence of ozone in the ion trap section, resulting in further fragmentation with higher regioselectivity. While the resulting fragment ion ratios are still influenced by the FAs, the method offers an interesting alternate approach for TG regioisomer analysis (Marshall et al., 2016).

2.2.5 Algorithmic interpretation of MS^n fragment data

As the fragmentation data of TG regioisomers in natural samples can be complex, and the manual interpretation time consuming and often extremely challenging, several tools have been developed to address this problem. One of the main challenges in the analysis of TG regioisomers in natural samples is the

overlapping structurally informative fragment ions from multiple isobaric TG species. Using calibration curves alone might not be enough, as the fragment ion ratios are distorted by interfering fragments from other TGs.

One of the first tools developed to tackle this issue was *MSPECTRA* (Kurvinen et al., 2001), which utilizes data obtained with a direct inlet shotgun method (CI(–)-CID-MS^2, $[M–H]^–$). The software first establishes the TG molecular species composition with the observed FA fragment ion $[RCOO]^–$ ratios. These fragments are not regiospecific, but instead they represent the total FA distribution over the fragmented TG species. By performing an optimization algorithm, the software uses the $[RCOO]^–$ ion intensities to find combinations of TGs, which result in the least amount of shortage or leftover $[RCOO]^–$ ions. The TG regioisomer ratios are then calculated with a similar optimization algorithm utilizing the regioselective $[M–H–100–RCOOH]^–$ fragments. One of the limitations of the software is that it effectively uses only one calibration curve for every TG (Kurvinen et al., 2001). The effect of using only one calibration curve was later demonstrated with a wide range of TG regioisomer standards. The calculated results for mixtures of reference standards were mostly accurate, however, there was an undeniable influence on the results caused by an increasing degree of unsaturation in the attached FAs (Fabritius et al., 2020). Considering this, while the accuracy of the calculations could be improved by implementing additional calibration curves, the *MSPECTRA* software is still a very efficient tool for evaluating relative differences in the TG regioisomer composition among different samples (Fabritius et al., 2020; Kalpio et al., 2021; Kurvinen et al., 2002; Linderborg et al., 2014).

A similar calculation software (*TAG analyzer*) has been developed recently (Sazzad et al., 2022). In addition to the optimization algorithm, the software has a built-in fragmentation model established with TG reference standards. The model takes into account differences in the fragmentation efficiencies of different TG species, including the acyl chain length and the number of double bonds in the *sn*-2 FA as was observed (ESI(+)-CID-MS^2, $[M+NH_4]^+$) in an earlier study (Tarvainen et al., 2019). The optimization algorithm looks at the fragment spectra and uses the fragmentation model to create a synthetic spectrum to match the observed one as closely as possible (**Figure 11**). The TG regioisomer abundances used to create the best matching synthetic spectra are then reported. The software can accurately identify the most abundant regioisomers within each isobaric TG species, but the accuracy decreases as the relative abundance of the TG molecular species decreases. When the algorithm optimizes the regioisomer abundances, the changes are accentuated in the low abundance TGs, likely resulting in proportionally larger errors (Sazzad et al., 2022). Similar behavior was observed with the *MSPECTRA* software, where the low abundance TGs within the species produced the highest relative deviations (Fabritius et al., 2020).

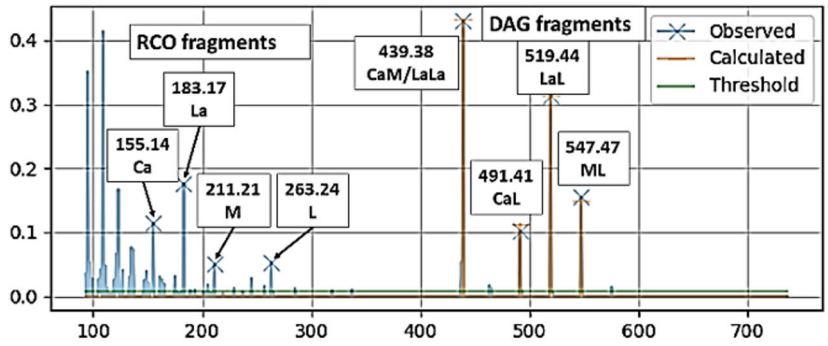

Figure 11 The synthetic DG spectrum of an ACN:DB 42:1 species overlaid on top of the measured fragment ion spectrum. Reprinted with permission from (Sazzad et al., 2022), copyright 2022 Elsevier.

An algorithm for analyzing palmitic acid containing TG regioisomers has been developed by constructing calibration curves with reference standards (ESI(+)-CID-MS^2, $[M+NH_4]^+$), and subsequently extrapolating fragmentation efficiencies for other TGs. As observed by other authors, the fragmentation was influenced by the double bond number and acyl chain length. Accuracy of the calculation model was demonstrated by comparing the results to manual calculations with the calibration curves. The results for ABC type TGs were more in line with the two calculation methods, with a maximum difference of 11 %, whereas with the AAB type TGs the differences were somewhat higher with a maximum of 27 %. As only palmitic acid containing TGs were analyzed, more reference standards are needed to expand the method further for a wider range of TGs (Zhang et al., 2022).

Modeling TG fragmentation patterns has been done using other published studies, including data obtained with various different MS instruments using both ESI-CID-MS^2 and APCI-MS (Balgoma et al., 2019). Fragmentation abundances were instrument and adduct specific. Common trends for fragmentation in each dataset were modeled, and the established model was applied to quantify TG regioisomers using their own instrument (ESI(+)-CID-MS^2, $[M+NH_4]^+$). The results were mostly in agreement with previous studies, including several TGs that were not used in creation of the calculation model. However, the regioisomer ratios of TGs containing two or more highly unsaturated FAs such as FA 20:4, FA 20:5 or FA 22:6 were more difficult to predict (Balgoma et al., 2019). TG regioisomer analysis methods based on algorithmic interpretation of MS^n fragment data are listed in **Table 7**.

Table 7 TG regioisomer analysis methods based on algorithmic interpretation of MS^n fragment data

Reference	LC separation / direct inlet type	MS instrument	Instrument configuration	TG adducts	Algorithmic calculation of TG isomers	Sample material
(Sazzad et al., 2022)	Reversed phase C18	Waters Quattro Premier Triple Quadrupole	ESI(+)-CID-MS^2	$[M+NH_4]^+$	Synthetic recreation of observed fragment ion spectra using a fragmentation model established with regiopure TG standards.	TG standards, olive oil, human milk
(Zhang et al., 2022)	Reversed phase C18	Waters MALDI Synapt Q-TOF	ESI(+)-CID-MS^2	$[M+NH_4]^+$	Extrapolating fragmentation efficiencies of TG molecular species based on the acyl chain lengths and numbers of double bonds.	Human milk, mammal milks, fish oil
(Marchand et al., 2021)	Direct infusion and Reversed phase C18	Sciex QTRAP 5500 and Waters Synapt G2S Q-TOF	ESI(+)-CID-MS^2	$[M+NH_4]^+$	Fragmentation model established with regiopure TG standards and implementing two separate TG analysis platforms for better validation of the results.	Animal blood
(Peng et al., 2021)	Reversed phase C18	Shimadzu 8050 Triple Quadrupole	ESI(+)-CID-MS^2	$[M+NH_4]^+$	Automated generation of MRM list for TG ammonium adducts and its FA neutral loss fragments. Mainly designed for TG molecular species profiling but is also capable of identifying chromatographically separated regioisomers.	Bovine milk, infant formulas
(Balgoma et al., 2019)	Not specified	Waters Synapt G2S Q-TOF	ESI(+)-CID-MS^2	$[M+NH_4]^+$	Fragmentation model established with data from various previously published studies.	Vegetable oils
(Kurvinen et al., 2001)	Direct exposure probe	Finnigan MAT TSQ-700 Triple Quadrupole	CI(–)-CID-MS^2	$[M–H]^–$	Optimization of TG molecular species proportions using FA fragments, followed by optimization of TG regioisomer proportions using DG-like fragments.	Human milk, infant formulas, human chylomicron, cocoa butter

2.3 Separation of PL *sn*-positional isomers

2.3.1 Chromatographic separation

In contrast to TGs, the chromatographic separation of PL *sn*-positional isomers remains largely unexplored, and only a handful of examples exist in the literature. Regioisomers of selected PC molecular species, such as PC 16:0_18:2, PC 16:0_20:4 and PC 16:0_22:6, were separated with Acquity C18 BEH (150 × 1 mm, 1.7 μm) reversed phase column (Nakanishi et al., 2010). The regioisomer standards were analyzed as such, and after oxidation as PC hydroxides. The regioisomers of PC 16:0_20:4 and PC 16:0_22:6 were separated in less than 30 min, allowing quantification of regioisomer ratios. PC 16:0_18:2 regioisomers were not separated in the non-oxidized form. Oxidation enhanced the separation, resulting in adequate resolution of PC 16:0_18:2 regioisomers during a 10 min gradient. The relative peak areas of non-oxidized PC regioisomers were approximately the same as the oxidized compounds, suggesting that the ratio of regioisomers is not influenced by oxidation. Therefore, oxidation could be used as a tool to improve chromatographic resolution of PC regioisomers that would not be properly separated in their conventional forms (Nakanishi et al., 2010). Similarly, PC 16:0_20:4 and PC 16:0_22:6 regioisomers were successfully separated using the same Acquity C18 BEH (150 × 1 mm, 1.7 μm) column, but almost no separation was observed for PC 16:0_18:1 regioisomers (Kozlowski et al., 2015b). The regioisomer with a more highly unsaturated FA in the *sn*-1 position always eluted earlier with the tested PC reference standards. As the degree of unsaturation and the relative differences in the FA acyl chains is reduced, the separation becomes more challenging (Kozlowski et al., 2015b; Nakanishi et al., 2010). Capillary columns packed with C18 BEH particles have been used for lipid separations, including some PC regioisomers. Larger differences in the FA chain lengths, such as molecular species PC 2:0_16:0, resulted in baseline separation of the two isomers, while regioisomers of PC 14:0_18:0 were only partially separated (Sorensen et al., 2020).

The examples of PL enantiomer (phosphate group in *sn*-1 or *sn*-3 position) separation are very limited. It is generally accepted that the phosphate head group in natural PLs is almost exclusively in *sn*-3 position. However, the experimental evidence supporting this assumption is lacking. Partial separation of racemic dipalmitoyl phosphatidylcholine (palmitic acids in *sn*-1/2 or *sn*-2/3 positions and phosphate group in *sn*-1 or *sn*-3 position) was achieved using a Chiralpak ID column (Itabashi, 2012). Later, a baseline separation of various PC enantiomers was achieved using a Chiralpak IE column with amylose tris(3,5-dichlorophenylcarbamate) stationary phase (Kuksis et al., 2016). Analysis methods based on chromatography separation of PL regioisomers or stereoisomers are listed in **Table 8**.

Table 8 Analysis methods based on chromatographic separation of PL regioisomers or stereoisomers

Reference	Column	Mobile phase	Separation category	Separated PL isomers	Sample material
(Sorensen et al., 2020)	Custom capillary columns	A: H_2O/ACN (60:40) with 10 mM ammonium formate and 0.1 % formic acid, B: IPA/ACN/H_2O (85:10:5) with 10 mM ammonium formate and 0.1 % formic acid	Reversed phase C18	PC regioisomers	PC standards
(Takeda et al., 2018)	Acquity UPC^2 Torus DEA (100 × 3 mm, 1.7 µm)	Mobile phase: Supercritical CO_2, Modifier: MeOH/H_2O (95:5) with 0.1 % ammonium acetate	Supercritical fluid chromatography	Lyso-PL regioisomers	Human plasma
(Kozlowski et al., 2015b)	Acquity C18 BEH (150 × 1 mm, 1.7 µm)	A: H_2O with 70 µM sodium acetate, B: ACN/IPA (66:34) with 70 µM sodium acetate	Reversed phase C18	PC regioisomers	PC standards
(Itabashi, 2012)	Chiralpak ID (unknown dimensions)	ACN/MeOH/Diethylamine (85:15:0.1)	Chiral phase	PC stereoisomers	Unknown
(Nakanishi et al., 2010)	Acquity C18 BEH (150 × 1 mm, 1.7 µm)	A: ACN/H_2O (90:10) with 15 mM ammonium formate, B: ACN/MeOH/IPA/H_2O (47.5:45:2.5:5) with 15 mM ammonium formate	Reversed phase C18	PC regioisomers, oxidized PC regioisomers	Mouse brain, liver and heart
(Itabashi & Kuksis, 1997)	YMC A-K03 (250 × 4.6 mm, 5 µm) and YMC A-L03 (250 × 4.6 mm, 5 µm)	Hexane/CH_2Cl_2/MeOH/Trifluoroacetic acid (60:20:20:0.2), isocratic	Chiral phase	PG stereoisomers	PG standards

2.3.2 Ion mobility

While ion mobility has seen some use for separation of PL regioisomers, most existing applications are only demonstrating the potential with specific compounds, and adaptation to a wider range of regioisomers and PL classes remains a challenge. Utilizing DMS, the effects of adduct type, chemical modifier and cell temperature were investigated to enhance the separation of molecular species PC 16:0_18:1 regioisomers (Ieritano et al., 2019). Five different adduct types $[M+X]^+$ (X = H, Ag, Li, Na, or K) were tested. PLs readily form protonated $[M+H]^+$ adducts in positive ESI mode, making them an obvious choice for further investigations. However, no regioisomer separation of $[M+H]^+$ adducts was observed after seeding the DMS cell with different chemical modifiers such as isopropanol, dichloromethane, acetonitrile or acetone. $[M+Li]^+$ adducts were partially separated, but required high gas pressures, resulting in significant loss of signal intensity. Best separation was achieved with $[M+Ag]^+$ adducts and low DMS cell temperature without a chemical modifier in addition to the methanol used as a sample solvent (Ieritano et al., 2019). In another study, $[M+Ag]^+$ adducts of PC 16:0_18:1 and 16:0_18:2 regioisomers were also successfully separated using DMS, but regioisomeric separation of the saturated molecular species PC 16:0_18:0 was not achieved (Maccarone et al., 2014). Like silver-ion chromatography, the amount of double bonds in the attached acyl chains seems to play a critical role in the ion mobility separation of $[M+Ag]^+$ adducts (Ieritano et al., 2019; Maccarone et al., 2014).

In a broader study for separation of various PL isomer types with drift tube ion mobility spectrometry (DTIMS), separation of saturated PC regioisomers was also attempted. The utilized adduct ion type was not specified, but only minor differences were observed in the drift times of PC 16:0_18:0 regioisomers, resulting in mostly overlapping peaks and inadequate separation (Kyle et al., 2016). Various adduct types have also been tested with DTIMS, including [M+X]+ (X = H, Ag, Na, or K) (Groessl et al., 2015). The [M+Ag]+ adducts of PC 16:0_18:1 were again the most easily separable ones with highest differences in the CCS values of the two regioisomers. The method was used to quantify PC 16:0_18:1 regioisomer ratios in porcine brain and yeast extract, while no other regioisomer pairs were investigated (Groessl et al., 2015). Partial separation of protonated [M+H]+ adducts of PC 16:0_18:1 regioisomers has been achieved using trapped ion mobility spectrometry (TIMS), allowing quantification of regioisomer ratios in human plasma (Fouque et al., 2019). Analysis methods based on ion mobility separation of PL regioisomers are listed in **Table 9**.

Table 9 Analysis methods based on ion mobility separation of PL regioisomers

Reference	Instrument	Ionization mode	Ion mobility category	Separated PL isomers	Sample material
(Fouque et al., 2019)	Bruker timsTOF	ESI(+)	Trapped ion mobility spectrometry	PC regioisomers	Human plasma
(Ieritano et al., 2019)	SCIEX SelexION DMS and SCIEX 5500 QTRAP	ESI(+)	Differential mobility spectrometry	PC regioisomers	PC standards
(Kyle et al., 2016)	Agilent 6560 IMS	ESI(+)	Drift tube ion mobility spectrometry	PC regioisomers	Human and mouse tissues
(Groessl et al., 2015)	Tofwerk IMS-TOF	ESI(+)	Drift tube ion mobility spectrometry	PC regioisomers	Porcine brain
(Maccarone et al., 2014)	SCIEX SelexION DMS and SCIEX 5500 QTRAP	ESI(+)	Differential mobility spectrometry	PC regioisomers	PC standards

2.4 Identification of PL regioisomers by MS methodologies

There are multiple examples of PL regioisomers analyzed with MS methodologies, but most of them are limited in scope, only focusing on a handful of individual regioisomers. The targeted compounds often consist of PCs only, while other PL classes are mostly neglected. ESI is the most commonly used ionization technique, but also direct surface imaging techniques such as desorption electrospray ionization (DESI) and especially matrix-assisted laser desorption/ionization (MALDI) are used. Similar to TG regioisomers, when employing MS methodologies the PL regioisomers are typically determined by the fragment ion ratios, which are influenced by the nature of the attached FAs.

2.4.1 Collision-induced dissociation

A single stage fragmentation with CID alone when using positive ionization ESI is often not enough for analysis of PL regioisomers, as the structurally informative fragment ions in most cases are of low abundance (F.-F. Hsu & Turk, 2009).

On negative polarity, sequential CID of chlorinated PC adducts (ESI(–)-CID-MS^3) has been observed to produce high abundance deprotonated FA $[RCOO]^-$ and lysophospholipid-like fragments that can be used for structural assignment of the FA chains (Ekroos et al., 2003a). **Figure 12A** shows the lack of structurally informative fragments after the first CID step, but the sequential fragmentation of the demethylated $[M–15]^-$ ions (**Figure 12B-C**) produces fragments that have reversed abundance ratios for PC 16:0/18:1 and PC 18:1/16:0 regioisomers, allowing identification of regioisomers. Similar methodologies utilizing ammonium adducts have been used to examine PC regioisomers in human plasma (Zacek et al., 2016) and for investigation of the impact of high-fat diets on PC regioisomer composition in mice (Sundaram et al., 2018). Using ammonium formate as the mobile phase modifier, PCs are ionized as formate adducts $[M+HCOO]^-$ that can produce the same structurally informative $[RCOO]^-$ and lysophospholipid-like fragments after a single stage CID fragmentation as was demonstrated by the comprehensive work earlier (F.-F. Hsu & Turk, 2009).

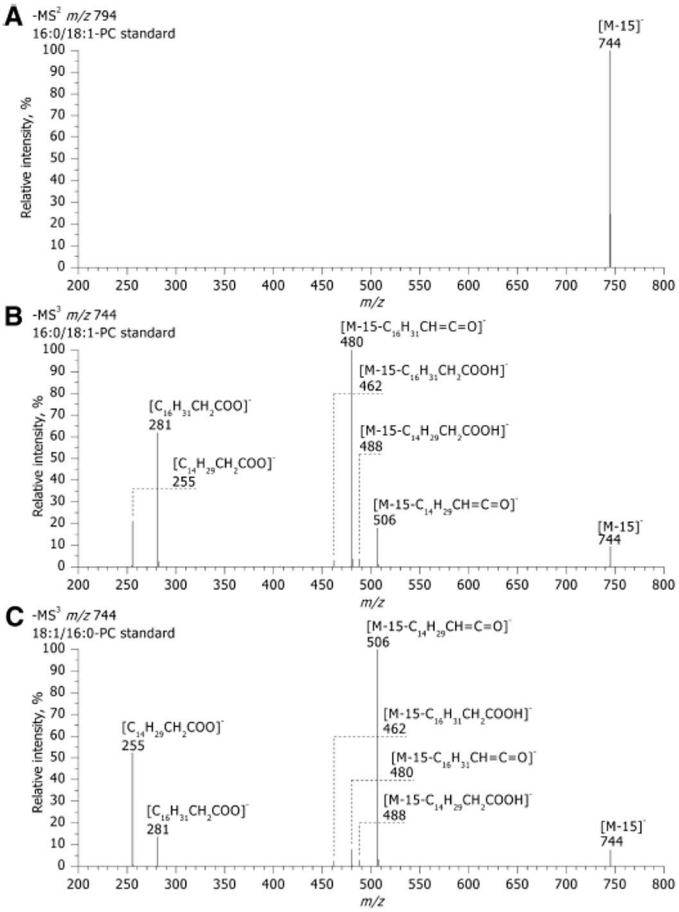

Figure 12 MS^2 spectrum of a chloride adduct of a PC 16:0/18:1 standard (A) and subsequent MS^3 spectra of demethylated $[M–15]^–$ ions of PC 16:0/18:1 (B) and PC 18:1/16:0 (C). Reprinted with permission from (Ekroos et al., 2003b), copyright 2003 Elsevier.

Several PC calibration curves, one PE and one PS calibration curve were established with reference standards in a recent study, allowing quantification of regioisomer ratios in standard mixtures (**Figure 13**) (Fabritius & Yang, 2021). The fragmentation of different PCs was influenced by the acyl chain lengths and the numbers of double bonds. Direct infusion of individual regioisomer standards yielded accurate results, but some challenges were encountered during a hydrophilic interaction liquid chromatography (HILIC) analysis of a mixture containing all studied reference compounds. As the HILIC method separated PLs primarily by class, many molecular species within the class are chromatographically overlapping. Due to inadequate precursor ion isolation capabilities of the instrument, regioisomers of molecular species such as PC

16:0_18:2 and PC 16:0_18:3 which only differ in one double bond, were difficult to analyze because interference by fragments from one another, distorting the fragment ion ratios (Fabritius & Yang, 2021). This issue could have been bypassed with better separation of the molecular species, for example using RP chromatography. For PC and PE classes, the fragments produced by cleavage of *sn*-2 FA from $[M+HCOO]^-$ or $[M–H]^-$ adducts, respectively, were more abundant than the fragments resulting from *sn*-1 FA cleavage. The fragmentation pattern for PS was less clear, as the abundance of FA fragments was $[R_1COO]– > [R_2COO]–$, but for the lysophospholipid-like fragments the abundance ratio was reversed $[M–H–87–R_2COOH]– > [M–H–87–R_1COOH]–$. This discrepancy could be explained by more complex fragmentation mechanisms as was theorized earlier (F.-F. Hsu & Turk, 2005; Hvattum et al., 1998). Nevertheless, a calibration curve was created with regiopure reference standards, and the fragment ion ratios were successfully used to determine regioisomers of PS 16:0_18:1 molecular species in a standard mixture. The use of both $[RCOO]^-$ and the lysophospholipid-like fragments for regioisomer calculations of PC, PE and PS classes was demonstrated (Fabritius & Yang, 2021). Using CID on negative polarity, PCs are commonly analyzed as formate $[M+HCOO]^-$ adducts. However, utilizing ammonium bicarbonate resulted in significantly higher sensitivity of the precursor ions (nanoESI(–)-CID-MS^2), forming $[M+HCO_3]^-$ adducts instead (X. Zhao et al., 2019). Additionally, CID of the $[M+HCO_3]^-$ adducts produced fragments with *sn*-1 FA connected to a dehydro-glycerol backbone with the *sn*-3 hydroxyl esterified by ethyl phosphate. This fragment was *sn*-1 specific, allowing analysis of PC regioisomers utilizing the *sn*-1 fragment ion ratios and calibration curves with standards (**Figure 14**). The developed method was used to investigate certain PC regioisomer ratios in human breast cancer tissue (X. Zhao et al., 2019).

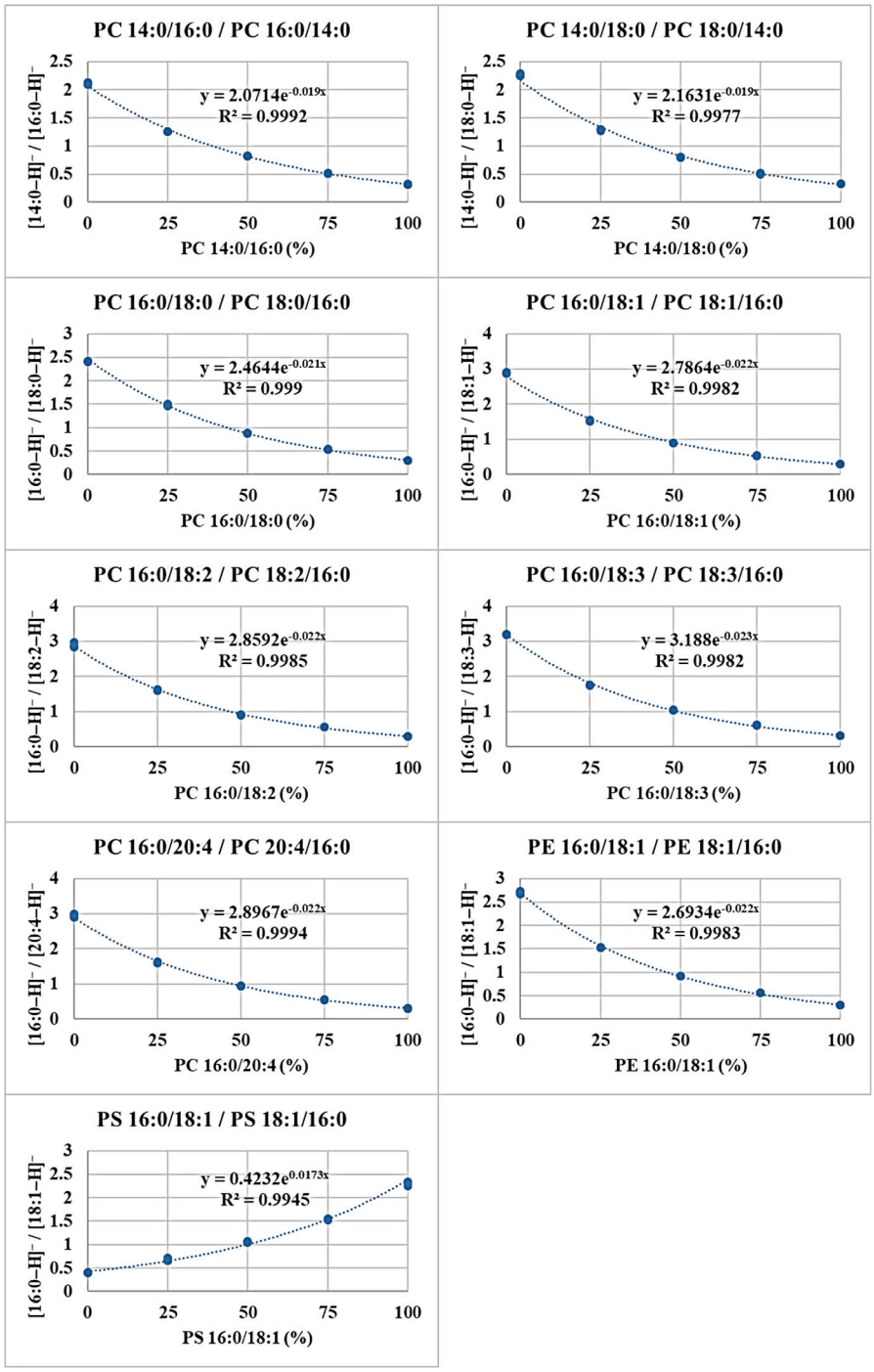

Figure 13 Calibration curves of various regiospecific PL reference standard pairs using $[RCOO]^-$ fragment ion ratios. Reprinted with permission from (Fabritius & Yang, 2021), copyright 2021 John Wiley and Sons.

This issue could have been bypassed with better separation of the molecular species, for example using RP chromatography. The fragmentation pattern for PS was less clear, as the abundance of FA fragments was $[R_1COO]^-$ > $[R_2COO]^-$, but for the lysophospholipid-like fragments the abundance ratio was reversed $[M–H–87–R_2COOH]^-$ > $[M–H–87–R_1COOH]^-$. This discrepancy could be explained by more complex fragmentation mechanisms as was theorized earlier (F.-F. Hsu & Turk, 2005; Hvattum et al., 1998). Nevertheless, a calibration curve was created with regiopure reference standards, and the fragment ion ratios were successfully used to determine regioisomers of PS 16:0_18:1 molecular species in a standard mixture. The use of both $[RCOO]^-$ and the lysophospholipid-like fragments for regioisomer calculations of PC, PE and PS classes was demonstrated (Fabritius & Yang, 2021). Using CID on negative polarity, PCs are commonly analyzed as formate $[M+HCOO]^-$ adducts. However, utilizing ammonium bicarbonate resulted in significantly higher sensitivity of the precursor ions (nanoESI(–)-CID-MS^2), forming $[M+HCO_3]^-$ adducts instead (X. Zhao et al., 2019). Additionally, CID of the $[M+HCO_3]^-$ adducts produced fragments with *sn*-1 FA connected to a dehydro-glycerol backbone with the *sn*-3 hydroxyl esterified by ethyl phosphate. This fragment was *sn*-1 specific, allowing analysis of PC regioisomers utilizing the *sn*-1 fragment ion ratios and calibration curves with standards (**Figure 14**). The developed method was used to investigate certain PC regioisomer ratios in human breast cancer tissue (X. Zhao et al., 2019).

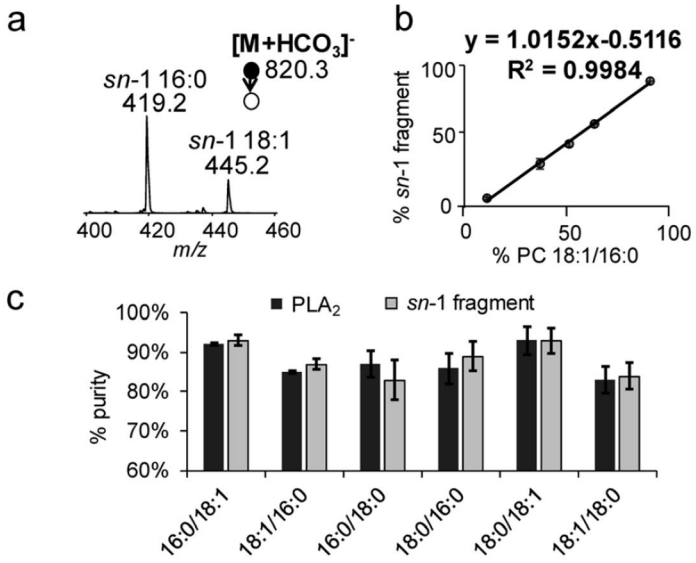

Figure 14 CID spectrum of $[M+HCO_3]^-$ derived from a 2:1 mixture of PC 16:0/18:1 and PC 18:1/16:0 **(a)**, Correlation between *sn*-1 specific fragment as a

function of molar ratio of PC 18:1/16:0 in the reference regioisomer standard mixture **(b)**, Comparisons of the purity of six PC standards measured by the *sn*-1 fragment and enzymatic PL_2 method **(c)**. Reprinted with permission from (X. Zhao et al., 2019), copyright 2019 Royal Society of Chemists.

A combination of the FA fragment $[RCOO]^-$ ion ratios and partial chromatographic separation has been used in calculating regioisomer ratios (Wozny et al., 2019). As the regioisomers such as PC 16:0_18:1 and PC 18:1_16:0 had only very minor difference in the retention time with the used C18 RP column, the fragment ion ratios in the leading edge, center and the tailing edge of the peak were also slightly different. These minor differences of individual regioisomer standards were used to create elution profiles that were used to monitor $[R_2COO]^- > [R_1COO]^-$ fragment ion ratios at specific retention times. The method was used to quantify regioisomers of PC 16:0_18:1 and PC 18:0_18:1 in bovine liver and *E. coli* lipid extracts (Wozny et al., 2019).

In positive ionization mode, sequential fragmentation with CID has been used (nanoESI(+)-CID-MS^3) to produce structurally informative fragments after Paterno-Buchi (PB) photochemical derivatization (Cao et al., 2020). After the loss of PC or PE head group in the first step, the resulting fragments were further fragmented, yielding *sn*-1 and *sn*-2-specific fragments. A total of seven different PB reagents were screened for highest abundance of *sn*-specific fragment ions and 2-acetylpyridine was selected. The regioisomer ratios within one species were calculated by dividing the *sn*-specific ion intensity of one isomer by intensities of all *sn*-specific ions within the species. The method was used for studying differences in PC regioisomer compositions of human lung cancer tissue, breast cancer cell lines and human plasma from diabetic patients (Cao et al., 2020). A similar method utilizing PB derivatization with 2-acetylpyridine and sequential CID was recently used for investigating (HESI(+)-CID-MS^3) PC regioisomers in bovine milk. The focus was on studying fragmentation behavior of different PC molecular species. Accurate quantification of regioisomer ratios was not attempted in this study, and it was noted that calibration curves would be needed for such analysis (Liu & Rochfort, 2022). Utilizing electrochemical reactions to form $[M+Co]^{2+}$ adduct ions, PC regioisomers were studied (nanoESI(+)-CID-MS^2) after fragmentation with CID (Tang et al., 2022). The nanoESI ion source was fitted with metallic cobalt wire, leading to anodic corrosion during the analysis and formation of the doubly charged cobalt adducts. Other metallic complexing agents such as Cu, Ag, Au and Fe were also tested, but the fragmentation patterns were not informative for *sn*-positional analysis. The PC 16:0_18:1 regioisomer ratios were calculated with a calibration curve using $[R_2COO+Co]^+$ and $[M+H–R_2COOH]^+$ fragments. Calculating accurate regioisomer ratios for other molecular species would have required additional

calibration standards, and the method was used for monitoring relative changes in the PC regioisomers of mouse prostate cancer tissue (Tang et al., 2022).

Surface imaging with three CID fragmentation steps was used (nanoDESI(+)-CID-MS^4) in analysis of silver adducts $[M+Ag]^+$ of PCs (Lillja & Lanekoff, 2022). The resulting fragments of PC 16:0_18:1 in MS^4 were mostly *sn*-2 specific, with a minor abundance of *sn*-1 specific fragments. The method was used for imaging regioisomers of molecular species such as PC 16:0_18:1, PC 18:0_18:1 and PC 16:0_20:1 in different regions of mouse brain. In addition to regioisomer ratios, also quantification of the PL regioisomer abundances was performed with this method (Lillja & Lanekoff, 2022). MALDI with a single stage CID has been used with a charge inversion technique, changing the initial positively charged adducts to negative using sequential ESI following MALDI (MALDI(+)/ESI(–)-CID-MS^2). The PCs are initially ionized as $[M+H]^+$, but utilizing 1,4-phenylenedipropionic acid (PDPA) and negative polarity ESI, complex $[M+PDPA–H]^–$ and demethylated $[M–CH_3]^–$ ions are formed. The $[M–CH_3]^–$ ions were further fragmented with CID, yielding $[RCOO]^–$ fragments and allowing regioisomer analysis of PCs utilizing calibration curves. The initial ionization on positive polarity allows for higher sensitivity, while the charge inversion to negative enables structural characterization (Randolph et al., 2020). MS methodologies used for PL regioisomer analysis are listed in **Table 10**.

Table 10 Mass spectrometric methodologies used for PL regioisomer analysis

Reference	LC separation / direct inlet type	MS instrument	Instrument configuration	PL regioisomers; Adducts	Sample material
(Young et al., 2022)	MS imaging (MALDI)	Thermo Scientific Orbitrap Elite	MALDI(+)-OzID-CID-OzID-MS^4	PC; $[M+Na]^+$	Prostate cancer cells
(Lillja & Lanekoff, 2022)	MS imaging (nanoDESI)	Thermo Scientific Orbitrap Velos Pro	nanoDESI(+)-CID-MS^4	PC; $[M+Ag]^+$	Mouse brain
(Liu & Rochfort, 2022)	Reversed phase C18	Thermo Scientific Orbitrap Elite	HESI(+)-CID-MS^3	PC; $[M_{PB}+Na]^+$ PE; $[M_{PB}+Na]^+$	Bovine milk
(Wang & Hsu, 2022)	MS imaging (MALDI)	Bruker UltrafleXtreme MALDI/TOF/TOF	MALDI(+)-MS	PC; $[M+H]^+$, $[M+Na]^+$ PE; $[M+Na]^+$	PL standards
(Tang et al., 2022)	Direct infusion	Thermo Scientific Orbitrap Velos Pro	nanoESI(+)-CID-MS^2	PC; $[M+Co]^{2+}$	Mouse prostate cancer tissue
(Fabritius & Yang, 2021)	Direct infusion or HILIC	Bruker Impact II QTOF	ESI(–)-CID-MS^2	PC; $[M+HCOO]^-$ PE; $[M–H]^-$ PS; $[M–H]^-$	PL standards
(Claes et al., 2021)	MS imaging (MALDI)	Waters SYNAPT HDMS G2-Si	MALDI(+)-CID-OzID-MS^3	PC; $[M+Na]^+$	Rat brain
(Specker et al., 2020)	MS imaging (MALDI)	Bruker 7T solariX XR FT-ICR	MALDI(+)/ ESI(–)-CID-MS^2	PC; $[M+H]^+$ to [M–H+1,4-phenylenedipropionic acid]$^-$ charge inversion	Rat brain

Reference	LC separation / direct inlet type	MS instrument	Instrument configuration	PL regioisomers; Adducts	Sample material
(Cao et al., 2020)	Direct infusion	Thermo Scientific LTQ Linear Ion Trap	nanoESI(+)-CID-MS^3	PC; $[M_{PB}+Na]^+$ PE; $[M_{PB}+Na]^+$	Breast cancer and lung cancer cells
(Born & Prentice, 2020)	MS imaging (MALDI)	Bruker 7T solariX XR FT-ICR	MALDI(+)-EID-MS^2	PC; $[M+H]^+$	Rat brain
(X. Zhao et al., 2019)	HILIC	SCIEX 4500 QTRAP Triple Quadrupole Linear Ion Trap	nanoESI(–)-CID-MS^2	PC; $[M+HCO_3]^-$	Human breast cancer tissue
(Wozny et al., 2019)	Reversed phase C18	Thermo Scientific Q Exactive	ESI(–)-CID-MS^2	PC; $[M+HCOO]^-$	Bovine liver
(Batarseh et al., 2018)	Direct infusion or C18 reversed phase	SCIEX 5500 QTRAP Triple Quadrupole Linear Ion Trap	ESI(+)-CID-OzID-MS^3	PC; $[M+Na]^+$	Human red blood cells
(Paine et al., 2018)	MS imaging (MALDI)	Thermo Scientific LTQ Orbitrap Elite	MALDI(+)-CID-OzID-MS^3	PC; $[M+Na]^+$	Rat brain
(Baba et al., 2018)	Direct infusion	Custom modified SCIEX QTOF	ESI(+)-EIEIO-MS^2	PC; $[M+H]^+$, $[M+Na]^+$ PE; $[M+H]^+$, $[M+Na]^+$	Porcine brain
(Becher et al., 2018)	Direct infusion	Thermo Scientific 7T LTQ FT Ultra or Thermo Scientific Q Exactive	HESI(+)-CID/HCD/UVPD-MS^2	PC; $[M+Fe]^{2+}$	Egg yolk, porcine brain, yeast extract

Reference	LC separation / direct inlet type	MS instrument	Instrument configuration	PL regioisomers; Adducts	Sample material
(Takahashi et al., 2018)	MS imaging (MALDI)	Custom MALDI quadrupole linear ion trap TOF	MALDI(+)-HAD-MS^2	PC; $[M+H]^+$	PL standards
(Williams et al., 2017)	Reversed phase C30	Thermo Scientific Fusion Lumos Orbitrap	nanoESI(+)-CID/HCD-UVPD-MS^3	PC; $[M+Na]^+$	Bovine liver and heart, porcine brain, *E. coli*
(Kozlowski et al., 2015a)	MS imaging (DESI)	Thermo Scientific LTQ Linear Ion Trap	DESI(+)-CID-OzID-MS^3	PC; $[M+Na]^+$	Animal tissues
(Jones et al., 2015)	MS imaging (MALDI)	Bruker 7T solariX XR FT-ICR	MALDI(+)-EID-MS^2	PC; $[M+H]^+$	PL standards
(Campbell & Baba, 2015)	Direct infusion	Custom modified SCIEX QTOF	ESI(+)-EIEIO-MS^2	PC; $[M+H]^+$	Egg yolk
(Pham et al., 2014)	Direct infusion	Thermo Scientific LTQ Linear Ion Trap and SCIEX 2000 QTRAP	ESI(+)-CID-OzID-MS^3	PC; $[M+Na]^+$	Bovine brain and kidney
(Ekroos et al., 2003a)	Direct infusion	Thermo Finnigan LCQ Quadrupole Ion Trap	nanoESI(–)-CID-MS^3	PC; $[M+CH_3COO]^-$, $[M+Cl]^-$	Human red blood cells

2.4.2 Ozone-induced dissociation

OzID is commonly used for identifying the double bond locations on the FA moieties, but it can also be utilized in PL regioisomer analysis, often in tandem with CID (CID-OzID). Chromatographic separation is rarely utilized with CID-OzID, instead, the commonly used methods include direct infusion with ESI (Batarseh et al., 2018; Pham et al., 2014) or MS imaging (Claes et al., 2021; Kozlowski et al., 2015a; Paine et al., 2018; Young et al., 2022) on positive polarity with sodiated $[M+Na]^+$ adducts. Applicability of CID-OzID for PL regioisomer analysis was demonstrated (ESI(+)-CID-OzID-MS^3) with reference standards of six different classes (PA 16:0/18:1, PC16:0/18:2, PE 16:0/18:1, PG 16:0/18:1, PI 16:0/18:2 and PS 16:0/18:1) (Pham et al., 2014). After loss of the head group in CID, the resulting ion was further fragmented with OzID. The CID-OzID fragment profiles of the six different classes (**Figure 15**) look remarkably similar (Pham et al., 2014), unlike with CID only where the PL class significantly influences the fragmentation pattern (Fabritius & Yang, 2021). This indicates that the removal of the head group in the first fragmentation step with CID followed by OzID could make analysis of PL classes such as PI or PS more approachable if the more readily available reference standards like PC or PE could be utilized to establish calibration curves.

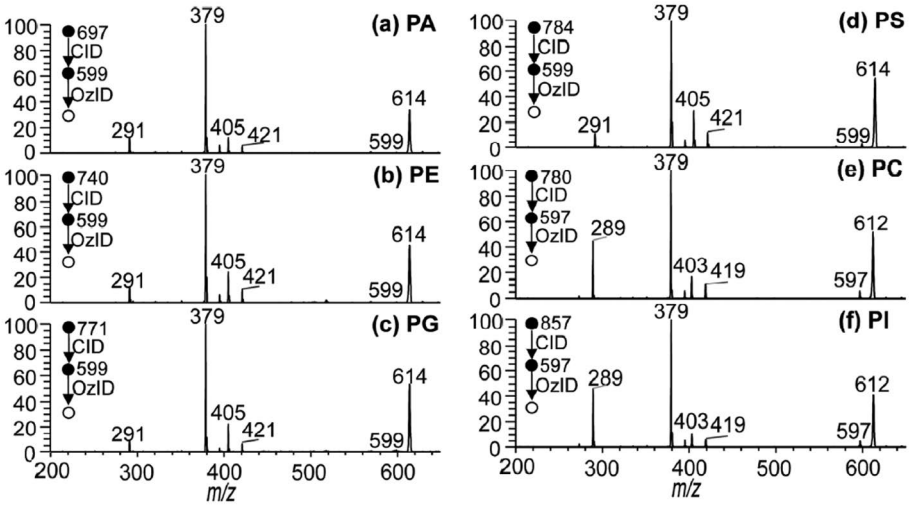

Figure 15 CID-OzID on the ions corresponding to complete phospholipid headgroup losses from precursors ions PA 16:0/18:1 **(a)**, PE 16:0/18:1 **(b)**, PG 16:0/18:1 **(c)**, PS 16:0/18:1 **(d)**, PC 16:0/18:2 **(e)** and PI 16:0/18:2 **(f)**. Reprinted with permission from (Pham et al., 2014), copyright 2014 Royal Society of Chemists.

A triple stage fragmentation (MALDI(+)-OzID-CID-OzID-MS^4) has been used for full structural characterization of certain PCs, including regioisomers and double bond locations (Young et al., 2022). In the first stage, the $[M+Na]^+$ precursor was subjected OzID, followed by selection of one aldehyde product ion of one DB position for CID fragmentation. After the loss of the head group, the final OzID stage produced fragments that enabled regioisomer analysis. PC regioisomers in prostate cancer tissue were analyzed (Young et al., 2022).

The ozonolysis for CID-OzID fragmentations can be performed for example in the trapping region of an ion trap instrument (Paine et al., 2018) or in the ion mobility region of an IMS instrument (Claes et al., 2021). Depending on the instrument type, the reaction rate for the ozonolysis can be a limiting factor with MS imaging if high enough ozone concentrations cannot be achieved. Significantly faster reaction rates resulting in shorter analysis times were observed when OzID was implemented in the high-pressure region of an ion mobility instrument (Claes et al., 2021). Both methods (MALDI(+)-CID-OzID-MS^3) were used to investigate PC regioisomers in different regions of rat brain (Claes et al., 2021; Paine et al., 2018). In addition to MS imaging with MALDI, also DESI has been used in conjunction with CID-OzID fragmentation for analysis of select PC regioisomers in various animal tissues and chicken egg yolk (Kozlowski et al., 2015a).

2.4.3 Other dissociation techniques

In-source fragmentation with MALDI on positive polarity has been used for PL regioisomer analysis without a dedicated fragmentation step (H. Y. J. Wang & Hsu, 2022). In-source fragmentation was generated by increased laser irradiation, resulting in structurally informative fragments after a preferential loss of *sn*-2 FA, similar to those observed with CID. While capable of resolving PL individual regioisomers, the method requires an efficient separation method for structural characterization of PLs in complex natural samples (H. Y. J. Wang & Hsu, 2022).

EID, including EIEIO of PLs produce a much wider variety of structural fragments compared with CID, which also allows differentiation of double bond isomers in addition to regioisomers (MALDI(+)-EID-MS^2) (Jones et al., 2015). A variety of different fragments obtained with EID could be used for studying PC 16:0_18:1 and PC 18:0_18:1 regioisomers in different rat brain regions utilizing calibration curves. *Sn*-specific fragments resulting from a cleavage along the glycerol backbone were also observed (MALDI(+)-EID-MS^2), but the intensities were low, limiting their usefulness in determining regioisomer ratios (Born & Prentice, 2020). The *sn*-specific fragments were more prominent in another study (ESI(+)-EIEIO-MS^2), where PC regioisomers were calculated using *sn*-1-specific ion ratios resulting from C_1-C_2 carbon bond cleavage on the

glycerol backbone (Campbell & Baba, 2015). When analyzing a PC 16:0/18:1 standard, a small amount of *sn*-2-specific fragment resulting from loss of FA 16:0 was observed. This was attributed to isomeric impurity of the standard, as the other regioisomer standard PC 18:1/16:0 produced only appropriate *sn*-1-specific 18:1 and *sn*-2-specific 16:0 fragments (Campbell & Baba, 2015). The method (ESI(+)-EIEIO-MS^2) was later used to analyse various other lipids, including regioisomers of PC, PE, PI and PS in porcine brain. The regioisomer ratios seem to have been calculated simply based on the *sn*-specific fragment ratios (Baba et al., 2018).

A comparison between CID, higher-energy collisional dissociation (HCD) and ultraviolet photodissociation (UVPD) on the structural fragments of PC standards has been performed (HESI(+)-CID/HCD/UVPD-MS^2) utilizing metal ion complexes as the precursor ions (Becher et al., 2018). A total of 11 different metal salts were screened for best suitability with UVPD, of which $FeCl_2$ forming $[M+Fe]^{2+}$ ions was selected due to the highest abundances of structurally informative fragments. Regardless of the higher *sn*-specificity of the UVPD fragments compared to those obtained with CID or HCD, calibration curves with reference standards are still required for accurate analysis of regioisomer ratios. UVPD fragmentation was used for analysis of PC regioisomers in mouse pancreas lipid extract (Becher et al., 2018). HCD has also been used in tandem with UVPD, resulting in loss of PL head group of the $[M+Na]^+$ precursors in the first fragmentation step and formation of structurally informative fragments in the second step (nanoESI(+)-HCD-UVPD-MS^3) (Williams et al., 2017). Similar to CID-OzID fragmentation of different PL classes (Pham et al., 2014), CID/HCD-UVPD also produced nearly identical fragment spectra for species with the same FA composition such as PA 16:0/18:1, PC 16:0/18:1, PE 16:0/18:1, PG 16:0/18:1, PI 16:0/18:1 and PS 16:0/18:1 after the initial head group loss (Williams et al., 2017).

2.5 Concluding remarks

Chromatography can offer targeted approaches for *sn*-positional isomers of specific TGs and PLs species of interest, but the methods are often very time consuming and not suitable for untargeted analysis of a wide spectrum of isomers. Various methods have been investigated for analysis of TG and PL regioisomers based on tandem mass spectrometry in shotgun mode or combined with liquid chromatography. Ion mobility for separation of regioisomers is an emerging technique and still quite unused, and the full potential remains likely to be explored. Collision-induced dissociation is the most frequently used fragmentation technique for regioisomeric analysis of both TGs and PLs taking advantage of differential dissociation energy of fatty acids from the primary and

secondary positions. Collision-induced dissociation in tandem with ozone-induced dissociation has shown potential to differentiate double bond isomers in addition to regioisomers. Determining the regioisomer ratios using MS methods usually requires calibration curves based on the structurally informative fragment ion ratios. Adapting the developed MS methods for use in another laboratories is not straightforward, as the fragment ion ratios can also be influenced by instrument and collision gas type. With TGs there is also the challenge of isobaric fragments resulting from multiple chromatographically overlapping molecular species distorting the fragment ion spectra. Calculating TG regioisomers from convoluted spectra with calibration curves alone is not viable, and automated optimization algorithms have been shown to offer useful solutions in such cases.

Regiopure standards can be expensive and often outright not available for certain PL classes. While most fragmentation methods produce fragments related to FA cleavage at different ratios from both *sn*-1 and *sn*-2 positions of PL, certain methods such as EIEIO can produce unique *sn*-specific fragments. However, the structural features of fatty acids i.e. the chain lengths as well as the number and position of double bonds of FAs likely influence the efficiency of *sn*-specific fragmentation; therefore, it is possible that calibration curves with different FA combinations are necessary for accurate quantification of regioisomers. Establishing fragmentation models using commercially available standards can help in properly investigating regioisomer abundances of complex samples, reducing the need for a much wider variety of reference standards. This has been done for TGs to assist calculations, and similar approach could be utilized for PL regioisomers as well.

Concluding this literature review, if no acceptable chromatographic separation of isobaric TG molecular species is achieved, each fragment ion spectrum needs careful assessment on the effects of interfering isobaric fragments when calculating the regioisomer ratios. Individual calibration curves are often not enough for complex natural samples as isobaric DG fragments might be product ions from multiple different TG species. Instead, using a general fragmentation model together with an optimization algorithm that recreates the observed spectrum by calculating regioisomer abundances that produced the original spectrum has shown potential for untargeted TG regioisomer analysis, mitigating the effects of isobaric fragments. With PLs the interference of isobaric fragment ions is of less importance, but lack of reference standards for various PL classes hinders development of fragmentation models. Future research should be directed to further development and integration of untargeted regioisomer analysis methods into standard lipidomics protocols to explore regioisomeric profiles of glycerolipids in tissues as biomarkers of health and diseases.

3 AIMS OF THE STUDY

The main aim of this research was to develop and validate methods for analysis of TG and PL regioisomer compositions in complex natural samples. The work is divided into four studies, the first two (**I**, **II**) of which focus on TG regioisomers and the latter two (**III**, **IV**) on PL regioisomers. The objectives of each study are briefly summarized as:

Transferring, testing and validation of an existing direct inlet analysis method for analysis of TG regioisomers (Kallio & Currie, 1993) to a new instrument, including a software update for a previously published *MSPECTRA* (Kurvinen et al., 2001) calculation program (**I**).

Development and validation of a new TG regioisomer calculation software to complement a previously developed (Tarvainen et al., 2019) LC-MS^2 method and the preliminary regioisomer calculation algorithm (Kallio et al., 2017) (**II**).

Investigation of PL fragmentation patterns and establishing a framework method for analysis of PL regioisomers utilizing calibration curves (**III**).

Further development of the PL regioisomer LC-MS^2 method and optimization of reversed phase chromatography for efficient separation of PL molecular species. Development of a fragmentation model and a calculation program for fully automated, untargeted PL regioisomer characterization (**IV**).

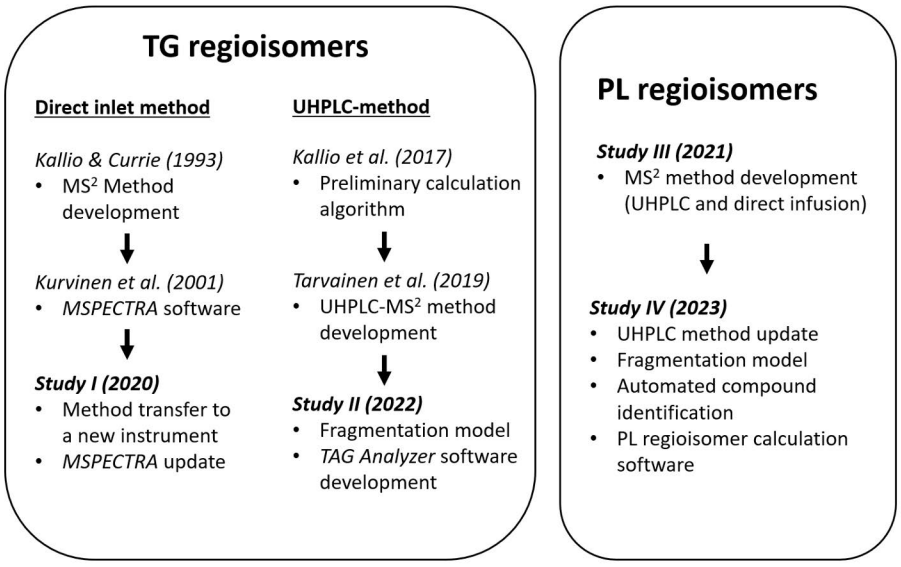

Figure 16 Overview of the thesis research and related previous work

4 MATERIALS AND METHODS

4.1 Materials

4.1.1 Reference standards

All TG reference standards (**Table 11**) were purchased from Larodan (Malmö, Sweden). The mixed acid TG standards were of high regioisomer purity (>98 %) according to the producer. All PL reference standards were purchased from Avanti Polar Lipids (Alabaster, AL, USA). For PLs (**Table 12**) there are two different purity categories: IsoPure and regular. The IsoPure product line is guaranteed to have >97 % regioisomer purity, whereas in the regular product line, while the molecular species purity is very good (>99%), the regioisomer purity is not specifically mentioned.

Table 11 TG reference standards

Shorthand notation	Full name	Purity (molecular species; regioisomer)[a]	Study
TG 8:0/8:0/8:0	1,2,3-tricaprylin	>99 %; not applicable	I
TG 10:0/10:0/10:0	1,2,3-tricaprin	>99 %; not applicable	I
TG 12:0/12:0/12:0	1,2,3-trilaurin	>99 %; not applicable	I
TG 14:0/14:0/14:0	1,2,3-trimyristin	>99 %; not applicable	I
TG 16:0/16:0/16:0	1,2,3-tripalmitin	>99 %; not applicable	I
TG 16:1/16:1/16:1	1,2,3-tripalmitolein	>99 %; not applicable	I
TG 18:0/18:0/18:0	1,2,3-tristearin	>99 %; not applicable	I
TG 18:1/18:1/18:1	1,2,3-triolein	>99 %; not applicable	I
TG 18:2/18:2/18:2	1,2,3-trilinolein	>99 %; not applicable	I
TG 18:2_18:2 *sn*-2_18:3	1(3),2-dilinolein-3(1)-linolenin	>98 %; >98 %	I, II
TG 18:2_18:3 *sn*-2_18:2	1,3-dilinolein-2-linolenin	>98 %; >98 %	I, II
TG 18:1_18:1 *sn*-2_18:3	1(3),2-diolein-3(1)-linolenin	>98 %; >98 %	I, II
TG 18:1_18:3 *sn*-2_18:1	1,3-diolein-2-linolenin	>98 %; >98 %	I, II
TG 18:0_18:0 *sn*-2_18:2	1(3),2-distearin-3(1)-linolein	>98 %; >98 %	I, II
TG 18:0_18:2 *sn*-2_18:0	1,3-distearin-2-linolein	>98 %; >98 %	I, II
TG 16:0_16:0 *sn*-2_18:2	1(3),2-dipalmitin-3(1)-linolein	>98 %; >98 %	I, II
TG 16:0_18:2 *sn*-2_16:0	1,3-dipalmitin-2-linolein	>98 %; >98 %	I, II
TG 18:1_18:1 *sn*-2_18:2	1(3),2-diolein-3(1)-linolein	>98 %; >98 %	I, II
TG 18:1_18:2 *sn*-2_18:1	1,3-diolein-2-linolein	>98 %; >98 %	I, II
TG 18:1_18:1 *sn*-2_14:0	1(3),2-diolein-3(1)-myristin	>98 %; >98 %	I, II
TG 18:1_14:0 *sn*-2_18:1	1,3-diolein-2-myristin	>98 %; >98 %	I, II
TG 18:1_18:1 *sn*-2_16:0	1(3),2-diolein-3(1)-palmitin	>98 %; >98 %	I, II
TG 18:1_16:0 *sn*-2_18:1	1,3-diolein-2-palmitin	>98 %; >98 %	I, II

Shorthand notation	Full name	Purity (molecular species; regioisomer)[a]	Study
TG 16:0_16:0 *sn*-2_18:0	1(3),2-dipalmitin-3(1)-stearin	>98 %; >98 %	I, II
TG 16:0_18:0 *sn*-2_16:0	1,3-dipalmitin-2-stearin	>98 %; >98 %	I, II
TG 16:0_16:0 *sn*-2_14:0	1(3),2-dipalmitin-3(1)-myristin	>98 %; >98 %	I, II
TG 16:0_14:0 *sn*-2_16:0	1,3-dipalmitin-2-myristin	>98 %; >98 %	I, II
TG 18:1_18:1 *sn*-2_12:0	1(3),2-diolein-3(1)-laurin	>98 %; >98 %	I, II
TG 18:1_12:0 *sn*-2_18:1	1,3-diolein-2-laurin	>98 %; >98 %	I, II
TG 14:0_14:0 *sn*-2_18:1	1(3),2-dimyristin-3(1)-olein	>98 %; >98 %	I, II
TG 14:0_18:1 *sn*-2_14:0	1,3-dimyristin-2-olein	>98 %; >98 %	I, II
TG 18:1_18:1 *sn*-2_18:0	1(3),2-diolein-3(1)-stearin	>98 %; >98 %	I, II
TG 18:1_18:0 *sn*-2_18:1	1,3-diolein-2-stearin	>98 %; >98 %	I, II
TG 18:0_18:0 *sn*-2_18:1	1(3),2-distearin-3(1)-olein	>98 %; >98 %	I, II
TG 18:0_18:1 *sn*-2_18:0	1,3-distearin-2-olein	>98 %; >98 %	I, II
TG 16:0_16:0 *sn*-2_18:1	1(3),2-dipalmitin-3(1)-olein	>98 %; >98 %	I, II
TG 16:0_18:1 *sn*-2_16:0	1,3-dipalmitin-2-olein	>98 %; >98 %	I, II
TG 18:2_18:2 *sn*-2_16:0	1(3),2-dilinolein-3(1)-palmitin	>98 %; >98 %	I, II
TG 18:2_16:0 *sn*-2_18:2	1,3-dilinolein-2-palmitin	>98 %; >98 %	I, II
TG 18:2_18:2 *sn*-2_18:1	1(3),2-dilinolein-3(1)-olein	>98 %; >98 %	I, II
TG 18:2_18:1 *sn*-2_18:2	1,3-dilinolein-2-olein	>98 %; >98 %	I, II
TG 18:1_16:0 *sn*-2_18:2	1(3)-olein-2-palmitin-3(1)-linolein	>98 %; >98 %	I, II
TG 18:1_18:2 *sn*-2_16:0	1(3)-olein-2-linolein-3(1)-palmitin	>98 %; >98 %	I, II
TG 16:0_18:1 *sn*-2_18:2	1(3)-palmitin-2-olein-3(1)-linolein	>98 %; >98 %	I, II
TG 18:2_18:1 *sn*-2_12:0	1(3)-linolein-2-olein-3(1)-laurin	>98 %; >98 %	I, II
TG 18:1_12:0 *sn*-2_18:2	1(3)-olein-2-laurin-3(1)-linolein	>98 %; >98 %	I, II
TG 18:1_18:2 *sn*-2_12:0	1(3)-olein-2-linolein-3(1)-laurin	>98 %; >98 %	I, II
TG 16:0_18:1 *sn*-2_12:0	1(3)-palmitin-2-olein-3(1)-laurin	>98 %; >98 %	I, II
TG 18:1_12:0 *sn*-2_16:0	1(3)-olein-2-laurin-3(1)-palmitin	>98 %; >98 %	I, II
TG 18:1_16:0 *sn*-2_12:0	1(3)-olein-2-palmitin-3(1)-laurin	>98 %; >98 %	I, II
TG 18:1_16:0 *sn*-2_18:0	1(3)-olein-2-palmitin-3(1)-stearin	>98 %; >98 %	II
TG 18:1_18:0 *sn*-2_16:0	1(3)-olein-2-stearin-3(1)-palmitin	>98 %; >98 %	II
TG 16:0_18:1 *sn*-2_18:0	1(3)-palmitin-2-olein-3(1)-stearin	>98 %; >98 %	II
TG 18:1_16:0 *sn*-2_20:0	1(3)-olein-2-palmitin-3(1)-arachidin	>98 %; >98 %	II
TG 18:1_20:0 *sn*-2_16:0	1(3)-olein-2-arachidin-3(1)-palmitin	>98 %; >98 %	II
TG 16:0_18:1 *sn*-2_20:0	1(3)-palmitin-2-olein-3(1)-arachidin	>98 %; >98 %	II
TG 16:0_16:0 *sn*-2_8:0	1(3),2-dipalmitin-3(1)-caprylin	>98 %; >98 %	II
TG 16:0_8:0 *sn*-2_16:0	1,3-dipalmitin-2-caprylin	>98 %; >98 %	II

[a] According to the supplier

Table 12 PL reference standards

Shorthand notation	Full name	Purity (molecular species; regioisomer)[a]	Study
PC 12:0/12:0	1,2-dilauroyl-*sn*-glycero-3-phosphocholine	>99 %; not applicable	III
PC 14:0/14:0	1,2-dimyristoyl-*sn*-glycero-3-phosphocholine	>99 %; not applicable	III
PC 14:1/14:1	1,2-dimyristoleoyl-*sn*-glycero-3-phosphocholine	>99 %; not applicable	III
PC 16:0/16:0	1,2-dipalmitoyl-*sn*-glycero-3-phosphocholine	>99 %; not applicable	III
PC 16:1/16:1	1,2-dipalmitoleoyl-*sn*-glycero-3-phosphocholine	>99 %; not applicable	III
PC 18:0/18:0	1,2-distearoyl-*sn*-glycero-3-phosphocholine	>99 %; not applicable	III
PC 18:1/18:1	1,2-dioleoyl-*sn*-glycero-3-phosphocholine	>99 %; not applicable	III
PC 18:2/18:2	1,2-dilinoleoyl-*sn*-glycero-3-phosphocholine	>99 %; not applicable	III
PC 18:3/18:3	1,2-dilinolenoyl-*sn*-glycero-3-phosphocholine	>99 %; not applicable	III
PC 20:0/20:0	1,2-diarachidoyl-*sn*-glycero-3-phosphocholine	>99 %; not applicable	III
PC 22:0/22:0	1,2-dibehenoyl-*sn*-glycero-3-phosphocholine	>99 %; not applicable	III
PC 14:0/16:0	1-myristoyl-2-palmitoyl-*sn*-glycero-3-phosphocholine	>99 %; not specified	III, IV
PC 16:0/14:0	1-palmitoyl-2-myristoyl-*sn*-glycero-3-phosphocholine	>99 %; not specified	III, IV
PC 14:0/18:0	1-myristoyl-2-stearoyl-*sn*-glycero-3-phosphocholine	>99 %; not specified	III, IV
PC 18:0/14:0	1-stearoyl-2-myristoyl-*sn*-glycero-3-phosphocholine	>99 %; not specified	III, IV
PC 16:0/18:0	1-palmitoyl-2-stearoyl-*sn*-glycero-3-phosphocholine	>99 %; not specified	III, IV
PC 18:0/16:0	1-stearoyl-2-palmitoyl-*sn*-glycero-3-phosphocholine	>99 %; not specified	III, IV
PC 18:0/18:1	1-stearoyl-2-oleoyl-*sn*-glycero-3-phosphocholine	>99 %; not specified	IV
PC 18:1/18:0	1-oleoyl-2-stearoyl-*sn*-glycero-3-phosphocholine	>99 %; not specified	IV

Shorthand notation	Full name	Purity (molecular species; regioisomer)[a]	Study
PC 16:0/22:6	1-palmitoyl-2-docosahexaenoyl-*sn*-glycero-3-phosphocholine	>99 %; not specified	IV
PC 18:0/18:2	1-stearoyl-2-linoleoyl-*sn*-glycero-3-phosphocholine	>99 %; not specified	IV
PC 18:0/20:4	1-stearoyl-2-arachidonoyl-*sn*-glycero-3-phosphocholine	>99 %; not specified	IV
PC 18:0/22:6	1-stearoyl-2-docosahexaenoyl-*sn*-glycero-3-phosphocholine	>99 %; not specified	IV
PC 16:0/18:1	1-palmitoyl-2-oleoyl-glycero-3-phosphocholine	>97 %; >97 %	III, IV
PC 18:1/16:0	1-oleoyl-2-palmitoyl-*sn*-glycero-3-phosphocholine	>97 %; >97 %	III, IV
PC 16:0/18:2[b]	1-palmitoyl-2-linoleoyl-glycero-3-phosphocholine	>97 %; >97 %	III, IV
PC 18:2/16:0[b]	1-linoleoyl-2-palmitoyl-*sn*-glycero-3-phosphocholine	>97 %; >97 %	III, IV
PC 16:0/18:3[b]	1-palmitoyl-2-linolenoyl-glycero-3-phosphocholine	>97 %; >97 %	III, IV
PC 18:3/16:0[b]	1-linolenoyl-2-palmitoyl-*sn*-glycero-3-phosphocholine	>97 %; >97 %	III, IV
PC 16:0/20:4	1-palmitoyl-2-arachidonoyl-*sn*-glycero-3-phosphocholine	>97 %; >97 %	III, IV
PC 20:4/16:0	1-arachidonoyl-2-palmitoyl-*sn*-glycero-3-phosphocholine	>97 %; >97 %	III, IV
PE 14:0/14:0	1,2-dimyristoyl-*sn*-glycero-3-phosphoethanolamine	>99 %; not applicable	III
PE 16:0/16:0	1,2-dipalmitoyl-*sn*-glycero-3-phosphoethanolamine	>99 %; not applicable	III
PE 18:0/18:0	1,2-distearoyl-*sn*-glycero-3-phosphoethanolamine	>99 %; not applicable	III
PE 18:1/18:1	1,2-dioleoyl-*sn*-glycero-3-phosphoethanolamine	>99 %; not applicable	III
PE 16:0/18:1	1-palmitoyl-2-oleoyl-*sn*-glycero-3-phosphoethanolamine	>97 %; >97 %	III
PE 18:1/16:0	1-oleoyl-2-palmitoyl-*sn*-glycero-3-phosphoethanolamine	>97 %; >97 %	III
PS 14:0/14:0	1,2-dimyristoyl-*sn*-glycero-3-phospho-L-serine (sodium salt)	>99 %; not applicable	III

Shorthand notation	Full name	Purity (molecular species; regioisomer)[a]	Study
PS 16:0/16:0	1,2-dipalmitoyl-*sn*-glycero-3-phospho-L-serine (sodium salt)	>99 %; not applicable	III
PS 18:0/18:0	1,2-distearoyl-*sn*-glycero-3-phospho-L-serine (sodium salt)	>99 %; not applicable	III
PS 18:1/18:1	1,2-dioleoyl-*sn*-glycero-3-phospho-L-serine (sodium salt)	>99 %; not applicable	III
PS 16:0/18:1	1-palmitoyl-2-oleoyl-*sn*-glycero-3-phospho-L-serine (sodium salt)	>97 %; >97 %	III
PS 18:1/16:0	1-oleoyl-2-palmitoyl-*sn*-glycero-3-phospho-L-serine (sodium salt)	>97 %; >97 %	III
PI extract (soybean)	L-α-phosphatidylinositol (Soy) (sodium salt)	>99 %; not applicable	III
SM extract (egg yolk)	Sphingomyelin (Egg)	>99 %; not applicable	III

[a] According to the supplier

[b] Custom synthesis product by Avanti

Standards of FA methyl esters (**I**), 37 component FA methyl ester mixture (Sigma-Aldrich, St. Louis, MO, USA), 68D and GLC-490 (both from Nu-Chek-Prep, Elysian, MN, USA), were used as external standards for FA composition analysis. All mobile phase solvents and additives were of MS-grade. Other solvents and reagents were of HPLC or MS-grade.

4.1.2 Sample materials

Infant formulas (IF), consisting of 7 liquid and 4 powdered formulas (**I**), were purchased from local grocery stores in Turku, Finland (**Table 13**). The selected formulas were all intended for infants younger than 6 months, representing a majority of infant formulas available on the Finnish retail market. The infant formulas were divided into four categories based on the most abundant source of fat according to the product information: palm oil and rapeseed oil (IF A1-A5), sunflower oil (IF B1-B3), bovine milk (IF C1-C2) and modified vegetable oil (IF D1). Two bovine milk samples (**I**, **IV**) were provided by Valio Ltd (Helsinki, Finland). The olive oil sample was purchased from a local grocery store.

The human milk sample (**I, II**) of Finnish origin was pooled from milk samples of volunteer mothers (n = 7) living in the Turku area, and the milk of Chinese origin was pooled from milk samples of mothers (n = 10) living in Beijing area. Approval for collecting and studying the Finnish and Chinese human milk samples was obtained from the Ethics Committee of Hospital District of Southwestern Finland and Medical Research Board of Peking University, respectively. All mothers gave written informed consent. Only

healthy mothers, who had given birth to a normally grown full term infant younger than 6 months of age, and were exclusively breastfeeding, were accepted.

Table 13 Sample material analyzed in the thesis work

Sample	Form	Source of fat	Study
IF A1	Liquid	Vegetable oil (palm oil, rapeseed oil, soy oil, coconut oil), *mortierella alpina oil*	I
IF A2	Liquid	Vegetable oil (palm oil, rapeseed oil, coconut oil, sunflower oil), fish oil, *mortierella alpina* oil	I
IF A3	Liquid	Vegetable oil (palm oil, rapeseed oil, coconut oil, sunflower oil), fish oil, *mortierella alpina oil*	I
IF A4	Liquid	Vegetable oil (palm oil, rapeseed oil, coconut oil, sunflower oil), fish oil, *mortierella alpina oil*	I
IF A5	Powder	Vegetable oil (palm oil, rapeseed oil, coconut oil sunflower oil), fish oil, *mortierella alpina oil*	I
IF B1	Liquid	Vegetable oil (sunflower oil, rapeseed oil), fish oil	I
IF B2	Powder	Vegetable oil (sunflower oil, coconut oil, soy oil), fish oil, *mortierella alpina* oil	I
IF B3	Powder	Vegetable oil (sunflower oil, coconut oil, rapeseed oil), fish oil, *mortierella alpina oil*	I
IF C1	Liquid	Bovine milk, vegetable oil (sunflower oil, rapeseed oil, palm oil, coconut oil), fish oil, *mortierella alpina oil*	I
IF C2	Liquid	Bovine milk, vegetable oil (rapeseed oil, sunflower oil), *mortierella alpina* oil	I
IF D1	Powder	Vegetable oil (modified vegetable oil, rapeseed oil, sunflower oil), fish oil, *mortierella alpina oil*	I
Bovine milk	Liquid	Bovine milk	I, IV
Bovine milk, organic	Liquid	Bovine milk	I
Human milk, Chinese	Liquid	Human milk	I
Human milk, Finnish	Liquid	Human milk	I, II
Olive oil, Italian	Liquid	Olive oil	II

4.2 Methods

4.2.1 Lipid extraction

The commercial olive oil sample (**II**) was analyzed as such without extraction or purification. 0.5 mL chloroform was added to 0.5 mL sample of infant formula (**I**), bovine milk (**I, IV**) or human milk (**I, II**), and the mixture was vortexed briefly. For further TG fractionation (**I, II**), 1 mL internal standard TG 17:0/17:0/17:0 in chloroform (0.85 mg/mL) was added to the sample. For PL fractionation (**IV**), 100 µL of internal standard PC 19:0/19:0 (100 µg/mL) was used.

1.5 mL methanol, 1.5 mL chloroform and 0.8 mL 0.88 % potassium chloride were added, and the sample was vortexed briefly after each addition. The samples were centrifuged at 1100 *g* for 5 min, and the lower chloroform phase was collected. Lipids were further extracted from the upper phase by adding 1.5 mL chloroform, vortexing briefly, centrifuging, and collecting the chloroform phase. The chloroform phase of the two extractions were combined and evaporated to dryness under gentle nitrogen flow at 50 °C, after which 1 mL dry diethyl ether (**I, II**) or hexane:diethyl ether (1:1, v/v) (**IV**) was added to dissolve the lipids.

4.2.2 FA composition analysis

FA composition analysis was done on the human milk, infant formulas, and bovine milk (**I**). 100 µg aliquot of the TG extract was taken for analysis. The solvent was first evaporated from the fractionated TGs. The samples were dissolved in 1 mL sodium-dried diethyl ether. 25 µL methyl acetate and 25 µL 1 M sodium methoxide were added. After a brief vortexing the sample was left to incubate at room temperature for 5 min and mixing it occasionally during the incubation. The reaction was stopped by adding 6 µL of acetic acid with brief agitation with vortex. The mixture was centrifuged at 1100 *g* for 5 min. The supernatant was collected into an autosampler vial. Solvent was gently evaporated under nitrogen flow at room temperature. TGs were dissolved in 1 mL hexane. Vials were thoroughly mixed before analysis.

Gas chromatographic analysis of fatty acid composition of TG fraction was carried out using a Shimadzu GC-2010 with AOC-20i auto injector and flame ionization detector (Shimadzu Corporation, Kyoto, Japan). The equipment was controlled by GC Solution software. The column was a wall coated open tubular column DB-23 (60 m × 0.25 mm, liquid film 0.25 µm, Agilent Technologies, Santa Clara, CA, USA). Helium was used as the carrier gas. Injector temperature was set at 270 °C. Split/splitless injection mode was used and the split was opened after 1 min. The injection volume was 0.5 µL. The column temperature

program was as follows: initial temperature 130 °C and hold for 1 min, increase at 4.5 °C/min to 170 °C, increase at 10 °C/min to 220 °C and hold for 14.5 min, increase at 60 °C/min to 230 °C and hold for 3 min. The detector temperature was set at 280 °C.

Fatty acids were identified using external fatty acid methyl ester standards 68D, GLC-490 and 37 component FAME mix. The quantification was performed by comparing the peak area of each fatty acid with that of the internal standard. Correction factors were determined by analysis of standard mixtures and applied in the quantification to correct the difference in detector response between each fatty acid and the internal standard. The fatty acid composition was calculated as weight percentage of the total fatty acids.

4.2.3 Lipid fractionation

For isolation of neutral lipids including TGs from the total lipids (**I, II**), a Sep-Pak Vac silica 6 cc (500 mg) solid phase extraction (SPE) column was conditioned by elution with 5 mL diethyl ether. The extracted lipid sample dissolved in 1 mL diethyl ether was applied to the SPE column. The sample vial was washed with 2 mL diethyl ether, which was transferred into the column. TG fraction was collected by elution with 9 mL diethyl ether. TG extract was evaporated to dryness under gentle nitrogen flow at 50 °C and dissolved in 1 mL hexane.

For PL fractionation (**IV**), the neutral lipids were first collected similarly as above, except diethyl ether was replaced by hexane/diethyl ether (1:1, v/v). After collection of neutral lipids, the collection tube was replaced by a clean one. The sample vial was washed with 2 mL methanol/chloroform/water (5:3:2, v/v), which was then transferred into the SPE column. Polar lipids, mainly phospholipids, were eluted with 8 mL methanol/chloroform/water (5:3:2, v/v), and the solvent was evaporated under gentle nitrogen flow. The polar lipid fraction was reconstituted in 1 mL chloroform/methanol (2:1, v/v).

4.2.4 TG molecular species and regioisomer analysis (Direct inlet MS^2 method)

The targeted direct inlet MS^2 analysis method consists of three phases. First, the TG molecular weight distribution is screened with an MS scan. Then, the most abundant or otherwise interesting TG species are selected for fragmentation and regioisomer analysis. The regioisomer compositions are finally calculated with *MSPECTRA* software based on the fragment ion ratios.

4.2.4.1 TG molecular weight distribution analysis

Molecular weight analysis of TGs (**I**) was carried out using a Thermo Scientific TSQ 8000 EVO mass spectrometer (Thermo Fisher Scientific, Waltham, MA, USA) equipped with a direct exposure probe. The equipment was controlled by Xcalibur software. The system was used in negative chemical ionization mode with ammonia (purity 6.0) as the ionization gas. 1 µL of the TG fraction of each sample containing approximately 20 µg of TGs was applied onto the rhenium wire on the tip of the probe. The probe was placed inside the ion source via the vacuum interlock and after a short period of vacuum stabilization the probe tip was heated at a steadily increasing rate. There was no gas flow coming from the GC side of the instrument and the transfer line was blocked.

Instrument parameters were optimized with regiopure TG 16:0_16:0 *sn*-2_18:1, TG 16:0_18:1 *sn*-2_16:0, TG 18:1_18:2 *sn*-2_18:2, and TG 18:2_18:1 *sn*-2_18:2 with the goal of having the highest obtainable intensity for deprotonated $[M-H]^-$ ions. The optimized instrument settings for molecular weight analysis were: ion source temperature 100 °C, ammonia gas flow rate 1.5 mL/min, electron energy 70 eV, emission current 300 mA and scan time 0.1 s.

In addition, the effects of probe heating rate were investigated, but the heating rate did not have a significant effect on the results, so a fast heating rate of 100 mA/s (0 – 800 mA) was chosen. MS scans between *m/z* 400-1000 were acquired in quadruplicate. The number of acyl carbons and double bonds (ACN:DB) were calculated according to the *m/z* values of $[M-H]^-$ ions. Relative molar proportions of different molecular weight species were calculated using the abundances of $[M-H]^-$ ions. The amount of naturally occurring ^{13}C was taken into account when the proportions of TGs were calculated. The monoacid TG standards listed in **Table 11** were used for determining whether correction factors for different ACN:DB species were needed.

4.2.4.2 TG regioisomer analysis

The initial MS scan data and molecular weight analysis was used to create a product ion scan method for each selected molecular $[M-H]^-$ ion (**I**). Fragmentation of molecular TG ions $[M-H]^-$ was performed using collision-induced dissociation (CID) with argon gas, which favors dissociation of FAs from *sn*-1/3 positions. Selection of precursor ions was performed within a range of $m/z \pm 0.5$ of the theoretical *m/z* value of the molecular TG ion.

Product ions were scanned between *m/z* 100-650 to determine the primary (*sn*-1/3) and secondary (*sn*-2) positions of FAs. Ion source temperature was set at 340 °C, ammonia gas flow rate at 1.5 mL/min, electron energy at 70 eV, emission current at 300 mA, collision energy at 20 eV and 0.1 s scan time was used. The

results were calculated using an updated version (v.1.4) of the *MSPECTRA* software (Kurvinen et al., 2001).

A total of 21 of the most abundant TG species, each representing at least 1 mol% of the total ACN:DB species in the human milk samples, were selected for regioisomeric analysis. In infant formulas and bovine milks out of the selected 21 TG species, only the ones containing more than 1 mol % of the total TGs were quantified. Seven different ACN:DB species could be tracked and analyzed during a single run. Each selected ACN:DB species was analyzed in quadruplicate.

4.2.4.3 *MSPECTRA* software

The TG regioisomer calculation algorithms with the direct inlet MS^2 method, including the *MSPECTRA* software, have been described previously (Kallio & Rua, 1994; Kurvinen et al., 2001). In the thesis work, the *MSPECTRA* calculation software was updated to handle data obtained with the TSQ 8000 EVO mass spectrometer (**I**). Briefly, the software uses three ion types for TG regioisomer analysis. The deprotonated molecular ion $[M–H]^–$ is first used for assigning the ACN:DB species based on the *m/z* ratio. The $[M–H]^–$ is fragmented with CID, yielding structurally informative $[M–H–RCOOH–100]^–$ and $[RCOO]^–$ ions.

The abundances of the $[RCOO]^–$ deprotonated FA anions represent the FA composition of the ACN:DB species, but they are not *sn*-specific. *MSPECTRA* first looks at the ACN:DB value determined by the $[M–H]^–$ precursor ion and calculates all the possible FA combinations that fulfill the ACN:DB requirements of the TG precursor ion. An optimization algorithm finds a combination and ratios of TG molecular species that match the abundances of the observed $[RCOO]^–$ ions. The resulting information from this step is the molecular species distribution within the ACN:DB species. Correction factors for FA abundances were calculated using relative proportions of $[RCOO]^–$ fragments in the TG standards. As the $[RCOO]^–$ fragment ion ratios are not regiospecific, but instead they represent the general FA composition of the ACN:DB species, the correction factors were calculated using AAB and ABA type TGs as follows:

$$C_B = \frac{\left(\frac{I_A}{2}\right) * C_A}{I_B}$$

where:

I_A = Intensity of the $[RCOO]^–$ fragment of A fatty acid
I_B = Intensity of the $[RCOO]^–$ fragment of B fatty acid
C_A = Correction factor for A fatty acid

As there are two A fatty acids in the AAB and ABA type TGs, their intensity is divided by two. Correction factor 1.00 was assigned to 18:0 and everything else was adjusted in relation to that. The first calculations were done using the TG 18:0_18:0 *sn*-2_X and TG 18:0_X *sn*-2_18:0 series, where the only unknown variable is the correction factor of B fatty acid. All correction factors could not be calculated using the FA 18:0 as a reference point. In such cases, for example FA 8:0, the calculations were performed using TG 16:0_8:0 *sn*-2_16:0 after the correction factor for 16:0 was established.

The TG regioisomers within the molecular species are subsequently calculated using the relative abundances of $[M–H–RCOOH–100]^-$ fragment ions using a similar optimization algorithm, considering the already determined TG molecular species composition and the fragmentation efficiency differential between the *sn*-2 and *sn*-1/3 positions. A discrimination factor, meaning the probability of a FA to be cleaved off from *sn*-2 position instead of *sn*-1/3 positions, was determined with ABA type TG standards as follows:

$$D = \frac{I_{M-B}}{I_{M-A} + I_{M-B}}$$

where:
$I_{M\text{-}A}$ = Intensity of the $[M–H–RCOOH–100]^-$ fragment resulting from loss of A fatty acid
$I_{M\text{-}B}$ = Intensity of the $[M–H–RCOOH–100]^-$ fragment resulting from loss of B fatty acid

An average discrimination factor of all analyzed TGs was used in further regioisomer calculations. AAB and ABA type TG standards were analyzed to test the accuracy of the calculations.

4.2.5 TG regioisomer analysis (UHPLC-MS^2 method)

4.2.5.1 TG regioisomer analysis

The UHPLC-MS^2 method (Tarvainen et al., 2019) for TG regioisomer analysis (**II**) utilized Acquity UHPLC coupled to Quattro Premier tandem mass spectrometer (Waters corp., Milford, MA, USA) with ESI source in positive ionization mode. A Waters Cortecs C18 column (150 mm × 2.1 mm, 1.6 µm particle size) with a Waters VanGuard C18 precolumn (1.6 µm particle size) was used for the separation of TGs. The mobile phase consisted of solvent A, which was methanol/water (1000:1, v/v) with ammonium acetate (10 mM), and solvent B, which was isopropanol/water (1000:1, v/v) with ammonium acetate (10 mM).

The column oven was held at 60 °C. A solvent gradient program was used with an initial composition of 99 % solvent A, which was changed linearly to 70 % solvent A in 30 min, then linearly to 50 % solvent A in 7 min, followed by isocratic 50 % A for 1 min, and then changed linearly to 30% A in 2 min, and changed back to 99 % A in 4 min, and finally isocratic until 50 min. Flow rate was set at 0.2 mL/min until 44 min, increased to 0.3 mL/min at 46 min and held at 0.3 mL/min for 4 min. The total analysis time was 50 min.

Capillary voltage was set at 4.9 kV, the cone voltage at 22 V, the extractor voltage at 6 V, and the RF lens voltage at 0.1 V. The source was held at 120 °C and the probe heater at 350 °C. Desolvation gas flow was set at 750 L/h and cone gas flow at 200 L/h. MS^2 product ion scans after CID at 35 eV were carried out with argon as the collision gas at a flow rate of 0.35 mL/min. Full scans of *m/z* 120-950, and MS^2 product ion scans of *m/z* 100-700 were acquired. For studying the human milk sample, the same 21 most abundant TG species that were analyzed with the direct inlet method were selected for analysis with the UHPLC-MS^2 method as well.

4.2.5.2 *TAG analyzer* software

The *TAG analyzer* calculation software used in conjunction with the UHPLC-MS^2 method was developed in the thesis work (**II**). A preliminary version of the calculation algorithm was first presented with another method utilizing lithium adduct $[M+Li]^+$ precursor ions (Kallio et al., 2017). However, due to issues of lithium salt precipitation within the LC-MS instrument, the method was not used further. Utilizing ESI on positive ionization mode and ammonium acetate in the mobile phase, the TGs are ionized as $[M+NH_4]^+$ ammonium adducts (**II**), avoiding precipitation issues. Fragmentation with CID produces high abundance of structurally informative DG fragments $[M+NH_4–RCOOH–NH_3]^+$ and a low abundance of FA ketene $[RCO]^+$ fragments.

The program works in two phases. The program first finds the candidate TGs consisting of specific fatty acid combinations that matches the ammonium adduct precursor ion. A TG is a candidate if corresponding DG and FA ketene fragments are found in the spectra. The result of the first phase is a list of candidate TGs that have appropriate fragments present in the spectra. In the second phase, the proportions of the regioisomers of the candidate TGs found in the first phase are calculated. The concentrations are mainly determined based on the DG fragments. The calculation is carried out based on recreating the DG fragment peaks in the spectrum based on a fragmentation model established with a wide range of calibration curves.

Before the candidate TGs are determined, preprocessing is done to enable matching the observed with the computed spectra. The spectra are first binned to integers within 1 Da (n-0.1, n+0.9) value so that each peak is mapped to values

representing the *m/z* ratios of the fragments. Due to low resolution of the used triple quadrupole instrument, if observed peaks are spaced within the range (n-0.1, n+0.9), they are summed up, meaning that they are considered to belong to the same *m/z* value. After the binning of the spectra, the candidate TGs can be found. The search space is formed by TGs containing fatty acids with even number (4–28) of carbon atoms and in addition fatty acids of length 15 and 17. The number of double bonds considered is determined by the length of the fatty acid in order to consider all realistic fatty acids.

The search is performed by looking at the possible fragments for each TG in the search space and checking if corresponding peaks are found in the observed spectra. If they are found, the TG is considered a candidate that is present in the spectra. A TG is considered to be found if the appropriate DG fragments and the FA ketene fragments have peaks above a user defined threshold. A fragmentation model has been developed that describes the probability that a fatty acid in each position of TG is detached. The fragmentation depends both on the relative lengths of the fatty acids and the number of double bonds in the *sn*-2 FA of the TG as described previously (Tarvainen et al., 2019).

The regioisomeric compositions of candidate TGs are determined by creating a synthetic fragment spectrum of the candidate TGs by adjusting the regioisomer abundances to produce a spectrum that matches the observed one. Only the DG fragments are used by default to calculate the regioisomer ratios since the DG fragments are produced in the most consistent and systematic manner. The synthetic spectra for each TG are obtained based on fragmentation model calibrated on a set of experiments with known concentrations of different TGs. All mixed FA TG standards used to establish the calibration model are listed in **Table 11**.

In the following equation, S_i denotes the spectra produced by the DG fragments of candidate TG $i \in 1 \ldots n$ where n is the number of candidate TGs:

$$S(mz) = \Sigma_{i \in C}\, c_i\, S_{i,DG}(mz)$$

To find the optimal set of TG regioisomer ratios that make the synthetic spectra match the observed one, the following optimization problem is solved to obtain the concentrations $c_1 \ldots c_n$ for TGs $1 \ldots n$:

$$\min_{c_1,\ldots,c_n} \Sigma_{mz}\big(S_0(mz) - S(mz)\big)^2$$

The sum of the square error of the difference in intensity value between the observed spectra S_0 and the calculated spectra S is minimized. This problem can be solved by numerical off-the-shelf optimization algorithms. The optimization problem above is based on the assumption that the fragmentation efficiency of a

TG into different DG and FA ketene fragments is known. The set of TGs with two or less different fatty acids, so called AAB/ABA pairs have been handled separately from those that contain three different fatty acids, ABC/ACB/BAC triplets. Conceptually they can be handled the same way. However, since AAB/ABA peaks give rise to two peaks instead of three, the precision of the analysis is increased when having a separate model for the two cases.

Only the above-mentioned optimization of the results was described in the published study (**II**) (Sazzad et al., 2022). Herein, also the established fragmentation model will be discussed in more detail. The fragmentation depends both on the relative lengths of the fatty acids and the double bonds in the different positions in the TG (Tarvainen et al., 2019). The developed fragmentation model describes the probability that a fatty acid in a given position is dissociated. To create a model the following features are derived for a TG *t*:

$x_{i,j} = |t_i| - |t_j|$ for all $i \in 1..3$, $j \in 1..3$ and $j \neq i$ where $|t_i|$ is the length of the fatty acid in position *i*.

$y_{i,j} = |d_i| - |d_j|$ for all $i \in 1..3$, $j \in 1..3$ and $j \neq i$ where $|d_i|$ is the number of double bonds in position *i*.

This gives the matrices $X(t) = \begin{bmatrix} x_{11} & x_{12} \\ x_{21} & x_{22} \\ x_{31} & x_{32} \end{bmatrix}$ and $Y(t) = \begin{bmatrix} y_{11} & y_{12} \\ y_{21} & y_{22} \\ y_{32} & y_{32} \end{bmatrix}$ for the positions 1..3 for TG *t*.

Fragmentation model has the form:

$$P(t) = C_{const} + C_x X + C_y Y + C_{x2} X^2 + C_{x3} X^3 + C_{y2} Y^{2/3},$$

where P_i ($i \in 1..3$) is the probability that the FA in position *i* is detached, *C* are the optimized parameters from TG standard data, and exponents of X and Y are results of trial and error producing the most accurate fragmentation model. The calibration takes advantage of the fact that for fragmentation of TGs is symmetric, that is, the TG ABC is the same as CBA. Hence, only one of the alternatives need to be considered and for all C, $C_{1i} = C_{3i}$.

This gives 22 parameters that need to be optimized against the calibration data. The calibration dataset for AAB/ABA type TGs consists of set of pairwise mixtures of DGs with known concentrations and known DG fragment ratios. For each AAB/ABA type TG each calibration data point consists of the TG pair t_{AAB}, t_{ABA}, the concentrations c_{AAB}, c_{ABA} and the fragment ratios p_{AA}, p_{AB}. For ABC/ACB/BAC type TGs the calibration datasets consist of mixtures of the three TGs with known concentrations combined with the associated DG fragment ratios p_{AB}, p_{AC} and p_{BC}.

The parameters *C* are determined by solving an optimization problem of fitting the model above to a calibration dataset. For each TG mixture of AAB/ABA type the difference of the observed fragmentation and the fragmentation obtained from the model is calculated:

$$E_{AA} = p_{AA} - \left(\frac{c_{AAB} P_3(t_{AAB})}{2} + \frac{c_{AAB} P_1(t_{BAA})}{2} + c_{ABA} P_2(t_{ABA}) \right)$$

$$E_{AB} = p_{AB} - \frac{c_{AAB}\left(P_1(t_{AAB}) + P_2(t_{AAB})\right)}{2} + \frac{c_{AAB}\left(P_2(t_{BAA}) + P_3(t_{BAA})\right)}{2} + \frac{c_{ABA}\left(P_1(t_{ABA}) + P_3(t_{ABA})\right)}{2}$$

The square errors *E* for each AAB/ABA type TG pair in the calibration dataset are then summed up and the following optimization problem is obtained:

$$\min_{C} \Sigma_i E_{i,AA}^2 + \Sigma_i E_{i,AB}^2$$

That is, the parameters *C* are optimized to make the fragmentation model match the observed fragmentation as close as possible.

The error for ABC/ACB/BAC type TGs is calculated the same way, but in this case, there are three DG fragments to consider:

$$E_{AB} = p_{AB} - \frac{c_{ABC}\left(P_3(t_{ABC}) + P_1(t_{CBA})\right)}{2} + \frac{c_{ACB}\left(P_2(t_{ACB}) + P_2(t_{BCA})\right)}{2} + \frac{c_{BAC}\left(P_3(t_{BAC}) + P_1(t_{CAB})\right)}{2}$$

$$E_{AC} = p_{AC} - \frac{c_{ABC}\left(P_2(t_{ABC}) + P_2(t_{CBA})\right)}{2} + \frac{c_{ACB}\left(P_3(t_{ACB}) + P_1(t_{BCA})\right)}{2} + \frac{c_{BAC}\left(P_1(t_{BAC}) + P_3(t_{CAB})\right)}{2}$$

$$E_{BC} = p_{BC} - \frac{c_{ABC}\left(P_1(t_{ABC}) + P_3(t_{CBA})\right)}{2} + \frac{c_{ACB}\left(P_1(t_{ACB}) + P_3(t_{BCA})\right)}{2} + \frac{c_{BAC}\left(P_2(t_{BAC}) + P_2(t_{CAB})\right)}{2}$$

The optimization problem to determine the parameters *C* is obtained in the same was as for AAB/ABA type TGs:

$$\min_{C} \Sigma_i (E_{i,AB}^2 + E_{i,AC}^2 + E_{i,BC}^2)$$

Trust-Region Constrained Algorithm (Byrd et al., 1999) from the open-source Python library SciPy (Virtanen et al., 2020) has been used.

4.2.6 PL molecular species and regioisomer analysis

For PL regioisomer analysis, a direct infusion (**III**) and two different chromatographic methods, including a HILIC (**III**) and RP (**IV**), were employed. The same data-dependent MS^2 acquisition method (**III**, **IV**) was used for both chromatographic systems, whereas targeted product ion scan method was used with direct infusion.

4.2.6.1 Hydrophilic interaction liquid chromatography

The HILIC system (**III**) consisted of a Cortecs UPLC HILIC column (2.1 × 150 mm, 1.6 µm particle size; Waters Corp.) and an Elute HPG 1300 pump unit (Bruker Corp., Billerica, MA, USA). The binary solvent gradient consisted of (A): water/acetonitrile (80:20, v/v) with 5 mM ammonium formate and (B): acetonitrile/water (95:5, v/v) with 5 mM ammonium formate. A stock solution of 100 mM ammonium formate in water (pH 3.0, adjusted with formic acid) was used when preparing the mobile phase solvents.

The mobile phase gradient was as follows: initial solvent composition was 6 % A, 6 to 9 % A (0–20 min), 9 to 20 % A (20–40 min), 20 to 70 % A (40–41 min), held at 70 % A (41–48 min), 70 to 6 % A (48–49 min) and held at 6 % A (49–65 min). Total solvent flow rate was 0.15 mL/min from 0 to 41 min, then changed to 0.3 mL/min during the column flushing and equilibration phase from 41 to 62 min and changed back to 0.15 mL/min at 62 min before the next injection. Column oven temperature was maintained at 25 °C.

4.2.6.2 Direct infusion

Direct infusion of the PL standards (**III**) was performed using a Model 300 syringe pump (New Era Pump Systems, Farmingdale, NY, USA) with a T-split connecting the syringe pump flow to the LC mobile phase flow. The syringe pump flow was set at 5 µL/min and the LC flow rate at 0.15 mL/min 15 % A and 85 % B of the same mobile phase solvents as with the HILIC method.

4.2.6.3 Reversed phase chromatography

The reversed phase system (**IV**) consisted of an Acquity Premier BEH C18 (2.1 × 150 mm, 1.7 µm particle size; Waters Corp) column equipped with a Vanguard FIT column guard and a Bruker Elute HPG 1300 pump unit (Bruker Corp.). The binary solvent gradient consisted of (A) water and (B) isopropanol/acetonitrile/water (50:45:5, v/v), both with 10 mM ammonium formate and 0.1 % formic acid added.

The mobile phase gradient was as follows: initial solvent composition was 35 % B, 35 to 85 % B (0–2 min), 85 to 99 % B (2–15 min), held at 99 % B (15–20 min), 99 to 35 % B (20–21 min) and held at 35% B (21–28 min). Total solvent flow rate was 0.4 mL/min and the column oven temperature was maintained at 60 °C.

4.2.6.4 MS^2 analysis

MS^2 analyses for PL regioisomer calculations (**III**, **IV**) were performed with an Impact II quadrupole time-of-flight (QTOF) tandem mass spectrometer (Bruker Corp.) using an electrospray ionization source on negative polarity. The capillary voltage was set at 3500 V and the end plate offset at 500 V. The nebulizer gas pressure was set at 2 bar, drying gas flow rate at 8 L/min and drying gas temperature was at 300 °C. The collision energy was set at 40 eV for all studied samples.

For direct infusion analyses (**III**), targeted product ion scans were used for the selected precursor ions of the PL reference standards and the fragment data was recorded from a 10 s window after the syringe pump flow had stabilized.

For the UHPLC-MS^2 analyses with both HILIC (**III**) and RP (**IV**), a non-targeted data-dependent acquisition (DDA) MS^2 method was used, which selects precursor ions for fragmentation when the intensity exceeds a set threshold. The precursor ion intensity threshold for fragmentation was set at 600 counts, which was slightly above background noise levels. The maximum number of simultaneous product ion scans was set at five, meaning that the system prioritizes fragmentation of the five most abundant ions at any given time. MS scan time was 0.25 s and MS^2 total cycle time for five consecutive scans was 1.4 s.

4.2.6.5 PL molecular weight distribution

The monoacid PC standards consisting of PC 12:0/12:0, PC 14:0/14:0, PC 14:1/14:1, PC 16:0/16:0, PC 16:1/16:1, PC 18:0/18:0, PC 18:1/18:1, PC 18:2/18:2, PC 18:3/18:3 and PC 20:0/20:0 were used to determine the detector response between different PCs of varying FA compositions. The equimolar

mixture consisted of each PC compound at 20 µM concentration. The analysis was performed with the RP method (**IV**).

4.2.6.6 PL regioisomer calculations with calibration curves

Five mixtures of the PL regioisomer pairs at different ratios (100:0, 75:25, 50:50, 25:75 and 0:100) were prepared in order to construct the calibration curves. Calibration curves (**III**) were established with PL regioisomer pairs listed in **Table 12** using the deprotonated FA $[RCOO]^-$ fragment ion ratios. Additionally, another set of calibration curves (**III**) was established with the lysophospholipid-like $[M+HCOO–RCOOH–42]^-$, $[M–H–RCOOH]^-$ and $[M–H–RCOOH–87]^-$ fragments for PC, PE, and PS, respectively.

To test the accuracy of the calibration curves and calculations, mixtures of PL regioisomers at 60/40 % ratios were analyzed (**III**). In order to expand the calibration data (**IV**), additional individual PC standards were analyzed in addition to the regioisomer pairs (**Table 12**).

4.2.6.7 Algorithmic calculation of PL regioisomers

A calculation software for PL regioisomers was developed in this work. The algorithms of the software are described in detail in **Study IV** (Fabritius et al., 2023, unpublished manuscript). In current work, the accurate analysis of regioisomer ratios is optimized for PC class only, but the software can also qualitatively identify PE, PI and PS molecular species. Briefly, a data preprocessing script for exporting all DDA event information was first created using the Bruker Data Analysis software. The script creates .csv files of each DDA event containing the fragment spectra of each compound. A separate compound table containing the retention time, peak area, and precursor ion m/z of each DDA event is also created.

The software then goes through the compound table and looks for precursor ions that match specific adducts of PL species. If a match is found within a specified *m/z* threshold, the software searches relevant FA $[RCOO]^-$ ions from the fragment spectra. Detection of matching $[RCOO]^-$ fragments leads to identification of the PL molecular species. For analysis of regioisomers, the software uses a fragmentation model influenced by the carbon chain lengths and numbers of double bonds in the FAs. The preliminary molecular species identification tells the software what parameters to use in the fragmentation model. The fragmentation model was calibrated with all mixed FA PC standards listed in **Table 12**.

Using the peak area, the software can determine the PL species abundance. Correction factors for various PC species were determined with an equimolar mixture of PC standards. The current version of the software does not yet include

the correction factors, and they were manually applied to the results afterwards. The molecular species abundance within each species is calculated using the relative abundances of $[RCOO]^-$ fragment pair abundances. Thus, the software can calculate the results at three levels of depth in structural information: PL species, molecular species and regioisomers.

5 RESULTS AND DISCUSSION

5.1.1 FA composition

A total of 37 different FAs were identified in the human milk, bovine milk, and infant formula samples (**I**). The most abundant FAs are displayed in **Figure 17**. Considering that human milk FA composition varies depending on the mother's diet (Much et al., 2013; Tian et al., 2019) as evidenced by the differences in Finnish and Chinese human milk samples, most studied infant formulas were good at mimicking the human milk FA composition.

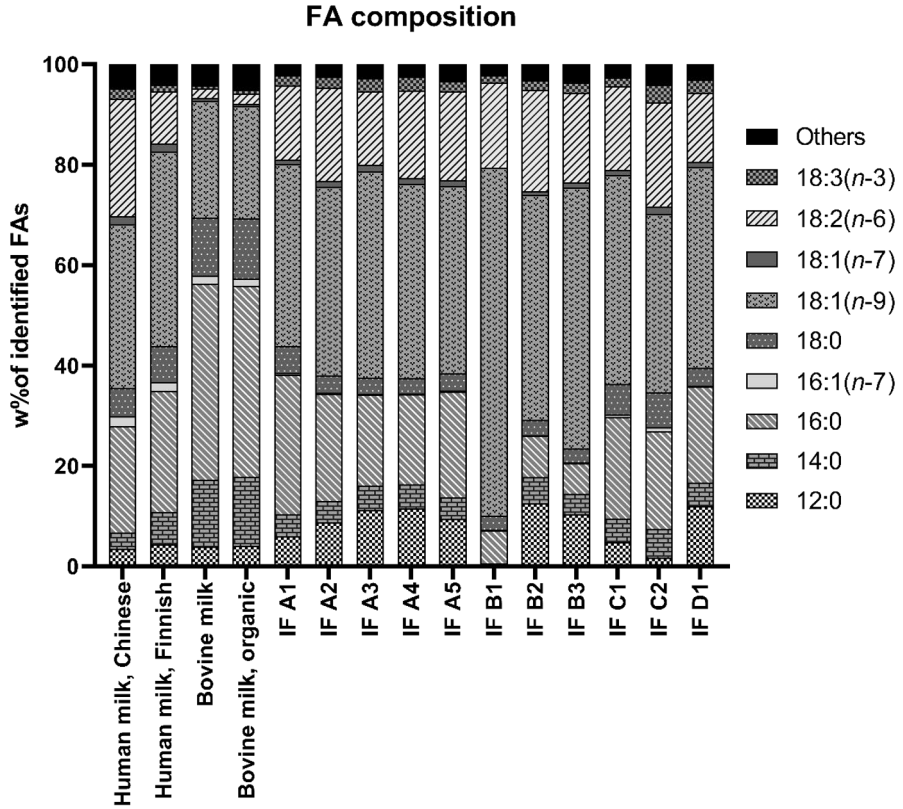

Figure 17 Identified FAs in the human milk, bovine milk, and infant formula samples (**I**)

Category A (fat mainly from palm oil, rapeseed oil), C (rapeseed oil, sunflower oil) and D (modified vegetable oil, rapeseed oil) infant formulas were fairly similar, with the main difference being the varying amount of 12:0. Within category A, the IF A1 was slightly different compared to IF A2-A5, likely due to the soy oil in addition to the palm oil, rapeseed oil, and coconut oil. Amount

of 18:1(*n*-9) in category B (sunflower oil, rapeseed oil) infant formulas was higher than the others, especially in IF B1. Bovine milk samples were significantly different compared to human milk, containing more 16:0, 14:0 and 12:0. It is worth noting that the GC-FID method was not able to resolve FAs at ACN 8 or below, which likely resulted in slightly distorted results, especially for bovine milk samples as they are known to contain short chain FAs (Yao et al., 2016; Zou et al., 2013).

5.1.2 TG molecular weight distribution

The molecular weight distribution of TGs (**I**) was analyzed with different ionization parameters compared to the regioisomer analysis. In the initial method development, low ion source temperature (100 °C) produced the highest abundance of $[M–H]^-$ ions used in calculating the corresponding ACN:DB abundances. However, the low temperature combined with high sample concentrations caused rapid contamination of the ion source. Ultimately, the low temperature was only used for the molecular weight distribution analysis, while the following regioisomer analyses were performed with much higher ion source temperature (340 °C) to significantly reduce ion source contamination and improve reproducibility.

Using Tukey test and Levene's test with Origin 2016 software (OriginLab, Northampton, MA, USA), analysis of the equimolar mixture of eight TGs ranging between ACN 30-54 (**I**) resulted in no statistically significant differences between the abundances of $[M–H]^-$ ions (**Figure 18a**). This was surprising, because with the older generation direct inlet method (Kallio & Rua, 1994; Kurvinen et al., 2002) and other methods (Linderborg et al., 2014) it has been reported that the ionization is affected by the ACN:DB value. However, in addition to the eight TGs with similar ionization, there was one outlier, TG 8:0/8:0/8:0 (TG 24:0), which had higher intensity compared to the others. The possibility of a dilution error was checked, but the higher intensity remained. Ultimately, the TG 24:0 was treated as an outlier and not included in the study, as this molecular weight range was not relevant for the studied sample material. No correction factors were used for molecular weight distribution analysis (**I**).

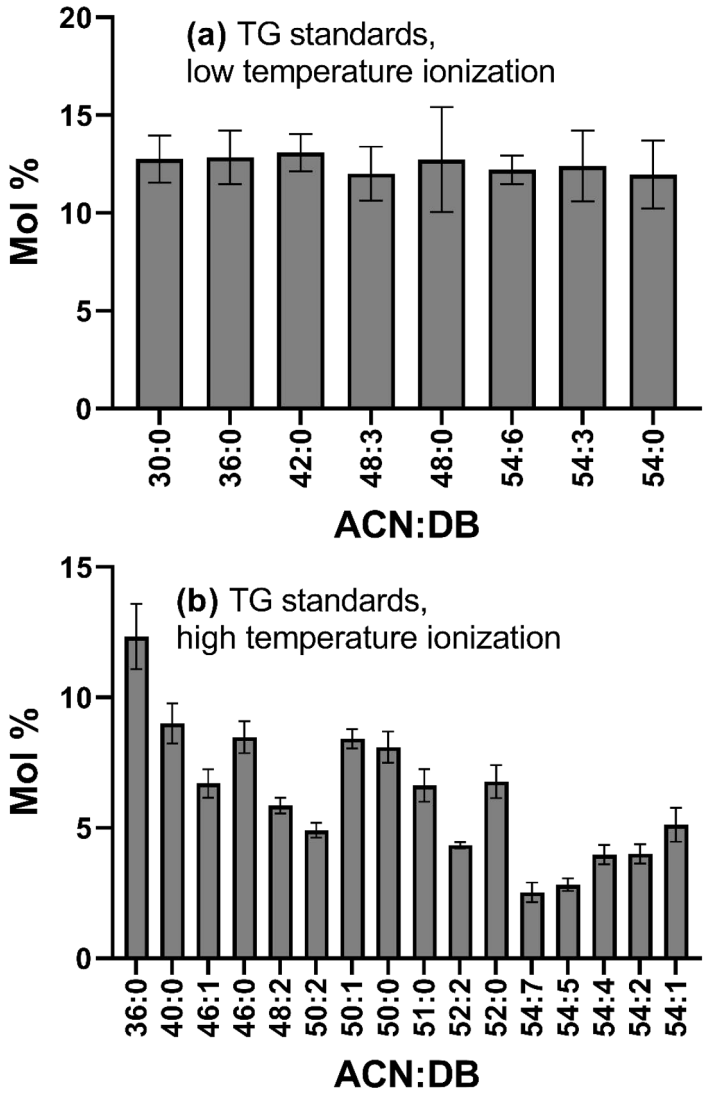

Figure 18 Measured molar proportions of two equimolar TG standard mixtures with the low-temperature (100°C) **(a)** and high-temperature (340 °C) **(b)** ionization methods.

An example of the molecular weight distribution analysis with 21 most abundant TG species in human milk is displayed in **Table 14** along with comparisons to the same TG species found in bovine milk and infant formulas. It is evident that the molecular weight distribution of human milk samples is different compared to bovine milk and infant formulas, highlighting the fact that

Table 14 TG molecular weight distribution of infant formula, bovine milk, and human milk samples (**I**)

	ACN:DB																				
Sample	**44:2**	**44:1**	**46:1**	**46:0**	**48:3**	**48:2**	**48:1**	**50:4**	**50:3**	**50:2**	**50:1**	**52:5**	**52:4**	**52:3**	**52:2**	**52:1**	**54:6**	**54:5**	**54:4**	**54:3**	**54:2**	Others[a]
Human milk, Chinese	1.2	2.0	2.5	1.0	1.8	2.6	1.5	1.1	2.2	3.7	3.1	1.3	5.5	11.0	10.4	2.9	1.8	4.2	4.3	3.5	1.3	30.9
Human milk, Finnish	1.1	3.0	3.4	1.3	1.5	3.4	3.4	0.7	2.2	4.7	4.3	0.6	2.3	6.7	12.2	3.8	0.8	1.6	3.3	4.1	1.7	34.0
Bovine milk	0.7	2.0	1.7	1.7	0.0	0.9	2.5	0.0	0.4	1.2	2.7	0.0	0.0	0.7	1.8	1.4	0.0	0.0	0.2	0.6	0.7	80.6
Bovine milk, organic	0.7	1.9	1.7	1.6	0.3	0.8	2.3	0.2	0.4	1.1	2.1	0.0	0.2	0.5	1.5	1.1	0.0	0.0	0.2	0.5	0.6	82.4
IF A1	0.3	0.7	0.7	0.6	0.0	0.7	1.3	0.0	0.5	3.9	7.7	0.5	2.9	5.6	10.0	2.9	2.6	3.4	6.8	5.3	3.6	40.1
IF A2	0.3	0.4	0.5	0.3	0.2	0.6	0.6	0.2	0.4	3.0	10.6	0.6	2.3	4.6	8.4	2.2	3.1	6.4	4.7	8.9	1.8	39.8
IF A3	0.2	0.5	0.4	0.3	0.0	0.3	0.6	0.0	0.4	4.0	6.0	0.3	1.5	2.9	7.3	3.3	2.7	7.0	10.4	13.6	1.0	37.2
IF A4	0.2	0.6	0.5	0.4	0.0	0.4	0.6	0.3	0.5	3.3	6.2	0.0	2.4	3.2	8.4	2.1	3.9	5.0	6.8	14.0	0.8	40.3
IF A5	0.2	0.4	0.4	0.2	0.2	0.4	0.6	0.0	0.4	3.6	6.6	0.5	1.9	3.7	7.2	4.1	3.8	7.7	7.8	10.4	2.9	37.1
IF B1	0.2	0.4	0.0	0.0	0.0	0.0	0.0	0.1	0.2	0.6	2.0	0.4	2.2	2.6	8.4	1.5	3.6	7.3	10.4	40.3	3.3	16.6
IF B2	0.3	0.6	0.4	0.2	0.2	0.4	0.3	0.2	0.3	0.6	0.8	0.7	2.7	2.4	3.9	0.5	4.5	8.3	7.8	21.2	2.4	41.5
IF B3	0.2	0.5	0.3	0.2	0.0	0.2	0.2	0.1	0.2	0.3	0.5	0.3	1.4	2.2	5.5	0.6	5.1	6.7	9.3	23.4	4.6	38.4
IF C1	0.4	0.7	0.7	0.7	0.0	0.6	0.9	0.0	0.5	2.4	6.2	0.3	1.8	4.7	6.3	1.5	4.1	5.5	5.3	14.2	3.4	39.6
IF C2	0.6	1.5	1.2	1.1	0.2	0.8	1.6	0.1	0.4	1.2	2.1	0.4	1.7	1.5	2.8	1.3	4.9	7.0	5.8	6.4	1.4	56.0
IF D1	0.3	1.0	0.8	0.3	0.0	0.6	0.8	0.1	0.4	1.7	7.6	1.0	2.5	4.8	10.8	3.7	2.8	5.8	7.5	7.4	3.6	36.6

[a] Other TG species not included in the 21 selected ACN:DB species.

while total FA compositions (**Figure 17**) might be similar, the TG compositions can be notably different. For example, ACN 54 species are the most abundant ones in infant formulas. In contrast, ACN 52 species are the most abundant in human milk samples, and overall, the TGs are more evenly distributed between ACN 44-54. The molecular weight distribution of bovine milk was significantly different with low abundances of TG between ACN 50-54, while most were concentrated in the lower range of ACN 30-40.

As the low-temperature ionization was not ideal for frequent, high-throughput analyses due to the contamination issues, additional validation was later performed (not included in the published studies of this thesis) to investigate suitability of higher ionization temperature for the molecular weight analysis. In contrast to the low temperature method, with a high temperature of 340 °C there were immediately noticeable differences between the various TG standards of an equimolar mixture (**Figure 18b**). Two distinct factors influencing the molecular ion abundances were observed: TGs with lower ACN were overrepresented and TGs with high DB number were underrepresented. Based on this experimental information, correction factors for various ACN:DB species were extrapolated (**Figure 19**). Correction factor 1.00 was set for TG 36:0, and everything else was adjusted in relation to this.

The experimentally measured correction factors in **Figure 19** are shown next to the extrapolated values. Based on this selection of 16 TG standards, the correction factors increased as the DB number increased, and decreased as the ACN decreased. Out of the 16 analyzed standards, there were only a few exceptions that did not follow the same pattern as well as the others, for example 50:1 and 54:4. Overall, the pattern was clear enough to justify using the extrapolated correction factors. Subsequently, molar proportions of the TG mixture were recalculated using the extrapolated correction factors. As an equimolar mixture, the molar proportion of each of the 16 TGs should be 6.25 mol%. **Figure 20** shows that after correction the calculated molar ratios are much closer to actual ratios than before correction.

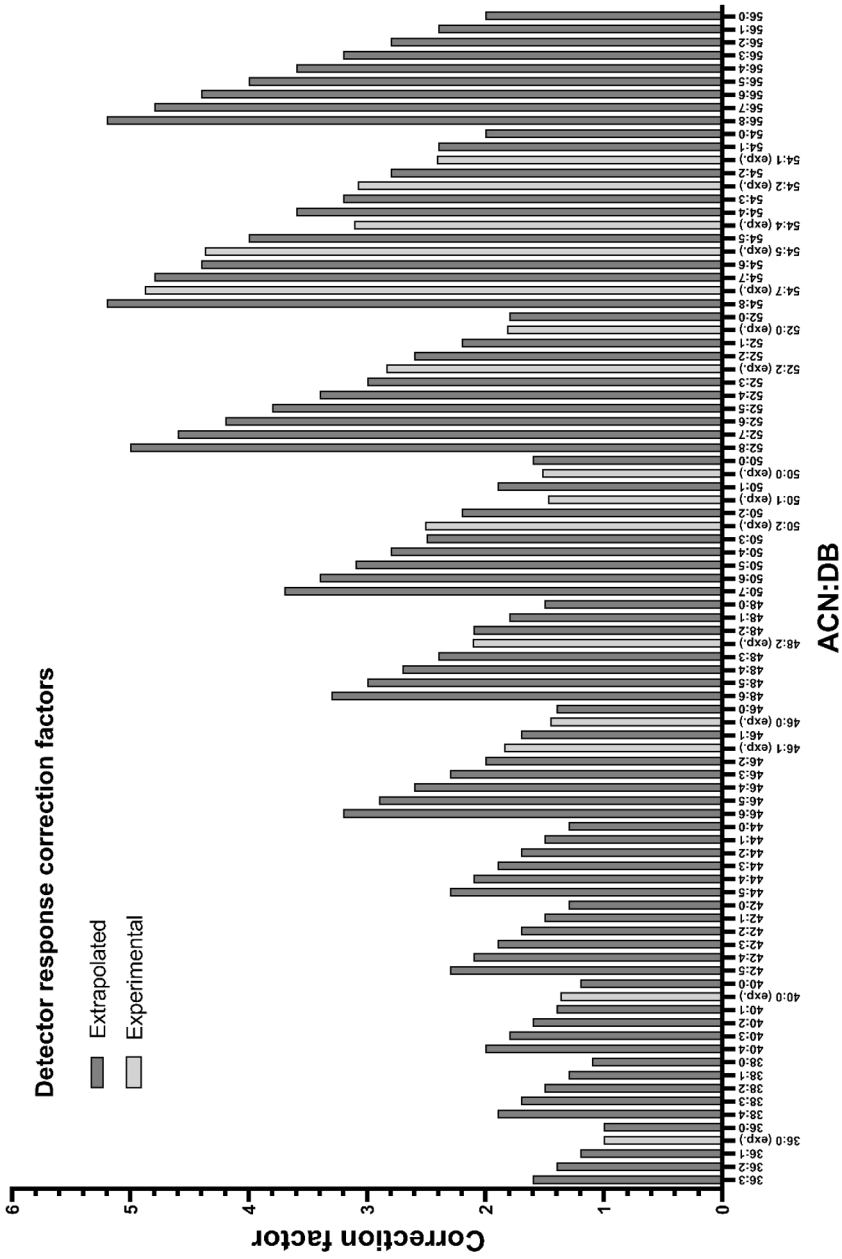

Figure 19 Experimental (exp.) and extrapolated correction factors for TG molecular weight distribution analysis

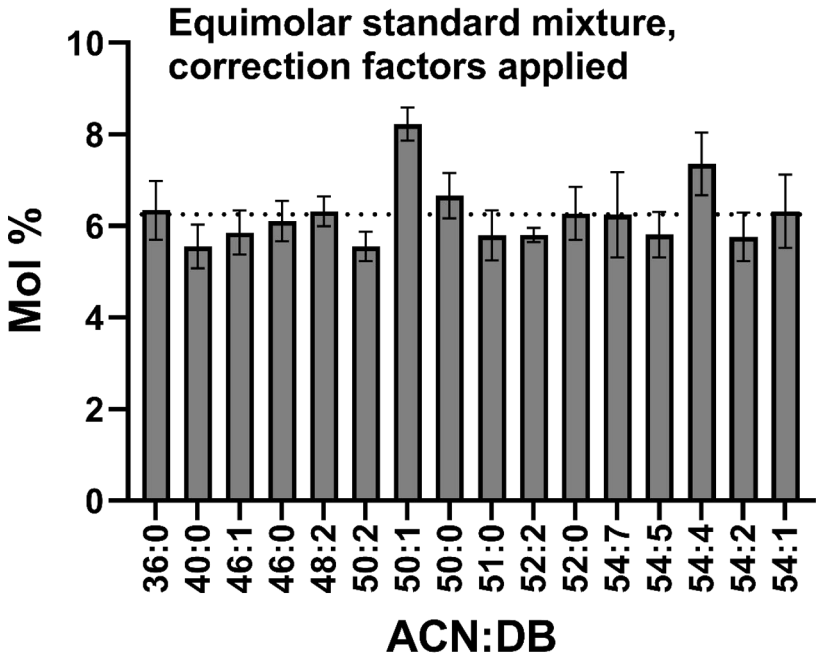

Figure 20 Calculated molar proportions of the equimolar TG standard mixture using extrapolated correction factors. The dotted line indicates the actual molar proportion (6.25 mol%)

The drastic differences in ionization efficiencies between the two temperatures could be explained by the amount of in-source fragmentation. Ideally, equimolar compounds with perfect ionization and no in-source fragmentation would produce similar signal response. With the lower 100 °C ion source temperature, there does not seem to be significant in-source fragmentation or thermal decomposition, resulting in similar detector response. With the high 340 °C ion source temperature, however, the TGs with longer acyl chains and more double bonds likely decompose easier due to the harsh ionization conditions, resulting in different detector response for each compound.

To test the influence of the new correction factors with a real sample using the high-temperature method, the Chinese human milk sample was reanalyzed. **Figure 21** shows a comparison of both the response-corrected and uncorrected results using the high-temperature method (unpublished) as well as the uncorrected results from the low temperature method (**I**)

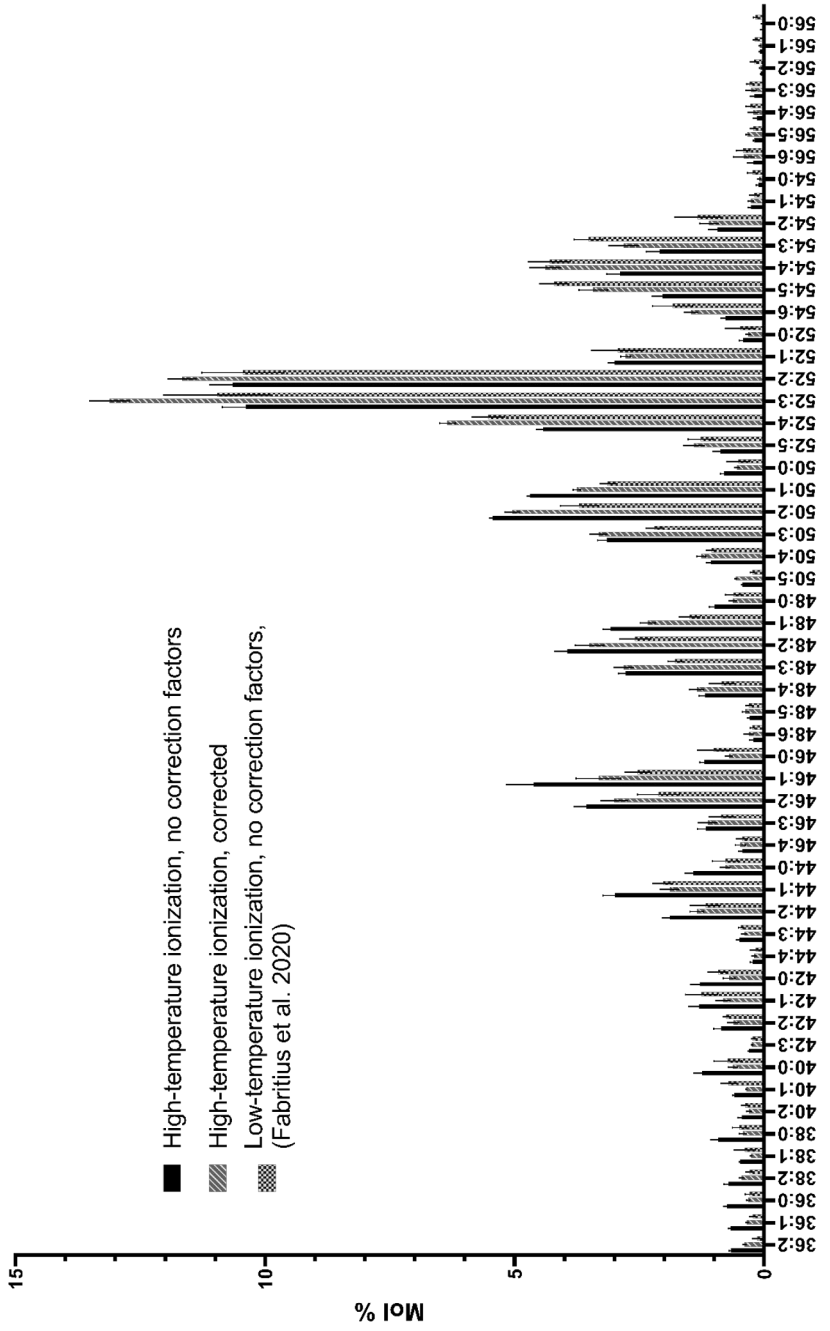

Figure 21 Comparison of the molecular weight distribution in Chinese milk sample using three different methods

While the overall profile of the molecular weight distribution in each case looks comparable, there are some noticeable differences. In the uncorrected high-temperature method the lower-mass TGs are proportionally more abundant compared to the other two methods, whereas the higher-mass TGs are less abundant. The results of the low-temperature method and corrected high-temperature method are fairly similar in most cases. Going further, only the high-temperature method with correction factors should be used in later studies due to the practicalities related to instrument performance and frequency of cleaning. Hundreds of samples can be analyzed with the high-temperature method without any meaningful degradation of signal intensity, whereas with the low-temperature method daily cleaning of the ion source was required.

5.1.3 TG regioisomer calculations

5.1.3.1 *MSPECTRA* software

Utilizing the deprotonated FA fragment ions $[RCOO]^-$, the initial determination of the TG molecular species composition within the selected ACN:DB is useful for setting boundaries for the subsequent regioisomer calculations. When the FA combinations of the molecular species and their abundances are known, there are less options for the regioisomer optimization algorithm to consider, possibly resulting in more accurate results than without initial molecular species composition analysis.

For accurate analysis of the preliminary molecular species composition, correction factors for the fragmentation efficiencies of the deprotonated FA fragment $[RCOO]^-$ ions are required. The relative abundance of the $[RCOO]^-$ fragments decreased as the length of the acyl chain decreased and number of double bonds increased, requiring higher correction factors (**Table 15**). Correction factors for 10:0 and 16:1 were extrapolated.

For regioisomer analyses utilizing the $[M–H–RCOOH–100]^-$ fragment ions, the average discrimination factor of 10 ABA type TGs was 13.9 %, meaning that on average, roughly 14 % of the observed $[M–H–RCOOH–100]^-$ fragments are resulting from a loss of FA from *sn*-2 position. *MSPECTRA* software takes this into account when optimizing the regioisomer abundances. Discrimination factors for individual TG standards varied between 9-17 %. Using a single, universal discrimination factor for all TGs is likely not ideal, as the fragmentation is known to be affected by the nature of the attached FAs (Gakwaya et al., 2007; Judge et al., 2017; X. Li & Evans, 2005; Tarvainen et al., 2019).

Table 15 FA correction factors for the initial TG molecular species composition determination with *MSPECTRA* software (**I**)

Fatty acid	Correction factor
8:0	4.16
10:0	3.50[a]
12:0	2.78
14:0	2.38
16:0	1.44
16:1	1.70[a]
18:0	1.00
18:1	1.33
18:2	1.56
18:3	1.80

[a] Extrapolated

Results for mixtures of 16 AAB/ABA type TG regioisomer pairs are shown in **Table 16**, showing the accuracy of the *MSPECTRA* calculation software. Despite the software using only a single discrimination factor for all TGs, the results were mostly accurate. However, higher deviations from the actual concentrations were observed with polyunsaturated TGs containing 18:3 or more than one 18:2 FAs, suggesting that establishing additional discrimination factors for TG species with higher degree of unsaturation might be useful to increase the accuracy of the calculations. Other than that, no clear trends affecting the results were observed. Overall, while the results for TGs with polyunsaturated FAs are more skewed than the others, the software is still useful for comparing their differences between samples.

Table 16 Analysis of TG standards at various regioisomer ratios using the *MSPECTRA* software (**I**)

	TG 1 abundance in pair (%)				
TG regioisomer 1	**100**	**75**	**50**	**25**	**0**
TG 14:0_14:0 *sn*-2_18:1	99.6 ± 0.8	76.2 ± 6.4	47.9 ± 7.6	25.0 ± 5.1	1.1 ± 2.2
TG 16:0_16:0 *sn*-2_14:0	97.6 ± 4.9	77.5 ± 10.3	41.3 ± 3.9	24.0 ± 4.7	0.6 ± 1.2
TG 16:0_16:0 *sn*-2_18:0	94.3 ± 3.5	77.6 ± 5.7	43.3 ± 4.4	22.5 ± 13.1	1.5 ± 3.1
TG 16:0_16:0 *sn*-2_18:1	91.7 ± 3.3	65.8 ± 3.8	40.7 ± 8.5	17.5 ± 4.0	0.0 ± 0.0
TG 16:0_16:0 *sn*-2_18:2	100.0 ± 0.0	85.2 ± 13.8	56.3 ± 6.5	35.3 ± 6.5	6.8 ± 4.6
TG 18:0_18:0 *sn*-2_18:1	95.0 ± 5.7	67.8 ± 5.2	46.4 ± 4.7	19.1 ± 3.3	1.2 ± 1.2
TG 18:0_18:0 *sn*-2_18:2	99.7 ± 0.6	90.1 ± 5.3	62.4 ± 5.5	36.4 ± 3.2	9.2 ± 2.6
TG 18:1_18:1 *sn*-2_12:0	99.1 ± 1.9	76.5 ± 6.8	45.6 ± 5.2	25.8 ± 4.9	0.0 ± 0.0
TG 18:1_18:1 *sn*-2_14:0	99.8 ± 0.3	80.4 ± 7.6	67.4 ± 7.7	28.0 ± 6.7	1.2 ± 1.7
TG 18:1_18:1 *sn*-2_16:0	100.0 ± 0.0	80.0 ± 11.7	60.9 ± 1.2	38.7 ± 6.7	9.0 ± 9.3

	TG 1 abundance in pair (%)				
TG regioisomer 1	**100**	**75**	**50**	**25**	**0**
TG 18:1_18:1 *sn*-2_18:0	99.3 ± 1.3	76.0 ± 4.5	39.1 ± 5.1	19.8 ± 3.8	0.0 ± 0.0
TG 18:1_18:1 *sn*-2_18:2	100.0 ± 0.0	80.6 ± 9.2	47.8 ± 4.5	29.3 ± 7.4	6.0 ± 3.8
TG 18:1_18:1 *sn*-2_18:3	100.0 ± 0.0	99.1 ± 1.8	76.4 ± 4.8	50.0 ± 3.5	28.2 ± 1.4
TG 18:2_18:2 *sn*-2_16:0	83.6 ± 9.9	62.7 ± 4.4	39.2 ± 7.6	19.5 ± 1.3	0.0 ± 0.0
TG 18:2_18:2 *sn*-2_18:1	82.4 ± 5.0	53.6 ± 9.0	23.8 ± 4.7	5.3 ± 5.8	0.1 ± 0.2
TG 18:2_18:2 *sn*-2_18:3	100.0 ± 0.0	100.0 ± 0.0	87.2 ± 2.9	54.9 ± 4.7	18.7 ± 4.2

One of the limitations of the direct inlet chemical ionization MS method is that in the lower ACN:DB range, starting from ACN 40 and below, sometimes the $[RCOO]^-$ and $[M–H–RCOOH–100]^-$ fragments overlap in the product ion spectra. This means that neither the preliminary molecular species nor regioisomer abundances can be calculated when one of the fragment ion peaks consists of both fragment types. The problem is illustrated in **Figure 22**, displaying the fragment spectrum of TG 10:0_10:0 *sn*-2_18:1 (ACN:DB 38:1). In this case, the observed *m/z* 281.33 fragment ion is a product of two different fragment types, making it impossible to calculate the regioisomer ratios.

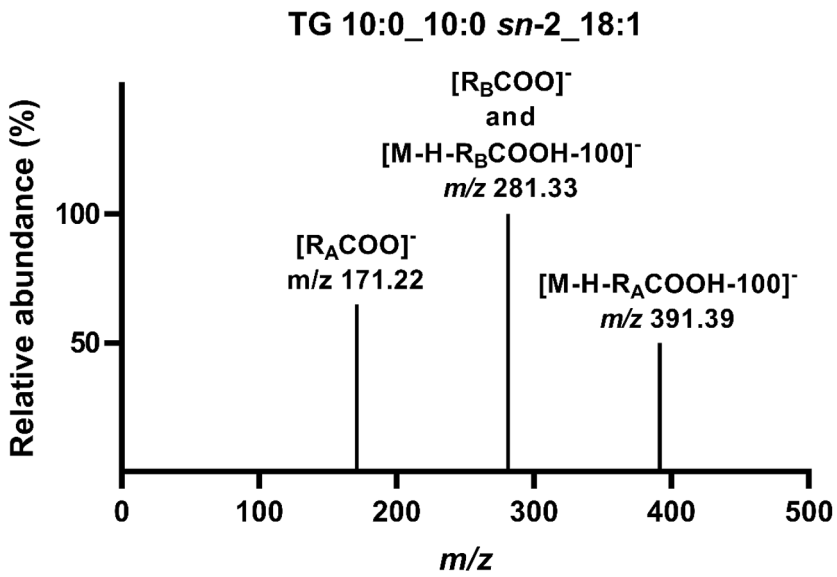

Figure 22 Example of overlapping $[RCOO]^-$ and $[M–H–RCOOH–100]^-$ fragments of TG 10:0_10:0 *sn*-2_18:1 (AAB type), preventing regioisomer calculations (**I**).

For analysis of human milk regioisomer composition (**I**), this problem was not significant as the TGs are mostly above ACN 40. However, the opposite is true for bovine milk, as the TGs are mainly concentrated at below ACN 40. For the purposes of the first study (**I**), the method was suitable, because the ACN:DB species of interest (**Table 14**) were selected based on high abundance in human milk, and no overlapping issues were encountered in ACN 44-54 range.
Selection of precursor ions was performed within a range of m/z ±0.5 of the theoretical *m/z* value of the molecular TG ion. For our triple quadrupole mass spectrometer this range was broad enough to allow acceptable sensitivity but narrow enough not to select adjacent monoisotopic TGs spaced 2 Da apart from one another. As a direct inlet method without chromatographic separation, the M+2 isotopes of a TG species with one more double bond always cause minor interference in the fragment pattern. In most cases of high abundance TGs, the interference is relatively low. However, when the ACN:DB species selected for analysis is of low abundance, and the adjacent species with one more double bond is of high abundance, the interference can be noticeable. For example, ACN:DB 54:2 results being interfered by M+2 isotopes of ACN:DB 54:3 in many of the infant formula samples as the ACN:DB 54:3 is significantly more abundant (**Table 14**).

An example of the effect of M+2 isotope interference with reference standards TG 16:0_16:0 *sn*-2_18:1 and TG 16:0_16:0 *sn*-2_18:0 is shown in **Figure 23**. As TG 16:0_16:0 *sn*-2_18:1 (*m/z* 831.8) has one more double bond, the M+2 isotope overlaps with the monoisotopic ion of TG 16:0_16:0 *sn*-2_18:0 (*m/z* 833.8). With a mixture of TG 16:0_16:0 *sn*-2_18:1 and TG 16:0_16:0 *sn*-2_18:0 (1:1), the M+2 isotope represents 16.2 % of the observed *m/z* 833.8 peak (**Figure 23a)** in MS scan. With another mixture of 9:1 ratios, respectively, the M+2 isotope represents 66.1 % of the observed *m/z* 833.8 peak, showing very significant isotopic overlap (**Figure 23b**). *MSPECTRA* software corrects the isotopic abundances when calculating the molecular weight distribution.

MS^2 product ion scans, however, are more susceptible to the isotope interference, as the software has no way of knowing if the observed fragments are coming from the targeted monoisotopic molecular ion, or M+2 isotope of the adjacent TG. **Figure 23c-d** show the product ion scans of the same 1:1 and 9:1 mixtures, respectively, both targeting the TG 16:0_16:0 *sn*-2_18:0 precursor ion *m/z* 833.8. In both mixtures, fragments *m/z* 281.3 and 451.5 are observed, related to loss of FA 18:1 from the TG. The intensities are fairly minor in the 1:1 mixture, but much more noticeable in the 9:1 mixture. Furthermore, what cannot be seen are the abundances of FA 16:0 $[RCOO]^-$ and $[M–H–16:0–100]^-$ ions fragmented from the M+2 isotope of TG 16:0_16:0 *sn*-2_18:1, as they are overlapping with the same fragments of TG 16:0_16:0 *sn*-2_18:0. This can distort the results of regioisomer calculations.

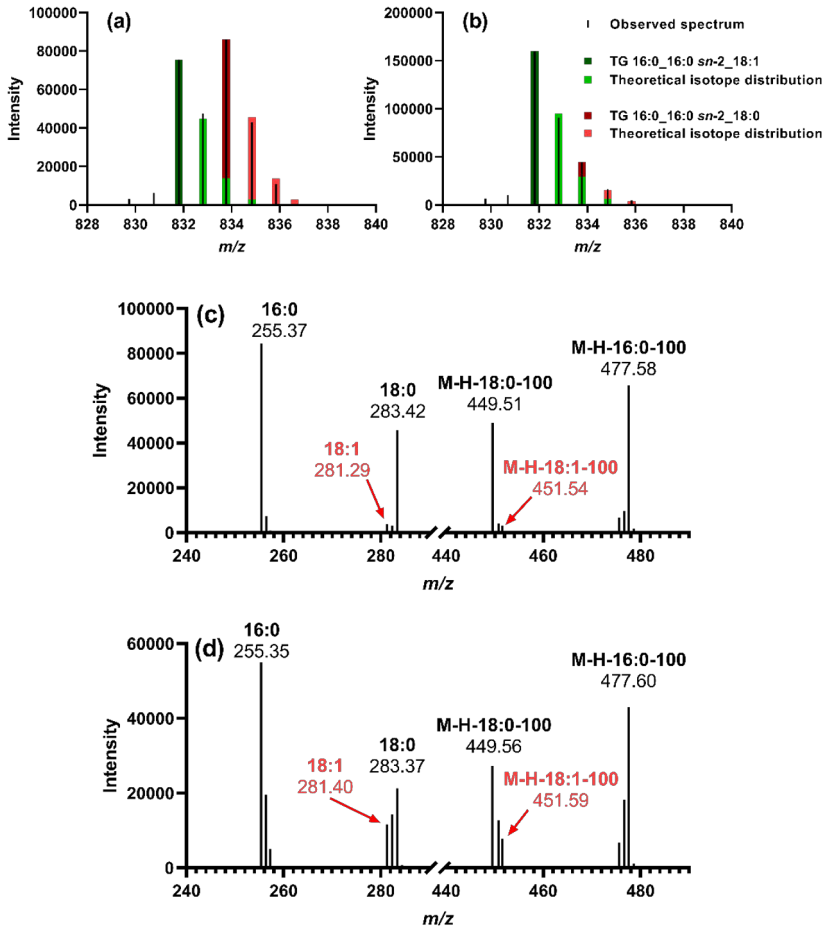

Figure 23 Analysis of TG 16:0_16:0 *sn*-2_18:1 (*m/z* 831.8) and TG 16:0_16:0 *sn*-2_18:0 (*m/z* 833.8) mixtures: MS scan of 1/1 mixture **(a)**, MS scan of 9/1 mixture **(b)**, 1/1 mixture MS^2 product ion scan of *m/z* 833.8 **(c)**, and 9/1 mixture MS^2 product ion scan of *m/z* 833.8 **(d)**.

The calculated average results of four replicates for TG 16:0_16:0_18:0 regioisomers are: 93.2 % TG 16:0_16:0 *sn*-2_18:0 in the 1:1 mixture and 80.9 % in the 9:1 mixture. With the 1:1 mixture, the results are quite close to the actual 100 % value, and while the results using the 9:1 mixture are more skewed, the results are still in the right direction. No other TG molecular species were detected in either case. When *MSPECTRA* calculates the results, it first identifies the precursor ion *m/z* 833.8 as TG 50:0. Because this ACN:DB does not have double bonds, any TGs containing FA 18:1 are left out of consideration. This helps in reducing false identifications, but nevertheless cannot correct the

distortions caused by shared fragments of both TG 16:0_16:0 *sn*-2_18:1 M+2 isotope and TG 16:0_16:0 *sn*-2_18:0. Overall, the effect of the M+2 isotopes is estimated as acceptable in study **I**.

5.1.3.2 *TAG analyzer* software

Utilizing the UHPLC-MS^2 method with ammoniated $[M+NH_4]^+$ precursor ion (**II**) the resulting fragment types are different compared to the direct inlet chemical ionization method (**I**). The *TAG analyzer* software mainly uses DG fragments $[M+NH_4–RCOOH–NH_3]^+$ for regioisomer calculations, but there is also an option to use FA ketene $[RCO]^+$ fragments, albeit they typically have low abundance, and are less reproducible. Furthermore, using only one fragment type means that similar preliminary TG molecular species abundances as with the *MSPECTRA* software is not obtained from the fragment ions. Only qualitative FA identifications are made using the corresponding $[RCO]^+$ fragments, and subsequently the possible TG molecular species combinations are determined.

Comparison of experimental calibration curves and the fragmentation model of TAG analyzer are shown in **Figure 24**. The MMP/MPM (TG 14:0_14:0_16:0) and PPBu/PBuP (TG 16:0_16:0_4:0) calibration plots only consist of one data point, because their regioisomer pair was not available. Regardless, having only one data point is still useful for creating the fragmentation model. The established model in most cases was very close to the actual, measured calibration curve. Largest deviations between the fragmentation model and the experimental calibration curves were observed with two 18:2 FA containing TG pairs LLO/LOL (TG 18:2_18:2_18:1) and LLP/LPL (TG 18:2_18:2_16:0).

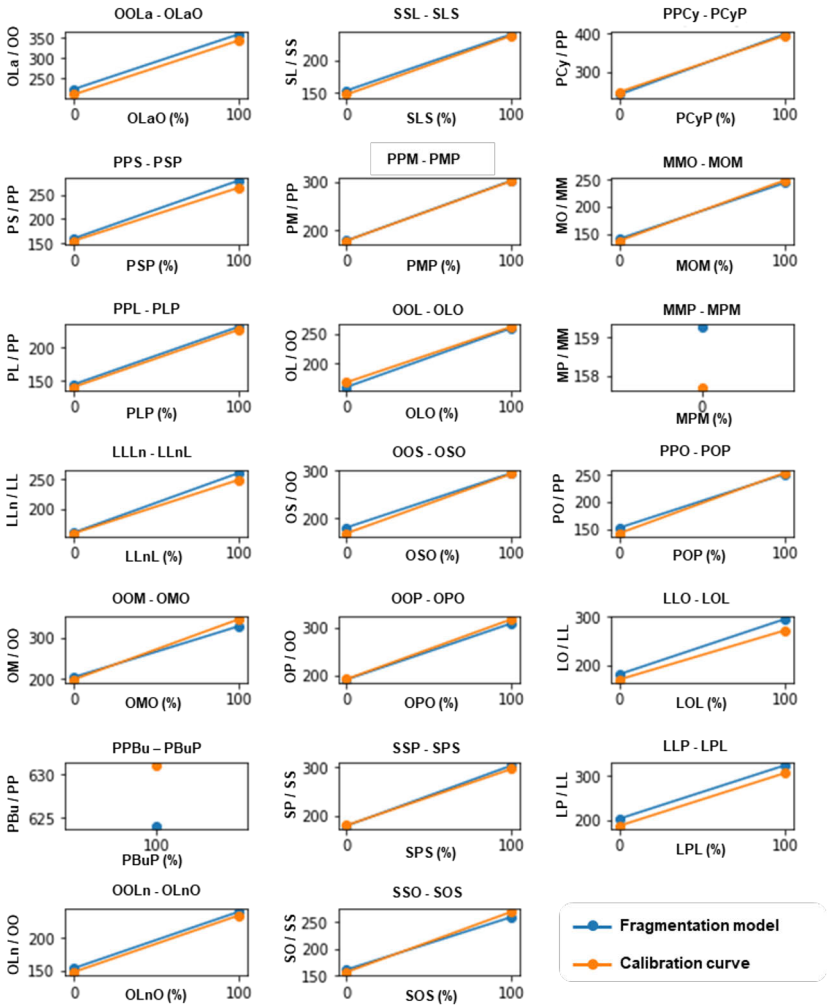

Figure 24 Comparison of original calibration plots and the *TAG analyzer* fragmentation model established with the calibration plots (**II**). For visual clarity, the TGs and their DG fragment ratios are labeled using the AAB/ABA shorthand notations.

TAG analyzer optimizes the TG regioisomer abundances within the ACN:DB species using the fragmentation model established with the TG regioisomer standards. A total of 18 regiospecific pairs of AAB/ABA type TGs were analyzed at five different molar ratios; 0/100, 25/75, 50/50, 75/25 and 100/0. In case of the ABC/ACB/BAC type TGs, the analysis for each regioisomer triplet was performed at 13 different ratios: 100/0/0, 0/100/0, 0/0/100, 80/10/10, 10/80/10, 10/10/80, 70/15/15/, 15/70/ 15, 15/15/70, 50/25/25, 25/50/25, 25/25/50 and 33.3/33.3/33.3. A comparison of the AAB/ABA (**Figure 25**) and

ABC/BAC/CAB (**Figure 26**) type TG standards calculated with original calibration curves and the *TAG analyzer* fragmentation model shows the similarity of the results between the two calculation methods.

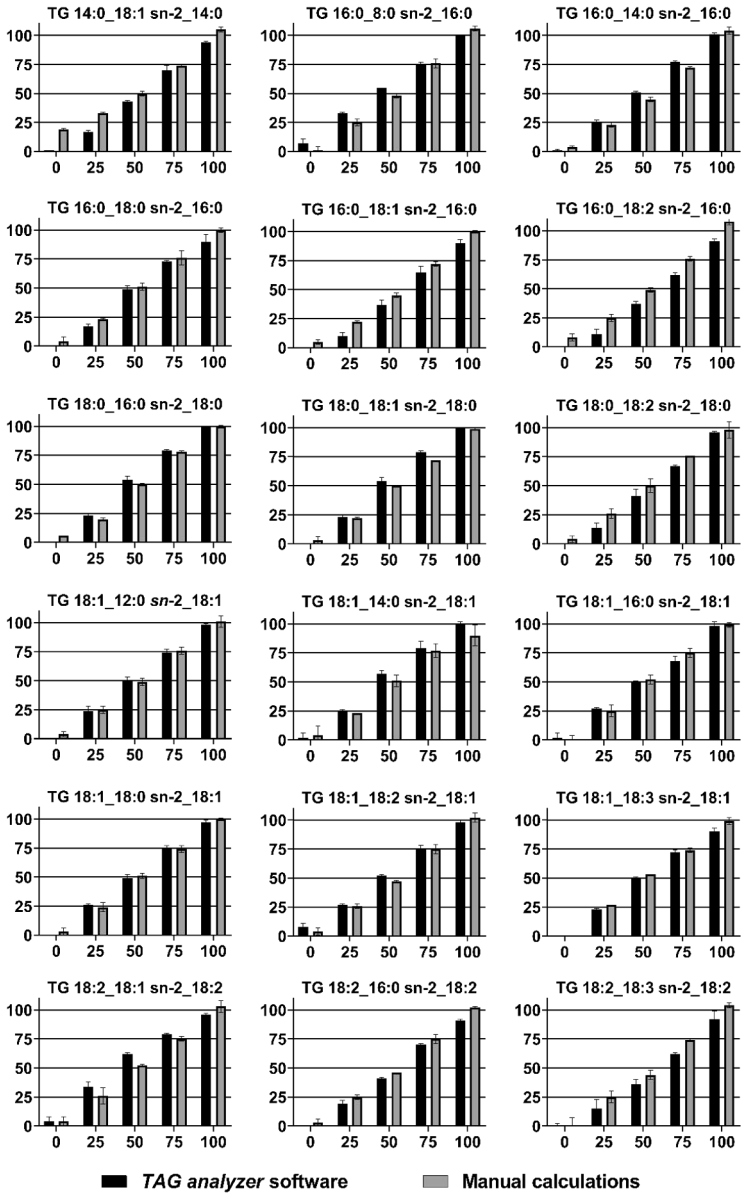

Figure 25 Calculated concentrations of AAB/ABA type regioisomer pairs (**II**). The labels below the bars represent the actual ABA concentrations of the mixtures and Y axis represents the calculated proportions of ABA type regioisomers using *TAG analyzer* or manual calculations.

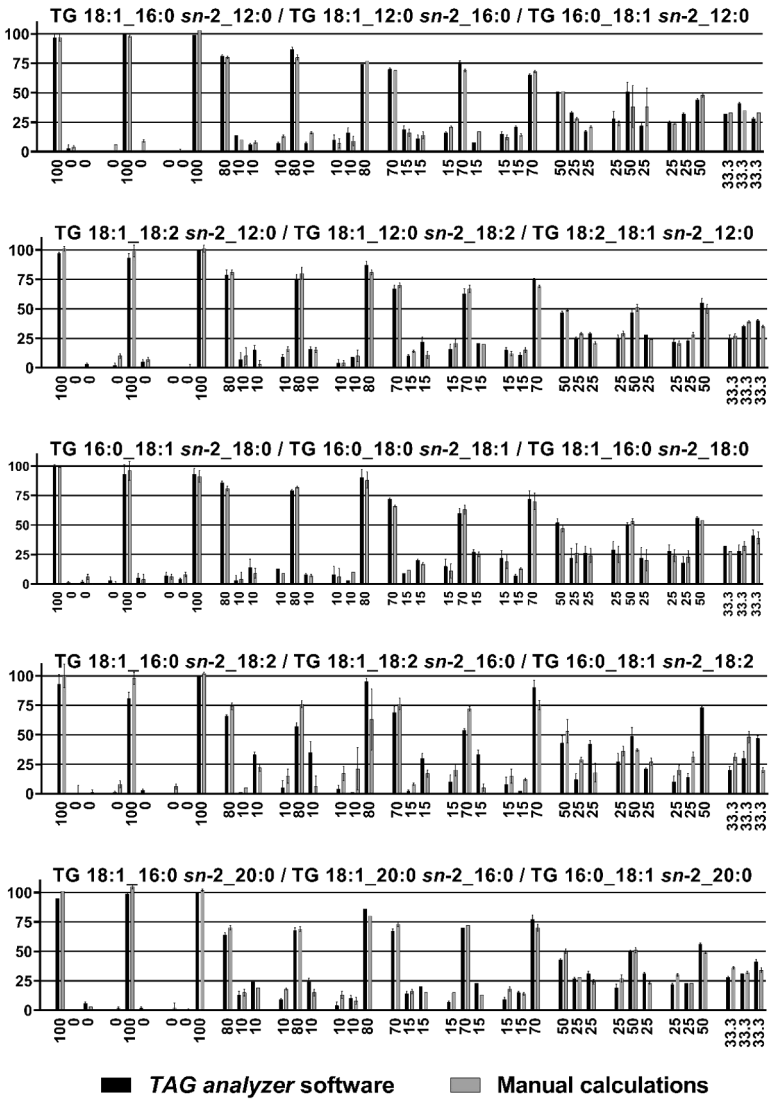

Figure 26 Calculated concentrations of ABC/ACB/BAC type regioisomer triplets (**II**). The labels below the bars represent the actual concentrations of the mixtures and Y axis represents the calculated proportions of the regioisomers using *TAG analyzer* or manual calculations.

All manual calculations of the regiospecific TG standards were performed using the calibration curves established in our previous study (Tarvainen et al., 2019). At all molar fractions, the ratios of most AAB/ABA type regioisomers calculated with the *TAG analyzer* fragmentation model were close to the values calculated manually. Some noticeable differences were also observed, most notably the

regioisomers of TG 16:0_16:0_18:2, TG 16:0_16:0_18:1, and TG 18:2_18:2_18:3 molecular species for the AAB/ABA type pairs. For ABC/BAC/CBA type TGs, the results of TG 16:0_18:1_18:2 deviated slightly more compared to other triplets. Some deviation is to be expected, as the software uses a general fragmentation model for all TGs. The accuracy of the fragmentation model could still be further increased by analyzing additional regioisomer pairs and triplets with varying relative FA chain lengths and degree of saturation. An output window of the *TAG analyz*er software is shown in **Figure 27**, offering a visual reference on the accuracy of the DG fragment optimizations. In this case, the analyzed regioisomers consist of TG 52:3 species in the Finnish human milk sample. The software has identified and optimized the abundances of four DG fragments, and the synthetic spectrum matches the observed spectrum very well. High deviations between the observed and synthetic spectra would mean that the software has challenges to find an optimal solution, leading to more inaccurate results.

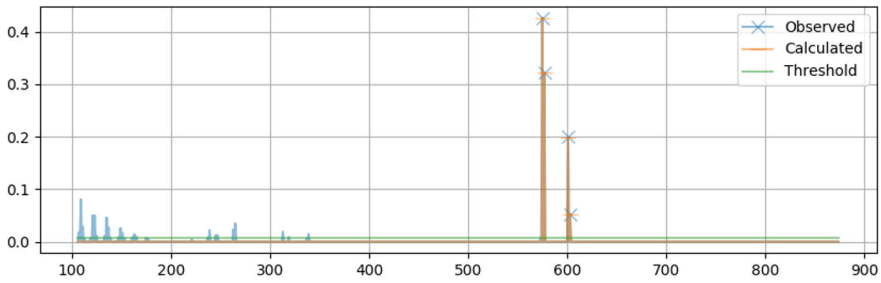

Figure 27 The synthetic DG spectrum of TG 52:3 species in Finnish human milk overlaid on top of the actual fragment spectra (**II**)

A further examination and a visualization of the synthetic spectrum is displayed in **Figure 28**, showing the optimized abundances of DG fragments. Each isobaric DG fragment can be a product of one or more TGs. For example, based on the initial qualitative molecular species identification, *m/z* 575.50 fragment is a mixture of DG 16:0_18:2 and DG 16:1_18:1, fragmented from TG 16:0_18:1_18:2 and TG 18:1_18:1_16:0, respectively. Furthermore, fragments *m/z* 577.52 (DG 16:0_18:1) and *m/z* 601.52 (DG 18:1_18:2) result from TG 16:0_18:1_18:2, and *m/z* 603.54 (DG 18:1_18:1) from TG 18:1_18:1_16:0. Based on the optimized DG fragment abundances, the calculated regioisomers within the TG 52:3 species are TG 18:1_16:0 *sn*-2_18:2 (66 %), TG 18:2_18:1 *sn*-2_16:0 (10 %), TG 18:1_18:2 *sn*-2_16:0 (4 %), TG 18:1_16:1 *sn*-2_18:1 (14 %), and TG 18:1_18:1 *sn*-2_16:1 (5 %).

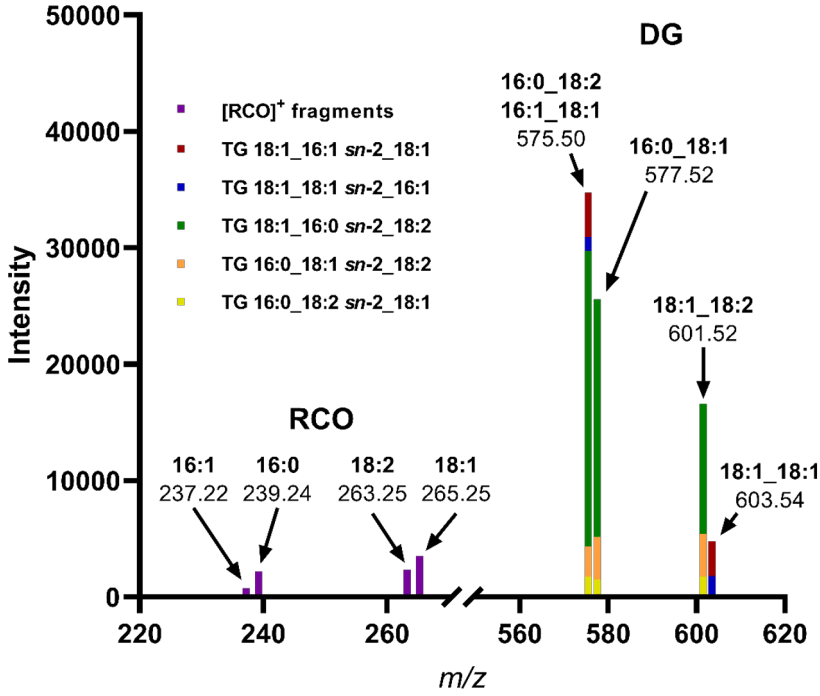

Figure 28 Visualization of the abundance optimization showing identified DG fragments belonging to each TG regioisomer in ACN:DB 52:3 species in Finnish human milk using the *TAG analyzer* software. The $[RCO]^+$ fragments are used for qualitative molecular species identification (**II**).

Without optimization algorithms, TG regioisomers would be difficult to resolve from spectra like this. With increasing sample complexity, more FA combinations and overlapping isobaric DG fragments from multiple sources, manual calculations using calibration curves become practically impossible.

5.1.3.3 Comparison of the TG regioisomer calculation methods

The results obtained with manual calculations using calibration curves, *TAG analyzer* and *MSPECTRA* are compared where applicable. First, most abundant TG regioisomers in olive oil (**Figure 29**) calculated with the *TAG analyzer* are compared with manual calculations (Tarvainen et al., 2019). Due to olive oil having a relatively simple TG composition, manual calculations with calibration curves are possible as the interference of isobaric TG fragments is mostly low. One major exception is the chromatographic overlap of isobaric TG 18:1_18:2_18:2 and TG 18:1_18:1_18:3 molecular species, both producing isobaric DG 36:4 fragments.

In the previous publication (Tarvainen et al., 2019), the results for these TG regioisomers were calculated by taking the spectra from the partially resolved peak using the rising edge of the TG 18:1_18:2_18:2 and the descending tail of the TG 18:1_18:1_18:3. This is not the ideal way of calculating the results, as there is likely some isobaric overlap that is difficult to quantify. Using only the front and back of the partially resolved peaks subjects the calculations to inaccuracies due to low number of data points. In addition to partial molecular species separation, there is also minor separation of the TG regioisomers themselves, likely leading to further distorted fragment ion spectra in the front and tail of the peak.

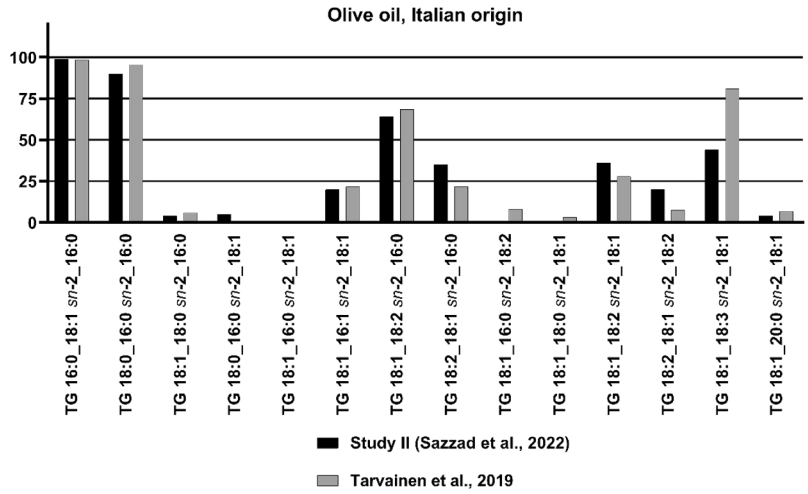

Figure 29 Comparison of olive oil TG regioisomer results using two different calculation methods: *TAG analyzer* (**II**) and manual calculations with calibration curves (Tarvainen et al., 2019)

Comparing the results, the TG 18:2_18:1 *sn*-2_18:2 ratios were reasonably close to one another using the manual calculations (7 %) and *TAG analyzer* (20 %). Higher differences were observed between the TG 18:1_18:3 *sn*-2_18:1 results (81 % and 44 %, respectively). As the TG 18:1_18:1_18:3 molecular species elutes slightly after TG 18:1_18:2_18:2, and it is evident that there is noticeable peak tailing (Tarvainen et al., 2019), the isobaric interference is significantly higher in the tail of the partially resolved peak compared to the front, subsequently leading to possibly inaccurate results using the manual calculation method. For the other studied abundant TGs in olive oil, the results between the two calculation methods were very similar (**Figure 29**).

As the human milk TG regioisomer composition has not been comprehensively resolved with methodologies other than the algorithmic

optimization of fragment spectra described in this thesis (*MSPECTRA* and *TAG analyzer*), results of the two calculation programs are mainly compared with one another, including the results from the preliminary algorithm development publication (Kallio et al., 2017) utilizing lithium adducts (**Table 17**). The comparison includes ten most abundant ACN:DB species in Finnish human milk, and two most abundant regioisomer pairs or triplets within each ACN:DB. The results obtained with the three different methods are mostly similar, especially for the most abundant TGs within each ACN:DB species. Larger differences between the methods are observed in some of the less abundant molecular species, such as TG 16:1_18:1 *sn*-2_18:1 within the TG 52:3 species, where the results calculated with *MSPECTRA* (**I**) are noticeably different compared to the other two methods. This could be explained by the differences in the fragmentation models. As *MSPECTRA* only uses the universal discrimination factor for all TGs, and *TAG analyzer* (**II**) and its predecessor algorithm (Kallio et al., 2017) use a more sophisticated fragmentation model for different TGs, some differences are to be expected.

Table 17 Comparison of human milk TG regioisomer results calculated with three different methodologies: *MSPECTRA* software with direct inlet CI(–)-MS^2 method using $[M–H]^–$ precursor ions (Study **I**), *TAG analyzer* software with RP chromatographic separation and ESI(+)-MS^2 method using $[M+NH_4]^+$ precursor ions (Study **II**), and the initial TG abundance optimization algorithm with RP chromatographic separation and ESI(+)-MS^2 method using $[M+Li]^+$ precursor ions (Kallio et al., 2017). Two most abundant TG regioisomer pairs or triplets within each ACN:DB are shown.

				Regioisomer ratios (Mol%)		
ACN:DB	Mol%	TG regioisomer	Abundance within ACN:DB (Mol%), Study **I**	Study **I**	Study **II**	Kallio et al., (2017)
54:4	3.3	TG 18:1_18:2 *sn*-2_18:1	89.5	64	69	57
		TG 18:1_18:1 *sn*-2_18:2		36	31	43
		TG 18:2_18:0 *sn*-2_18:2	6.7	63	n.d.	n.d.
		TG 18:0_18:2 *sn*-2_18:2		37	n.d.	n.d.
54:3	4.1	TG 18:1_18:1 *sn*-2_18:1	76.2	100	100	100
		TG 18:1_18:0 *sn*-2_18:2	23.2	23	25	25
		TG 18:0_18:1 *sn*-2_18:2		37	5	40
		TG 18:0_18:2 *sn*-2_18:1		40	75	35
52:3	6.7	TG 16:0_18:1 *sn*-2_18:2	76.4	7	13	0
		TG 18:1_18:2 *sn*-2_16:0		1	2	2
		TG 18:1_16:0 *sn*-2_18:2		93	85	98
		TG 18:1_16:1 *sn*-2_18:1	19.6	35	78	85
		TG 16:1_18:1 *sn*-2_18:1		65	22	15

				Regioisomer ratios (Mol%)		
ACN:DB	Mol%	TG regioisomer	Abundance within ACN:DB (Mol%), Study **I**	Study **I**	Study **II**	Kallio et al., (2017)
52:2	12.2	TG 18:1_16:0 *sn*-2_18:1	89.3	81	100	100
		TG 16:0_18:1 *sn*-2_18:1		19	0	0
		TG 16:0_18:0 *sn*-2_18:2	5.2	25	n.d.	4
		TG 18:0_18:2 *sn*-2_16:0		8	n.d.	4
		TG 18:0_16:0 *sn*-2_18:2		67	n.d.	92
52:1	3.8	TG 16:0_18:0 *sn*-2_18:1	97.6	7	2	4
		TG 16:0_18:1 *sn*-2_18:0		1	9	2
		TG 18:1_16:0 *sn*-2_18:0		92	89	93
		TG 18:0_16:1 *sn*-2_18:0	2.4	79	n.d.	100
		TG 16:1_18:0 *sn*-2_18:0		21	n.d.	0
50:2	4.7	TG 18:1_14:0 *sn*-2_18:1	55.6	81	94	99
		TG 14:0_18:1 *sn*-2_18:1		19	6	1
		TG 16:0_18:2 *sn*-2_16:0	15.7	0	2	7
		TG 16:0_16:0 *sn*-2_18:2		100	98	93
50:1	4.3	TG 16:0_18:1 *sn*-2_16:0	70.3	6	0	0
		TG 16:0_16:0 *sn*-2_18:1		94	100	100
		TG 14:0_18:1 *sn*-2_18:0	23.6	14	20	0
		TG 18:0_14:0 *sn*-2_18:1		85	72	90
		TG 14:0_18:0 *sn*-2_18:1		0	8	10
48:2	3.4	TG 18:1_12:0 *sn*-2_18:1	59	61	95	96
		TG 12:0_18:1 *sn*-2_18:1		39	5	4
		TG 16:0_14:0 *sn*-2_18:2	21.8	61	55	32
		TG 14:0_16:0 *sn*-2_18:2		39	35	38
		TG 16:0_18:2 *sn*-2_14:0		0	0	30
48:1	3.4	TG 14:0_18:1 *sn*-2_16:0	74.1	8	0	0
		TG 16:0_14:0 *sn*-2_18:1		25	45	44
		TG 14:0_16:0 *sn*-2_18:1		67	55	56
		TG 18:0_18:1 *sn*-2_12:0	18.8	22	n.d.	7
		TG 18:1_18:0 *sn*-2_12:0		10	n.d.	31
		TG 18:1_12:0 *sn*-2_18:0		68	n.d.	61
46:1	3.4	TG 16:0_18:1 *sn*-2_12:0	69	5	3	1
		TG 18:1_16:0 *sn*-2_12:0		93	74	76
		TG 18:1_12:0 *sn*-2_16:0		2	23	24
		TG 14:0_18:1 *sn*-2_14:0	18.7	9	15	1
		TG 14:0_14:0 *sn*-2_18:1		91	85	99

n.d. = not determined

Another factor contributing to the differences is the fact that when the algorithms are finding the optimal abundances of TG regioisomers, the changes are

proportionally higher in the lower-abundance TGs. This can result in larger inaccuracies for the low abundance TG compared to the more abundant ones.

Both calculation programs *MSPECTRA* and *TAG analyzer* have a configurable threshold for peak detection. Some TGs such as molecular species TG 18:0_18:2_18:2, TG 16:0_18:0_18:2, TG 16:1_18:0_18:0 and TG 12:0_18:0_18:1 identified with *MSPECTRA* in human milk were not identified using the *TAG analyzer* when analyzing the same sample. This might be caused by the intensity threshold being set too high. Great care should be used when assessing the proper intensity threshold for detection, as both too low and too high values have their own problems. If the value is set too low, the software might find additional peaks matching the structurally informative fragments, when in reality they are just background noise, resulting in convoluted and inaccurate results. Conversely, setting the threshold too high may discard valid low abundance TG regioisomers. More importantly, discarding some of the TGs from consideration will also distort the results of other, high abundance TGs if there is isobaric overlap of the fragments, as the software is trying to find an optimal solution without all the potential TG combinations in consideration.

Despite the differences of some individual results, the overall TG regioisomer profile calculated with the three methods is quite similar. The results of Finnish human milk clearly show that when paired with unsaturated FAs, the saturated FAs are heavily concentrated in *sn*-2 position, while unsaturated FAs seem to preferentially be located in *sn*-1/3 positions. When accompanied by FA 18:0, shorter saturated FAs such as 16:0, 14:0 and 12:0 are more concentrated in *sn*-2 position. When both FA 16:0 and 14:0 are present, no clear preference is observed between the two, as both are roughly equally found in *sn*-2 position.

One of the limitations of this comparison is that all three methods are published by our group, based on similar principles using optimization of the fragment ion spectra, and there are no other studies that have comprehensively investigated TG regioisomers in human milk. The results for certain abundant molecular species such as TG 16:0_18:1_18:1, TG 16:0_18:1_18:2 and TG 16:0_16:0_18:1 are well in agreement with previous literature (Chen et al., 2020; Zhang et al., 2022) that have analyzed specific regioisomers, showing that TG regioisomers in human milk containing FA 16:0 in *sn*-2 position are much more abundant compared to regioisomers with FA 16:0 in *sn*-1/3 positions (**Table 18**).

Table 18 Comparison of different methodologies for analysis of specific TG regioisomers in human milk

		Regioisomer ratios (Mol%)				
ACN:DB	TG regioisomer	Study **I**	Study **II**	Kallio et al., (2017)	Chen et al., (2020)	Zhang et al., (2022)
48:2	TG 18:1_12:0 *sn*-2_18:1	61	95	96	73	n.d.
	TG 12:0_18:1 *sn*-2_18:1	39	5	4	27	n.d.
50:1	TG 16:0_18:1 *sn*-2_16:0	6	0	0	6	11
	TG 16:0_16:0 *sn*-2_18:1	94	100	100	94	89
52:2	TG 18:1_16:0 *sn*-2_18:1	81	100	100	88	83
	TG 16:0_18:1 *sn*-2_18:1	19	0	0	12	17
52:3	TG 16:0_18:1 *sn*-2_18:2	7	13	0	4	0
	TG 18:1_18:2 *sn*-2_16:0	1	2	2	5	9
	TG 18:1_16:0 *sn*-2_18:2	93	85	98	91	91

n.d. = not determined

Some of the differences could be explained by sample variation between studies. Mother's diet (Much et al., 2013; Tian et al., 2019) and other external factors such as age (Kim et al., 2017) and BMI (Mäkelä et al., 2013) have been shown to affect the overall FA composition and subsequently TG species composition (Linderborg et al., 2014) in human milk. While there were minor statistical differences between the human milk regioisomers of mothers in three different regions of China (Chen et al., 2020), in other studies background factors have not been shown to cause significant differences in human milk TG regioisomer ratios (Linderborg et al., 2014).

The other two studies listed in **Table 18** were based on chromatographic separation of the regioisomers (Chen et al., 2020) or calibration curves using fragment ion ratios (Zhang et al., 2022). While the results reported by (Zhang et al., 2022) are well in agreement with the other four studies, the authors did not specify whether isobaric interference of the fragment ions was considered, and based on the chromatographic method used, it could have a significant influence on the results.

Even though the accuracy of the developed programs *MSPECTRA* and *TAG analyzer* was tested with a wide range of mixtures of pure reference standards, additional mixtures with TG standards containing isobaric fragments, for example regioisomers of both TG 18:1_18:1_18:3 and TG 18:1_18:2_18:2 species in the same sample, should have been analyzed. In hindsight, this would have greatly benefited the credibility of the validation, as analyzing TGs with isobaric fragments is a core feature of both calculation programs. Additionally, with the fragmentation model of the *TAG* analyzer program, a cross-validation of the TG reference standard mixtures would have been useful, meaning that with

each TG standard pair or triplet, the accuracy of the model would have been tested by dropping out the fragmentation data obtained from that specific TG species.

While external references are limited on TG regioisomer composition of complex samples such as human milk, there is a strong basis to conclude that the three methods published by our group (Study **I** (Fabritius et al., 2020), Study **II** (Sazzad et al., 2022) and (Kallio et al., 2017)) can be validated against one another. The methods use different instrumentation, ionization mode, adduct type, fragment type, fragmentation model and optimization algorithm. Despite these fundamental differences, the methods still produce comparable results, showing that using optimization algorithms to determine the TG regioisomers from complex data with overlapping isobaric fragments is a viable solution.

5.1.4 Correction factors for PL molecular weight distribution

Determination of the PL molecular weight correction factors resulting from differences in the detector response is described in more detail in **Study IV** (Fabritius et al., 2023, unpublished manuscript). Briefly, the correction factors are influenced by the attached FAs and the numbers of acyl carbons and double bonds. Increased FA chain length resulted in lower detector response, and increased double bond number resulted in higher detector response. PC 24:0 was used as a baseline (1.00) for the correction factors.

5.1.5 PL regioisomer calculations

5.1.5.1 Manual calculation of PL standards using the calibration curves

All investigated PL classes produced abundant deprotonated FA fragments at varying ratios. Additionally, different PL classes produced lysophospholipid-like fragment ions, structural differences in these fragments arising from the polar head group. Two types of calibration curves were established for manual calculations of the PL regioisomer ratios: one using the FA fragments and the other using the lysophospholipid-like fragments.

The first set of calibration curves used for manual calculations was initially established by determining the FA fragment ion $[RCOO]^-$ ratio in PL A_B molecular species by dividing the intensity of $[R_ACOO]^-$ by the intensity of $[R_BCOO]^-$. Similarly, the other set of calibration curves was established by dividing the intensities of the lysophospholipid-like fragments. This resulted in non-linear calibration curves (**III**) with best fitting obtained using exponential functions.

The calibration curves of various PL standards using the FA fragment ion ratios are shown in **Figure 30**. The coefficient of determination for each

calibration curve was very good ($R^2 > 0.99$), showing that the FA fragment ion ratios predictably represent the regioisomer ratios in each of the tested PL regioisomer pairs. While the general trend for the changing fragment ion ratios as different concentrations was similar, there were minor differences that could be explained by the nature of the PL molecular species. For example, with PCs the fragment ion ratios seem to be dependent on the lengths of the FAs and their numbers of double bonds. The calibration curves of various PL standards using the lysophospholipid-like fragment ion ratios are shown in **Figure 31**.

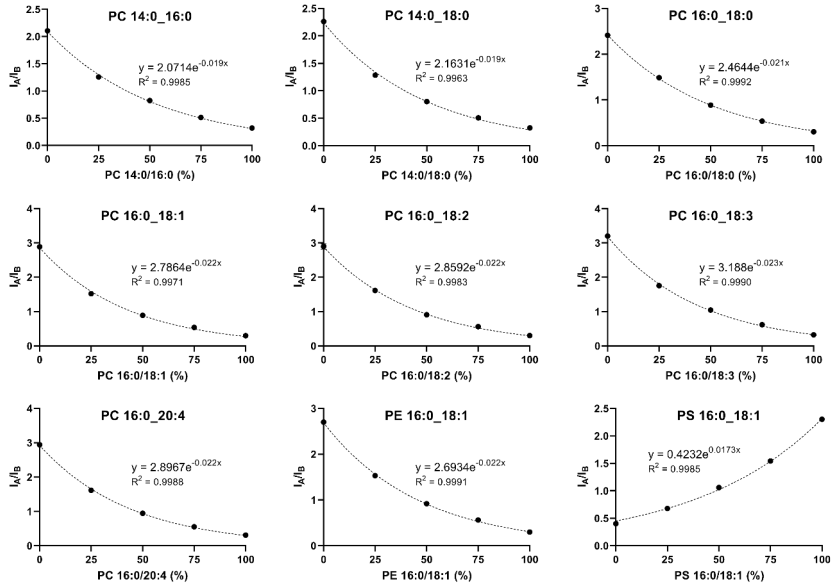

Figure 30 Calibration curves of the PL A_B reference standard pairs calculated using the deprotonated FA fragment $[RCOO]^-$ ion ratios (**III**)

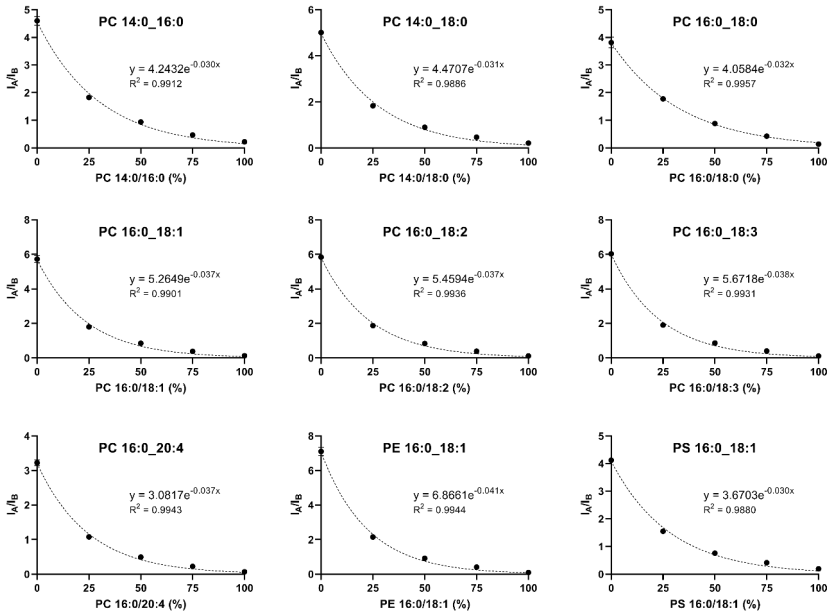

Figure 31 Calibration curves of the PL A_B reference standard pairs calculated using the lysophospholipid-like fragment ion ratios of $[M+HCOO–RCOOH–42]^-$, $[M–H–RCOOH]^-$ and $[M–H–RCOOH–87]^-$ for PC, PE and PS, respectively (**III**).

Utilizing both sets of calibration curves, mixtures of PL reference standard pairs at 60:40 % ratios were analyzed with both direct infusion and the HILIC method. For direct infusion, individual pairs were analyzed separately, whereas with the HILIC method a mixture containing all pairs was analyzed. The results for each method and calibration curve type are shown in **Table 19**. The results show that the calculations are accurate using direct infusion method and either fragment type. In addition to good accuracy, the results were also highly reproducible, indicating that the fragmentation occurs reliably.

However, some challenges were encountered with the HILIC method. As HILIC separates the PLs primarily based on the polar head group of the class, the molecular species within a class typically elute in clusters and many are partially overlapping with each other. Normally this would only cause minor M+2 isotope interference similar to what was discussed in the direct inlet TG analysis section, but in this case the precursor ion isolation capabilities of the instrument used are limited. Many of the overlapping peaks only differ by one double bond, for example PC 16:0_18:2 and PC 16:0_18:3, resulting in a 2 Da mass difference. The quadrupole responsible for precursor ion isolation is not capable of resolving these ions within ±2 *m/z*, and when selecting PC 16:0_18:3 for fragmentation, also the chromatographically overlapping part of PC

16:0_18:2 is fragmented, heavily distorting the product ion spectra. As FA 16:0 is a shared FA in both of these molecular species, the structurally informative fragment ion ratios are influenced by one another, resulting in inaccurate calculations (**Table 19**). This issue was solved by changing the chromatography from HILIC to RP (**IV**), which primarily separates the molecular species based on the FA composition, not class. Even if molecular species from different classes have the same FA composition and are chromatographically overlapping, they can be differentiated by the precursor ion m/z, because the *m/z* differences of most head groups of the PL classes are high enough for acceptable precursor ion isolation. Two exceptions are PC and PS, where the difference is less than 2 Da for the intact molecules. However, as PCs are ionized and detected as $[M+HCOO]^-$ formate adducts and PSs as deprotonated $[M–H]^-$ ions, this creates a 44 Da difference.

Table 19 Results of regioisomer mixtures calculated with both methods and fragment types.

Individual regioisomer pairs analyzed separately, 60/40% ratios, direct infusion method, product ion scan, n=3				Complex mixture with all reference standard regioisomer pairs, 60/40% ratios, HILIC method, autoMSMS, n=3			
PL composition	**Actual ratios (%)**	**Calculations using $[RCOO]^-$ ions (%)**	**Calculations using lysophospholipid-like ions (%)**	**PL composition**	**Actual ratios (%)**	**Calculations using $[RCOO]^-$ ions (%)**	**Calculations using lysophospholipid-like ions (%)**
		$[RCOO]^-$	**$[M+HCOO-RCOOH-42]^-$**			**$[RCOO]^-$**	**$[M+HCOO-RCOOH-42]^-$**
PC 14:0/16:0	60	61.2 ± 1.1	59.4 ± 1.1	PC 14:0/16:0	60	60.4 ± 1.4	59.9 ± 1.0
PC 16:0/14:0	40	38.8 ± 1.1	40.6 ± 1.1	PC 16:0/14:0	40	39.6 ± 1.4	40.1 ± 1.0
PC 14:0/18:0	60	62.8 ± 1.6	61.5 ± 3.8	PC 14:0/18:0	60	66.3 ± 2.7	63.0 ± 1.4
PC 18:0/14:0	40	37.2 ± 1.6	38.5 ± 3.8	PC 18:0/14:0	40	33.7 ± 2.7	37.0 ± 1.4
PC 16:0/18:0	60	60.7 ± 1.2	62.9 ± 1.7	PC 16:0/18:0	60	56.3 ± 1.7	58.4 ± 1.2
PC 18:0/16:0	40	39.3 ± 1.2	37.1 ± 1.7	PC 18:0/16:0	40	43.7 ± 1.7	41.6 ± 1.2
PC 16:0/18:1	60	59.2 ± 0.7	63.6 ± 2.4	PC 16:0/18:1	60	65.1 ± 0.3	69.8 ± 0.5
PC 18:1/16:0	40	40.8 ± 0.7	36.4 ± 2.4	PC 18:1/16:0	40	34.9 ± 0.3	30.2 ± 0.5
PC 16:0/18:2	60	63.3 ± 1.8	61.7 ± 0.8	PC 16:0/18:2	60	n.d.	n.d.
PC 18:2/16:0	40	36.7 ± 1.8	38.3 ± 0.8	PC 18:2/16:0	40	n.d.	n.d.
PC 16:0/18:3	60	61.9 ± 2.2	58.6 ± 1.5	PC 16:0/18:3	60	n.d.	n.d.
PC 18:3/16:0	40	38.1 ± 2.2	41.4 ± 1.5	PC 18:3/16:0	40	n.d.	n.d.
PC 16:0/20:4	60	64.1 ± 1.7	62.2 ± 0.9	PC 16:0/20:4	60	65.6 ± 0.7	61.8 ± 1.3
PC 20:4/16:0	40	35.9 ± 1.7	37.8 ± 0.9	PC 20:4/16:0	40	34.4 ± 0.7	38.2 ± 1.3
		$[RCOO]^-$	**$[M-H-RCOOH]^-$**			**$[RCOO]^-$**	**$[M-H-RCOOH]^-$**
PE 16:0/18:1	60	58.9 ± 0.9	59.4 ± 1.0	PE 16:0/18:1	60	58.2 ± 0.6	57.7 ± 1.4
PE 18:1/16:0	40	41.1 ± 0.9	40.6 ± 1.0	PE 18:1/16:0	40	41.8 ± 0.6	42.3 ± 1.4
		$[RCOO]^-$	**$[M-H-RCOOH-87]^-$**			**$[RCOO]^-$**	**$[M-H-RCOOH-87]^-$**
PS 16:0/18:1	60	63.6 ± 1.4	64.1 ± 1.8	PS 16:0/18:1	60	64.5 ± 1.2	62.5 ± 0.5
PS 18:1/16:0	40	36.4 ± 1.4	35.9 ± 1.8	PS 18:1/16:0	40	35.5 ± 1.2	37.5 ± 0.5

All established PC calibration curves are overlaid in **Figure 32**, showing the effects of different FA combinations. When comparing the $[RCOO]^-$ fragment ion calibration curves of PC 16:0_18:0, PC 16:0_18:1, PC 16:0_18:2 and PC 16:0_18:3, where the only difference is the degree of saturation in one FA, the presence of more unsaturated FAs seems to cause stronger differentiation in fragmentation of FAs between the *sn*-1 and *sn*-2 positions. Similarly, stronger differentiation seems to be caused by increasing ACN of the attached FAs. These observations were utilized in the development of the fragmentation model in the following study (**IV**). Calibration curves established with the lysophospholipid-like $[M+HCOO–RCOOH–42]^-$ fragment ions did not follow the same pattern, and were seemingly more random, the differences between individual calibration curves being higher. All things considered, including significantly higher sensitivity, the use of $[RCOO]^-$ fragments for PC regioisomer calculations was deemed more applicable.

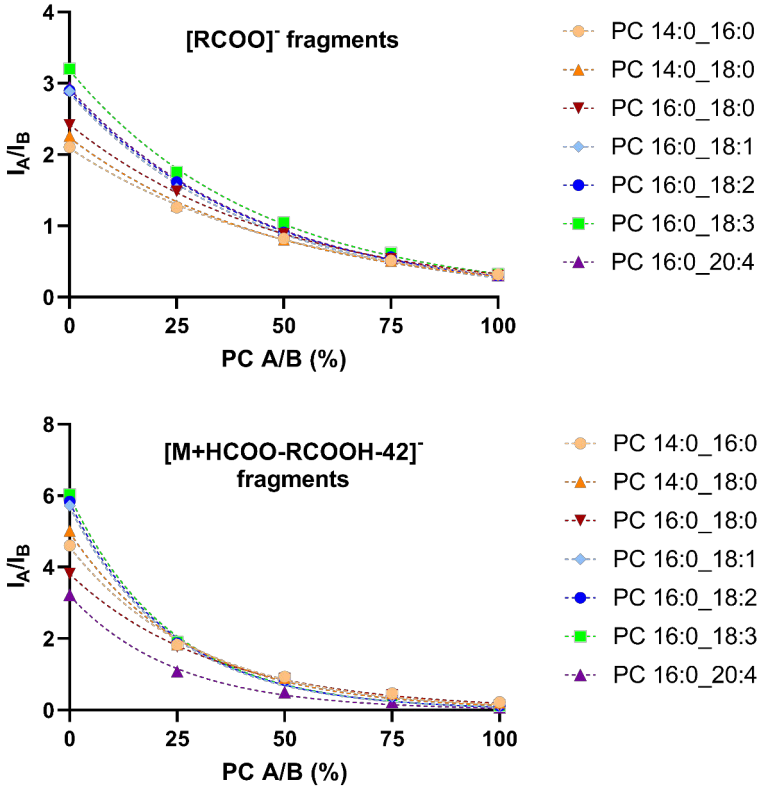

Figure 32 Calibration curves of PC standards overlaid in the same graph (**III**).

Investigating the PC calibration data further with a different approach, **Figure 33** shows the proportion of $[R_ACOO]^-$ or $[M+HCOO–R_ACOOH–42]^-$ of all

fragments of the same type. Using a linear regression model, the new calibration curves calculated with the $[RCOO]^-$ fragments are highly linear ($R^2 > 0.995$), meaning that as the proportions of the regioisomers change, the changes to $[RCOO]^-$ fragment ions are also linear. Because the change is linear, multiple mixtures of regioisomers at different ratios are not required, and similar calibration curves can be obtained with just the end points of the curves, i.e., pure PC A/B and PC B/A. However, using the $[M+HCOO–RCOOH–42]^-$ fragment calibration data, the situation is somewhat different. While most PC mixtures fit the linear regression model well, there is some observable curvature, especially with PC 16:0_20:4 (**Figure 33**). While this can be corrected by using non-linear calibration curves, as was done in Study **III**, it will be more difficult to create a universal fragmentation model if different molecular species need different regression models to fit the data. This again supports the use of $[RCOO]^-$ fragments in further fragmentation model development.

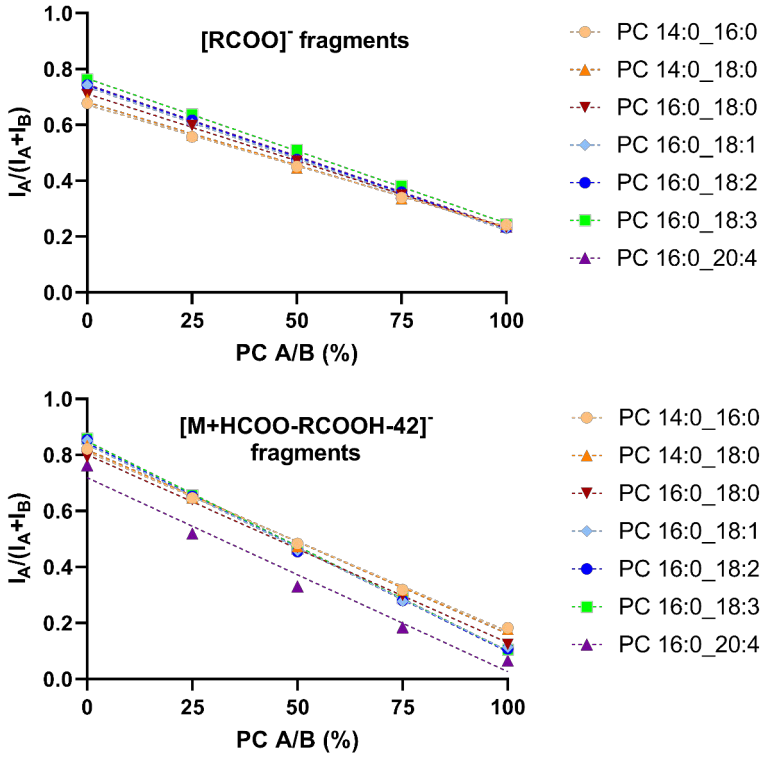

Figure 33 Proportions of $[R_ACOO]^-$ or $[M+HCOO–R_ACOOH–42]^-$ of all fragments of the same type.

Furthermore, another interesting observation can be made from the $[RCOO]^-$ calibration data. With all PC standards the $[R_ACOO]^-$ fragment ion proportions are very similar at 100 % PC A/B ratios (0.231-0.245) (**Figure 33**). A common factor for all the investigated PC A_B standards is that in PC A/B configuration the FAs in *sn*-1 position are of similar length and degree of saturation (FA 14:0 or 16:0). Even though the FAs in *sn*-2 position range from ACN 14 to 20, with DB number between 0-4, the fragment ion proportions are remarkably similar. As the ratio of PC B/A increases, the calibration curves start to diverge, resulting in proportionally higher differences at 100 % PC B/A (0.678-0.762). This suggests that the identity of FA in *sn*-1 position could be more responsible for causing the differences between the fragmentation efficiencies of various PC molecular species compared to *sn*-2 FA.

5.1.5.2 Calculation software

Detailed software validation is described in **Study IV** (Fabritius et al., 2023, unpublished manuscript). Briefly, the fragmentation stability was good over a wide concentration range (0.1-100 µg/mL) for PC, PE, PI and PS. No significant changes in the fragment ion ratios were detected, as both high and low concentrations produced mostly similar results. The limiting factor for the analysis became the triggering threshold of the DDA. This shows that the fragmentation is not influenced by the concentration, and the software can be used to accurately analyze PL regioisomers in samples of different concentrations.

The software has adjustable *m/z* thresholds for precursor and fragment ion detection. Without appropriate thresholds, the software incorrectly finds additional PL compounds that in reality are something else. For example, background noise can sometimes be interpreted as PL compounds if the m/z threshold is too wide, producing very convoluted and inaccurate results. More importantly, sometimes isotopes of other PLs can be incorrectly identified as other PLs. Adequate *m/z* threshold for removing the isotope misidentifications was set at *m/z* 0.002. This also removes the misidentifications resulting from background noise. In addition to the *m/z* threshold, there is also a sensitivity threshold that can be used to filter out background noise. 1 % relative sensitivity threshold was used for FA detection and identification, meaning that within each DDA event, fragments with less than 1 % intensity of the highest fragment peak were filtered out.

Different fragmentation models were tested. Briefly, the fragmentation models were calibrated with all mixed acid PC standards listed in **Table 12**. The first type of fragmentation model consisting of the average parameters obtained with all standards was used as a baseline. This is equivalent to using a single, average calibration curve for all PC compounds. Another, a more sophisticated fragmentation model that takes into account the differences of individual

molecular species produced more accurate results than the model with average parameters, and thus it was used in the subsequent analysis of PC regioisomers in bovine milk.

5.1.5.3 Analysis of bovine milk PC regioisomers

Most abundant PC species, molecular species and regioisomers found in bovine milk are described in detail in the **Study IV** (Fabritius et al., 2023, unpublished manuscript). Overall, three different calculation protocols were tested. The first method consisted of fully manual peak identification, integration and calculation with calibration curves. As we do not have calibration curves for all identified PC molecular species, a curve with similar FA composition was used instead. For example, regioisomers of PC 16:1_18:0 were calculated using the PC 16:0_18:1 calibration curve.

The second calculation protocol consisted of manual peak integrations, but automated calculation with the software. Finally, the third protocol consisted of fully automated peak integration and identification with the software. Comparison of these two methods shows that while there are some differences in the results of low-abundance PLs, most results are fairly well in line with each other. This shows that the fully automated peak integration script can be used for PL regioisomers analysis. Overall, the regioisomer results calculated with calibration curves and fragmentation model are also in agreement with each other.

Some general observations can be made from the bovine milk PC results **Study IV** (Fabritius et al., 2023, unpublished manuscript). In most cases, when an unsaturated FA is paired with a saturated FA, the unsaturated FA seems to be preferentially located in *sn*-2 position. When both FAs are unsaturated, there does not seem to be a clear preference between the *sn*-positions, as they are nearly equally distributed in *sn*-1 and *sn*-2 positions in each observed case. When both FAs are saturated, the preference was somewhat more unclear, but it seems that the shorter FA might have a preference for the *sn*-2 position.

There is limited information in the literature about the accurate PL regioisomer ratios in bovine milk, but some recent studies (Liu et al., 2020; Zhao et al., 2022) have investigated the PL fragment ion ratios and determined the most abundant regioisomers in each pair. Both methods for PL regioisomer analysis were relatively similar to our setup, consisting of single stage fragmentation with CID, ammonium formate as the mobile phase modifier, and PL regioisomer identifications performed on negative ionization mode. While regioisomer ratios were not accurately determined in these two studies, a comparison (**Table 20**) shows that most of the results are in agreement between the studies when looking at the major regioisomer in each pair.

Table 20 Comparison of the major bovine milk PC regioisomer (**IV**) with two lipidomics studies investigating bovine milk. Bolded text shows the major regioisomer identified in each study.

Species	**Study IV** (Fabritius et al., 2023, unpublished)		Zhao et al., 2022	Liu et al., 2020
PC 28:0	**PC 12:0/16:0**	**76.9 ± 25.7**	n.d.	PC 12:0/16:0
	PC 16:0/12:0	23.1 ± 25.7	n.d.	**PC 16:0/12:0**
PC 30:0	PC 14:0/16:0	42.7 ± 4.2	PC 14:0/16:0	PC 14:0/16:0
	PC 16:0/14:0	**57.3 ± 4.2**	**PC 16:0/14:0**	**PC 16:0/14:0**
PC 32:0	PC 14:0/18:0	23.4 ± 1.3	n.d.	PC 14:0/18:0
	PC 18:0/14:0	**76.6 ± 1.3**	n.d.	**PC 18:0/14:0**
PC 34:0	PC 16:0/18:0	24.6 ± 2.6	PC 16:0/18:0	PC 16:0/18:0
	PC 18:0/16:0	**75.4 ± 2.6**	**PC 18:0/16:0**	**PC 18:0/16:0**
PC 34:1	**PC 16:0/18:1**	**71.1 ± 1.8**	**PC 16:0/18:1**	**PC 16:0/18:1**
	PC 18:1/16:0	28.9 ± 1.8	PC 18:1/16:0	PC 18:1/16:0
PC 34:2	**PC 16:0/18:2**	**85.5 ± 1.7**	**PC 16:0/18:2**	**PC 16:0/18:2**
	PC 18:2/16:0	14.5 ± 1.7	PC 18:2/16:0	PC 18:2/16:0
PC 34:3	**PC 16:0/18:3**	**72.7 ± 6.1**	**PC 16:0/18:3**	**PC 16:0/18:3**
	PC 18:3/16:0	27.3 ± 6.1	PC 18:3/16:0	PC 18:3/16:0
PC 36:1	**PC 18:0/18:1**	**96.2 ± 1.9**	**PC 18:0/18:1**	**PC 18:0/18:1**
	PC 18:1/18:0	3.8 ± 1.9	PC 18:1/18:0	PC 18:1/18:0
PC 36:2	**PC 18:0/18:2**	**67.6 ± 10.1**	**PC 18:0/18:2**	**PC 18:0/18:2**
	PC 18:2/18:0	32.4 ± 10.1	PC 18:2/18:0	PC 18:2/18:0
PC 36:3	PC 18:1/18:2	44.2 ± 3.2	**PC 18:1/18:2**	**PC 18:1/18:2**
	PC 18:2/18:1	**55.8 ± 3.2**	PC 18:2/18:1	PC 18:2/18:1

[n.d.] Not determined.

In the most abundant PCs in bovine milk, there were only a few exceptions where the regioisomer ratios were not in the same direction. For example, with our method in PC 12:0_16:0 molecular species, the regioisomer PC 12:0/16:0 was the most abundant with roughly 75 % abundance. However, the deviation between the replicates in this case was very significant. Liu et al., (2020) reported that PC 16:0/12:0 was the major regioisomer in their study. Another discrepancy was with PC 18:1_18:2, where both FAs are unsaturated and our method showed that the ratios are close to equal with PC 18:2/18:1 being slightly more abundant, whereas the other two methods reported that the PC 18:1/18:2 was the major regioisomer. Especially in the high abundance cases where one FA was unsaturated and the other was saturated, all three methods were consistently in agreement with one another. Overall, this shows that our method with the calculation software (**IV**) can be a powerful tool in characterizing accurate regioisomer profiles in complex natural samples.

5.1.6 General discussion

5.1.6.1 TG regioisomer analysis methods

For both of the TG regioisomer analysis methods used in the thesis work, there are some advantages and limitations that might favor the use of one over the other method. The direct inlet MS^2 method with *MSPECTRA* software (**I**) is a separate platform dedicated to TG regioisomers and molecular species only. The method is very simple, requires little preparation and the analysis itself is fast, taking roughly 3 minutes per sample. One of the main disadvantages of the direct inlet methodology is the lack of an autosampler, requiring constant user involvement. Additionally, depending on the complexity of the sample, not all TG regioisomers can be analyzed during the same run. As the vaporization of the sample on the probe filament is quite rapid, we can only track a limited number of simultaneous product ion scans. Currently, the highest number of simultaneous product ion scans used with complex samples has been seven. Consequently, the lack of autosampler somewhat limits the usage of this method in large-scale analyses with a high number of samples. The method is, however, very useful for characterizing TG regioisomer profiles of a limited number of samples. *MSPECTRA* software is simple to use and can rapidly process the data to calculate the TG regioisomers.

The UHPLC-MS^2 method utilizing the *TAG analyzer* software (**II**) has the advantage of a more accurate fragmentation model for various TG species. Additionally, the chromatographic separation of the TG species mitigates the effects of adjacent M+2 isotopes affecting the fragment ion ratios. The chromatographic separation of the TG species is currently quite long (50 min), and further method development might be useful in the future to increase the throughput of the method. In the current state, the *TAG analyzer* software is still in quite early stage of development. While it can calculate the TG regioisomers of interest, processing the results requires a lot of user effort as the software can only process one ACN:DB species at a time.

Going further, the UHPLC-MS^2 method has potential to be developed into a truly untargeted, accurate, and high-throughput analysis method for TG regioisomers. The currently used triple quadrupole MS^2 platform is perfectly fine for targeted work, but the instrument is lacking in capabilities for untargeted analyses. Therefore, the method should be transferred to the QTOF platform, enabling DDA with high mass-accuracy. Additionally, the data processing and calculations need to be streamlined and automated. There are still some factors that might be useful to explore in method development, such as using different adduct types for fragmentation. For example, $[M+Na]^+$ sodium adducts fragment more predictably (Makarov et al., 2018) compared to $[M+NH_4]^+$ ammonium adducts used in this work. Changing the adduct type could result in more accurate

fragmentation model. One advantage of the direct inlet MS^2 method is that the deprotonated FA fragments $[RCOO]^-$ can be used to calculate the initial molecular species distribution within the fragmented TG species, as the abundances of the $[RCOO]^-$ fragments represent the overall FA composition. This information can be used to construct the possible molecular species compositions, setting boundaries for the regioisomer optimizations. This possibly results in more accurate regioisomer abundances. The UHPLC-MS^2 method with $[M+NH_4]^+$ adducts does not have this feature. Testing other adduct types might be useful in this regard as well.

Combining the observations from both methodologies, a realistic ideal method would have the following features: chromatographic separation of TG species; untargeted data-dependent fragmentation with high mass accuracy; initial molecular species composition calculated with FA fragments; fragmentation model accounting for differences in TGs; an optimization algorithm accounting for the isobaric overlap of fragments from different TGs; an automated calculation software to identify and calculate the regioisomers from the vast amounts of untargeted data.

5.1.6.2 PL regioisomer analysis methods

Even though the existing PL regioisomer analysis methods are less established compared to TG regioisomer methods, the process seems more straightforward. One significant factor for this is the lack of interfering isobaric fragments from multiple PL molecular species. Because PLs have only two FAs, the resulting FA pairs are unique within the species. This allows the use of simple calibration curves even in complex samples to quantify PL regioisomers of interest. However, one major obstacle for PL regioisomer analysis has traditionally been the lack of reference standards, especially for classes other than PC. This limitation could be mitigated by developing a fragmentation model, as was done for PC class in the thesis work (**IV**). This does require a certain number of reference standards, however. Having more standards will likely result in a more accurate model. Preliminary work for developing fragmentation models for PE and PS classes was done, but the low number of available standards resulted in inadequate models.

As the PL classes have very different fragmentation patterns and efficiencies with ESI on negative ionization mode, establishing the fragment ion ratios of various compounds is essential for the fragmentation model development. One potential way of reducing the reliance on expensive regiopure reference standards could be chromatographic separation of non-regiopure standards or other samples that contain both regioisomers at varying ratios. While the chromatographic method would not be applicable for high-throughput routine analyses, it could be used for establishing fragment ion ratios of the separated

regioisomers. Our aim is to further develop the method and calculation software to cover the other PL classes in addition to PC.

Overall, there is a strong need for a comprehensive and untargeted PL regioisomer analysis method. Lipidomics methods are mostly limited on molecular species level, incapable of resolving accurate regioisomer ratios (Heiles, 2021; Züllig & Köfeler, 2021). Current chromatographic (Kozlowski et al., 2015b; Sorensen et al., 2020) or ion mobility (Fouque et al., 2019; Ieritano et al., 2019; Kyle et al., 2016) methods are only capable of separating specific regioisomer pairs and have not yet proven to be effective in simultaneous separation of a wide range of PL regioisomers. Using MS based methodologies, there are several examples of untargeted identification of the major regioisomers within each pair using the relative fragment ion abundances without calibration curves (Liu et al., 2020; L. Zhao et al., 2022). This approach does not give accurate information on the regioisomer ratios within the pairs as it only attempts to identify the most abundant regioisomer. Additionally, identifying the major regioisomer using the fragment ion abundances alone is not always straightforward as the ratios are influenced by the attached FAs, and natural PL mixtures can contain regioisomers that have almost equal abundances.

Some methods use a dual stage fragmentation consisting of CID-OzID with an ion trap instrument (Batarseh et al., 2018; Pham et al., 2014) for PL regioisomer analysis. Using positive ionization mode, the polar head group can be dissociated in the first fragmentation step with CID. One benefit from this approach is that the resulting fragments of different PL classes behave in a relatively similar manner in the following OzID fragmentation step (Pham et al., 2014), potentially reducing the need for multiple regioisomer standards within each class. Certain dissociation techniques can produce *sn*-specific fragments, for example EIEIO (Baba et al., 2018; Campbell & Baba, 2015), multi-stage CID (Lillja & Lanekoff, 2022) or UVPD (Becher et al., 2018). This means that the origin of the fragments can be traced to either *sn*-1 or *sn*-2 positions. While the fragments are *sn*-specific, calibration curves are still required to determine the accurate regioisomer ratios, because the dissociation efficiencies and the observed fragment ion ratios can still be influenced by a multitude of factors such as FA chain lengths and double bond numbers.

One of the advantages of our approach is that it uses fragmentation with CID only, making it usable with virtually any MS^2 instrument. This would allow for the method to be incorporated in standard lipidomics methods utilizing DDA with ESI(–)-CID-MS^2. While the fragmentation model could also be adapted for usage with low-resolution instruments such as triple quadrupole MS, untargeted analysis and data processing with the software require a high-resolution instrument.

6 SUMMARY AND CONCLUSION

Comprehensive analysis of TG and PL regioisomers in natural samples is very challenging, and no perfect methods exist. Traditionally, chromatographic separation has been common in targeted TG regioisomer analysis methods, but they are often time consuming and tailored for specific regioisomers of interest. Mass spectrometric analysis methods utilizing structurally informative fragment ion ratios have been used by many researchers to study TG regioisomers. However, untargeted high-throughput methods have not seen wide adaptation mainly due to interfering isobaric fragment ions from multiple co-eluting TG species. Additionally, the fragmentation efficiencies of various TG and PL species vary significantly based on the identities of the attached FAs, and in case of PLs, the polar head group of the class is a very significant contributor to the differences in fragmentation patterns. For PL regioisomers, one of the main obstacles has been the lack of available reference standards.

In the thesis work, several major steps were taken forward towards the goal of developing comprehensive, untargeted TG and PL regioisomer analysis methods. In studies **I** and **II**, unique optimization algorithms were used for determining TG regioisomer abundances in complex natural samples. Both *MSPECTRA* (**I**) and *TAG analyzer* (**II**) calculation programs can mitigate the effects of interfering isobaric fragment ions by looking at the measured spectra and finding TG regioisomer concentrations that produce the observed spectra. *TAG analyzer* also has built-in fragmentation model calibrated with reference standards. The use of optimization algorithms is critical when analyzing TG regioisomer in complex samples, and even a comprehensive set of calibration curves or a perfect fragmentation model would not yield accurate results if the effects of overlapping fragment ions are not taken into consideration. The UHPLC-MS^2 method in combination with the *TAG analyzer* software (**II**) has potential to be further refined into an untargeted comprehensive method and used in lipidomics applications, while the direct inlet MS^2 method (**I**) primarily remains a simple and rapid method for specific targeted analyses.

The PL analysis method and the developed calculation software (**IV**) already provide an untargeted platform for analysis of PC regioisomers. With further method development, the software and the fragmentation model can be updated to process other PL classes as well, which we are focusing on in the future work. Analysis of TG and PL regioisomers has not been covered by current existing lipidomics applications. Overall, the methods, fragmentation models and optimization algorithms developed in this thesis work act as a proof of concept, potentially allowing standard lipidomics methods to be taken one step further into the structural analysis of regioisomers.

ACKNOWLEDGEMENTS

The thesis work was carried out at the Food Sciences unit at University of Turku. I'm extremely grateful for the Doctoral Programme in Technology who granted me a four-year salaried position to pursue my doctoral degree, covering most of my personal funding and allowing me to fully focus on my research. The Finnish Food Research Foundation is thanked for providing funding for the final few months leading to my thesis defense.

The research was also partially funded by the Academy of Finland as part of the project *Chiral lipids in chiral nature: a novel strategy for regio- and stereospecific research of human milk and omega-3 lipids*, as well as Valio Ltd, which facilitated the purchase of many important reference compounds vital to my thesis work. I am grateful to the American Oil Chemists' Society and Turku University Foundation for providing travel grants that enabled me to network with other professionals and present my research findings internationally.

I would like to extend my gratitude to my supervisors Baoru Yang, Jukka-Pekka Suomela, and Marko Tarvainen for their guidance and for fostering my growth into the independent researcher I am today. Your trust in my abilities to undertake this challenging research and the freedom you granted me in planning and conducting the work are deeply appreciated.

I also want to acknowledge the steering committee members Kaisa Linderborg and Heikki Kallio, as both of you have been really supportive during this time, especially Kaisa for providing a lot of help during the early stages of my research. My sincere gratitude also goes to my co-authors Marika Kalpio, Pontus Boström and Mohammed Sazzad. I wish to thank Yuqing Zhang for helping me with sample extractions and Linda Intonen for doing fatty acid composition analyses as part of her advanced laboratory work.

I would also like to offer my thanks to my fellow peers and colleagues Ella Aitta, Niina Kelanne, Eija Ahonen, Hany Ahmed, Annelie Damerau, Gabriele Beltrame, Anna Puganen, Ye Tian, Maaria Kortesniemi, Oskar Laaksonen and everyone else at our unit for all the help and lunchtime conversations.

For my parents I want to express my deepest gratitude for the unwavering support throughout my life, and for instilling in me the values and work ethic that have driven me to achieve this milestone.

And finally, Tanja. Our journey began as fellow students, progressed to coworkers and friends, and has now blossomed into something much more. Thank you for the endless love, support and understanding. This whole process has been significantly easier because of you.

Turku, June 2023

REFERENCES

Abreu, S., Heron, S., Solgadi, A., Joffre, F., Tchapla, A., & Chaminade, P. (2021). Rapid assessment of triacylglycerol fatty acyls composition by LC-APPI+-HRMS using monoacylglycerol like fragments intensities. *Analytica Chimica Acta*, *1178*, 338809. https://doi.org/10.1016/j.aca.2021.338809

Adlof, R., & List, G. (2004). Analysis of triglyceride isomers by silver-ion high-performance liquid chromatography: Effect of column temperature on retention times. *Journal of Chromatography A*, *1046*(1–2), 109–113. https://doi.org/10.1016/j.chroma.2004.06.012

Alvarez-Rivera, G., Bueno, M., Ballesteros-Vivas, D., & Cifuentes, A. (2020). Chiral analysis in food science. *TrAC Trends in Analytical Chemistry*, *123*, 115761. https://doi.org/10.1016/j.trac.2019.115761

Arena, P., Sciarrone, D., Dugo, P., Donato, P., & Mondello, L. (2021). Pattern-Type Separation of Triacylglycerols by Silver Thiolate×Non-Aqueous Reversed Phase Comprehensive Liquid Chromatography. *Separations*, *8*(6), 88. https://doi.org/10.3390/separations8060088

Baba, T., Campbell, J. L., Le Blanc, J. C. Y., & Baker, P. R. S. (2016). Structural identification of triacylglycerol isomers using electron impact excitation of ions from organics (EIEIO). *Journal of Lipid Research*, *57*(11), 2015–2027. https://doi.org/10.1194/jlr.M070177

Baba, T., Campbell, J. L., le Blanc, J. C. Y., Baker, PaulR. S., & Ikeda, K. (2018). Quantitative structural multiclass lipidomics using differential mobility: electron impact excitation of ions from organics (EIEIO) mass spectrometry. *Journal of Lipid Research*, *59*(5), 910–919. https://doi.org/10.1194/jlr.D083261

Baiocchi, C., Medana, C., Dal Bello, F., Giancotti, V., Aigotti, R., & Gastaldi, D. (2015). Analysis of regioisomers of polyunsaturated triacylglycerols in marine matrices by HPLC/HRMS. *Food Chemistry*, *166*, 551–560. https://doi.org/10.1016/j.foodchem.2014.06.067

Balgoma, D., Guitton, Y., Evans, J. J., Le Bizec, B., Dervilly-Pinel, G., & Meynier, A. (2019). Modeling the fragmentation patterns of triacylglycerides in mass spectrometry allows the quantification of the regioisomers with a minimal number of standards. *Analytica Chimica Acta*, *1057*, 60–69. https://doi.org/10.1016/j.aca.2019.01.017

Bar-Yoseph, F., Lifshitz, Y., & Cohen, T. (2013). Review of sn-2 palmitate oil implications for infant health. *Prostaglandins, Leukotrienes and Essential Fatty Acids*, *89*(4), 139–143. https://doi.org/10.1016/j.plefa.2013.03.002

Batarseh, A. M., Abbott, S. K., Duchoslav, E., Alqarni, A., Blanksby, S. J., & Mitchell, T. W. (2018). Discrimination of isobaric and isomeric lipids in complex mixtures by combining ultra-high pressure liquid chromatography with collision and ozone-induced dissociation. *International Journal of Mass Spectrometry*, *431*, 27–36. https://doi.org/10.1016/j.ijms.2018.05.016

Becher, S., Esch, P., & Heiles, S. (2018). Relative Quantification of Phosphatidylcholine sn-Isomers Using Positive Doubly Charged Lipid-Metal Ion Complexes. *Analytical Chemistry*, *90*(19), 11486–11494. https://doi.org/10.1021/acs.analchem.8b02731

Born, M. E. N., & Prentice, B. M. (2020). Structural elucidation of phosphatidylcholines from tissue using electron induced dissociation. *International Journal of Mass Spectrometry*, *452*. https://doi.org/10.1016/j.ijms.2020.116338

Bouzidi, L., & Narine, S. S. (2012). Phase Behavior of Saturated Triacylglycerides—Influence of Symmetry and Chain Length Mismatch. In *Cocoa Butter and Related Compounds* (pp. 73–101). Elsevier. https://doi.org/10.1016/B978-0-9830791-2-5.50007-4

Bowman, A. P., Abzalimov, R. R., & Shvartsburg, A. A. (2017). Broad Separation of Isomeric Lipids by High-Resolution Differential Ion Mobility Spectrometry with Tandem Mass Spectrometry. *Journal of the American Society for Mass Spectrometry*, *28*(8), 1552–1561. https://doi.org/10.1007/s13361-017-1675-2

Byrd, R. H., Hribar, M. E., & Nocedal, J. (1999). An Interior Point Algorithm for Large-Scale Nonlinear Programming. *SIAM Journal on Optimization*, *9*(4), 877–900. https://doi.org/10.1137/S1052623497325107

Campbell, J. L., & Baba, T. (2015). Near-complete structural characterization of phosphatidylcholines using electron impact excitation of ions from organics. *Analytical Chemistry*, *87*(11), 5837–5845. https://doi.org/10.1021/acs.analchem.5b01460

Cao, W., Cheng, S., Yang, J., Feng, J., Zhang, W., Li, Z., Chen, Q., Xia, Y., Ouyang, Z., & Ma, X. (2020). Large-scale lipid analysis with C=C location and sn-position isomer resolving power. *Nature Communications*, *11*(1). https://doi.org/10.1038/s41467-019-14180-4

Causevic, A., Olofsson, K., Adlercreutz, P., & Grey, C. (2021). Non-aqueous reversed phase liquid chromatography with charged aerosol detection for quantitative lipid analysis with improved accuracy. *Journal of Chromatography A*, *1652*, 462374. https://doi.org/10.1016/j.chroma.2021.462374

Cavazzini, A., Pasti, L., Massi, A., Marchetti, N., & Dondi, F. (2011). Recent applications in chiral high performance liquid chromatography: A review. *Analytica Chimica Acta*, *706*(2), 205–222. https://doi.org/10.1016/j.aca.2011.08.038

Chen, Y., Zhang, X., Li, D., Yi, H., Xu, T., Li, S., & Zhang, L. (2019). Fatty acid and triacylglycerol comparison of infant formulas on the Chinese market. *International Dairy Journal*, *95*, 35–43. https://doi.org/10.1016/j.idairyj.2019.02.017

Chen, Y., Zhou, X. H., Han, B., Yu, Z., Yi, H. X., Jiang, S. L., Li, Y. Y., Pan, J. C., & Zhang, L. W. (2020). Regioisomeric and enantiomeric analysis of primary triglycerides in human milk by silver ion and chiral HPLC atmospheric pressure chemical ionization-MS. *Journal of Dairy Science*, *103*(9), 7761–7774. https://doi.org/10.3168/jds.2019-17353

Claes, B. S. R., Bowman, A. P., Poad, B. L. J., Young, R. S. E., Heeren, R. M. A., Blanksby, S. J., & Ellis, S. R. (2021). Mass Spectrometry Imaging of Lipids with Isomer Resolution Using High-Pressure Ozone-Induced Dissociation. *Analytical Chemistry*, *93*(28), 9826–9834. https://doi.org/10.1021/acs.analchem.1c01377

Cubero Herrera, L., Ramaley, L., Potvin, M. A., & Melanson, J. E. (2013). A method for determining regioisomer abundances of polyunsaturated triacylglycerols in omega-3 enriched fish oils using reversed-phase liquid chromatography and triple-stage mass spectrometry. *Food Chemistry*, *139*(1–4), 655–662. https://doi.org/10.1016/j.foodchem.2012.12.059

Dai, Y., Tang, H., & Pang, S. (2021). The Crucial Roles of Phospholipids in Aging and Lifespan Regulation. *Frontiers in Physiology*, *12*. https://doi.org/10.3389/fphys.2021.775648

Damerau, A., Ahonen, E., Kortesniemi, M., Gudmundsson, H. G., Yang, B., Haraldsson, G. G., & Linderborg, K. M. (2023). Docosahexaenoic acid in regio- and enantiopure triacylglycerols: Oxidative stability and influence of chiral antioxidant. *Food Chemistry*, *402*, 134271. https://doi.org/10.1016/j.foodchem.2022.134271

Dillon, J. T., Aponte, J. C., Tarozo, R., & Huang, Y. (2012). Efficient liquid chromatographic analysis of mono-, di-, and triglycerols using silver thiolate stationary phase. *Journal of Chromatography A*, *1240*, 90–95. https://doi.org/10.1016/j.chroma.2012.03.083

Dobson, G., Christie, W. W., & Nikolova-Damyanova, B. (1995). Silver ion chromatography of lipids and fatty acids. *Journal of Chromatography B: Biomedical Sciences and Applications*, *671*(1–2), 197–222. https://doi.org/10.1016/0378-4347(95)00157-E

Dote, S., Yamamoto, Y., & Hara, S. (2016). Effects of Triacylglycerol Molecular Species on the Oxidation Behavior of Oils Containing α-Linolenic Acid. *Journal of Oleo Science*, *65*(3), 193–199. https://doi.org/10.5650/jos.ess15272

Dugo, P., Favoino, O., Tranchida, P. Q., Dugo, G., & Mondello, L. (2004). Off-line coupling of non-aqueous reversed-phase and silver ion high-performance liquid chromatography-mass spectrometry for the characterization of rice oil triacylglycerol positional isomers. *Journal of Chromatography A*, *1041*(1–2), 135–142. https://doi.org/10.1016/j.chroma.2004.04.063

Ekroos, K., Ejsing, C. S., Bahr, U., Karas, M., Simons, K., & Shevchenko, A. (2003a). Charting molecular composition of phosphatidylcholines by fatty acid scanning and ion trap MS3 fragmentation. *Journal of Lipid Research*, *44*(11), 2181–2192. https://doi.org/10.1194/jlr.D300020-JLR200

Ekroos, K., Ejsing, C. S., Bahr, U., Karas, M., Simons, K., & Shevchenko, A. (2003b). Charting molecular composition of phosphatidylcholines by fatty acid scanning and ion trap MS3 fragmentation. *Journal of Lipid Research*, *44*(11), 2181–2192. https://doi.org/10.1194/jlr.D300020-JLR200

Fabritius, M., Linderborg, K. M., Tarvainen, M., Kalpio, M., Zhang, Y., & Yang, B. (2020). Direct inlet negative ion chemical ionization tandem mass spectrometric analysis of triacylglycerol regioisomers in human milk and infant formulas. *Food Chemistry*, *328*, 126991. https://doi.org/10.1016/j.foodchem.2020.126991

Fabritius, M., & Yang, B. (2021). Direct infusion and ultra-high-performance liquid chromatography/electrospray ionization tandem mass spectrometry analysis of phospholipid regioisomers. *Rapid Communications in Mass Spectrometry*, *35*(18). https://doi.org/10.1002/rcm.9151

Fauconnot, L., Hau, J., Aeschlimann, J. M., Fay, L. B., & Dionisi, F. (2004). Quantitative analysis of triacylglycerol regioisomers in fats and oils using reversed-phase high-performance liquid chromatography and atmospheric pressure

chemical ionization mass spectrometry. *Rapid Communications in Mass Spectrometry*, *18*(2), 218–224. https://doi.org/10.1002/rcm.1317

Fouque, K. J. D., Ramirez, C. E., Lewis, R. L., Koelmel, J. P., Garrett, T. J., Yost, R. A., & Fernandez-Lima, F. (2019). Effective Liquid Chromatography-Trapped Ion Mobility Spectrometry-Mass Spectrometry Separation of Isomeric Lipid Species. *Analytical Chemistry*, *91*(8), 5021–5027. https://doi.org/10.1021/acs.analchem.8b04979

Gakwaya, R., Li, X., Wong, Y. L., Chivukula, S., Collins, E. J., & Evans, J. J. (2007). Examining the collision-induced decomposition spectra of ammoniated triglycerides. III. The linoleate and arachidonate series. *Rapid Communications in Mass Spectrometry*, *21*(20), 3262–3268. https://doi.org/10.1002/rcm.3208

Gazlay, W., & Evans, J. J. (2022). The impact of the complexing agent on the sensitivity of collision-induced dissociation spectra to fatty acid position for a set of XYZ-type triglycerides. *Rapid Communications in Mass Spectrometry*, *36*(4), 6–14. https://doi.org/10.1002/rcm.9226

George, A. D., Gay, M. C. L., Wlodek, M. E., Trengove, R. D., Murray, K., & Geddes, D. T. (2020). Untargeted lipidomics using liquid chromatography-ion mobility-mass spectrometry reveals novel triacylglycerides in human milk. *Scientific Reports*, *10*(1), 1–10. https://doi.org/10.1038/s41598-020-66235-y

Gotoh, N., Matsumoto, Y., Nagai, T., Mizobe, H., Otake, I., Ichioka, K., Kuroda, I., Watanabe, H., Noguchi, N., & Wada, S. (2011). Actual ratios of triacylglycerol positional isomers consisting of saturated and highly unsaturated fatty acids in fishes and marine mammals. *Food Chemistry*, *127*(2), 467–472. https://doi.org/10.1016/j.foodchem.2011.01.020

Gotoh, N., Matsumoto, Y., Nagai, T., Mizobe, H., Yoshinaga, K., Kojima, K., Kuroda, I., Kitamura, Y., Shimizu, T., Ishida, H., & Wada, S. (2012). Actual ratio of triacylglycerol positional isomers in milk and cheese. *Journal of Oleo Science*, *61*(4), 173–180. https://doi.org/10.5650/jos.61.173

Groessl, M., Graf, S., & Knochenmuss, R. (2015). High resolution ion mobility-mass spectrometry for separation and identification of isomeric lipids. *Analyst*, *140*(20), 6904–6911. https://doi.org/10.1039/c5an00838g

Gros, Q., Wolniaczyk, M., Duval, J., West, C., Horie, S., Toyota, Y., Funada, Y., & Lesellier, E. (2023). Comparison of the triglyceride composition of vegetable samples with ultra-high efficiency / low-pressure supercritical fluid chromatography – mass spectrometry. *Journal of Food Composition and Analysis*, *115*(October 2022), 104960. https://doi.org/10.1016/j.jfca.2022.104960

Grossert, J. S., Herrera, L. C., Ramaley, L., & Melanson, J. E. (2014). Studying the Chemistry of Cationized Triacylglycerols Using Electrospray Ionization Mass Spectrometry and Density Functional Theory Computations. *Journal of the American Society for Mass Spectrometry*, *25*(8), 1421–1440. https://doi.org/10.1007/s13361-014-0917-9

Grossert, J. S., Melanson, J. E., & Ramaley, L. (2020). Fragmentation pathways of cationized, saturated, short-chain triacylglycerols: Lithiated and sodiated tripropanoyl- And trihexanoylglycerol. *Journal of the American Society for Mass Spectrometry*, *31*(1), 34–46. https://doi.org/10.1021/jasms.9b00046

Heiles, S. (2021). Advanced tandem mass spectrometry in metabolomics and lipidomics—methods and applications. *Analytical and Bioanalytical Chemistry*, *413*(24), 5927–5948. https://doi.org/10.1007/s00216-021-03425-1

Herrera, L. C., Potvin, M. A., & Melanson, J. E. (2010). Quantitative analysis of positional isomers of triacylglycerols via electrospray ionization tandem mass spectrometry of sodiated adducts. *Rapid Communications in Mass Spectrometry*, *24*(18), 2745–2752. https://doi.org/10.1002/rcm.4700

Holčapek, M., Dvořáková, H., Lísa, M., Girón, A. J., Sandra, P., & Cvačka, J. (2010). Regioisomeric analysis of triacylglycerols using silver-ion liquid chromatography–atmospheric pressure chemical ionization mass spectrometry: Comparison of five different mass analyzers. *Journal of Chromatography A*, *1217*(52), 8186–8194. https://doi.org/10.1016/j.chroma.2010.10.064

Holčapek, M., & Lísa, M. (2017). Silver-Ion Liquid Chromatography–Mass Spectrometry. In *Handbook of Advanced Chromatography /mass Spectrometry Techniques* (pp. 115–140). Elsevier. https://doi.org/10.1016/B978-0-12-811732-3.00004-2

Holčapek, M., Velínská, H., Lísa, M., & Česla, P. (2009). Orthogonality of silver-ion and non-aqueous reversed-phase HPLC/MS in the analysis of complex natural mixtures of triacylglycerols. *Journal of Separation Science*, *32*(21), 3672–3680. https://doi.org/10.1002/jssc.200900401

Hsu, F.-F., & Turk, J. (2005). Studies on phosphatidylserine by tandem quadrupole and multiple stage quadrupole ion-trap mass

spectrometry with electrospray ionization: Structural characterization and the fragmentation processes. *Journal of the American Society for Mass Spectrometry*, *16*(9), 1510–1522. https://doi.org/10.1016/j.jasms.2005.04.018

Hsu, F.-F., & Turk, J. (2009). Electrospray ionization with low-energy collisionally activated dissociation tandem mass spectrometry of glycerophospholipids: Mechanisms of fragmentation and structural characterization. *Journal of Chromatography B*, *877*(26), 2673–2695. https://doi.org/10.1016/j.jchromb.2009.02.033

Hvattum, E., Hagelin, G., & Larsen, Å. (1998). Study of mechanisms involved in the collision-induced dissociation of carboxylate anions from glycerophospholipids using negative ion electrospray tandem quadrupole mass spectrometry. *Rapid Communications in Mass Spectrometry*, *12*(19), 1405–1409. https://doi.org/10.1002/(SICI)1097-0231(19981015)12:19<1405::AID-RCM338>3.0.CO;2-B

Ieritano, C., Campbell, J. L., & Hopkins, W. S. (2019). Unravelling the factors that drive separation in differential mobility spectrometry: A case study of regioisomeric phosphatidylcholine adducts. *International Journal of Mass Spectrometry*, *444*. https://doi.org/10.1016/j.ijms.2019.116182

Ikeda, I., Yoshida, H., Tomooka, M., Yosef, A., Imaizumi, K., Tsuji, H., & Seto, A. (1998). Effects of long-term feeding of marine oils with different positional distribution of eicosapentaenoic and docosahexaenoic acids on lipid metabolism, eicosanoid production, and platelet aggregation in hypercholesterolemic rats. *Lipids*, *33*(9), 897–904. https://doi.org/10.1007/s11745-998-0286-7

Innis, S. M. (2011). Dietary Triacylglycerol Structure and Its Role in Infant Nutrition. *Advances in Nutrition*, *2*(3), 275–283. https://doi.org/10.3945/an.111.000448

Itabashi, Y. (2012). Chiral separation of glycerolipids by high-performance liquid chromatography. *Journal of Lipid Nutrition*, *21*(1), 27–34. https://doi.org/10.4010/jln.21.27

Itabashi, Y., & Kuksis, A. (1997). Reassessment of Stereochemical Configuration of Natural Phosphatidylglycerols by Chiral-Phase High-Performance Liquid Chromatography and Electrospray Mass Spectrometry. In *ANALYTICAL BIOCHEMISTRY* (Vol. 254).

Jones, J. W., Thompson, C. J., Carter, C. L., & Kane, M. A. (2015). Electron-induced dissociation (EID) for structure characterization of glycerophosphatidylcholine: determination of double-bond positions and localization of acyl chains. *Journal of Mass Spectrometry*, *50*(12), 1327–1339. https://doi.org/10.1002/jms.3698

Judge, E. J., Zheng, D., Chivukula, S., Gakwaya, R., Schostarez, S., Li, X., Liriano, M., & Evans, J. J. (2017). A simple and economical strategy for obtaining calibration plots for relative quantification of positional isomers of YYX/YXY triglycerides using high-performance liquid chromatography/tandem mass spectrometry. *Rapid Communications in Mass Spectrometry*, *31*(20), 1690–1698. https://doi.org/10.1002/rcm.7953

Kallio, H., & Currie, G. (1993). Analysis of low erucic acid turnip rapeseed oil (Brassica campestris) by negative ion chemical ionization tandem mass spectrometry. A method giving information on the fatty acid composition in positions sn-2 and sn-1/3 of triacylglycerols. *Lipids*, *28*(3), 207–215. https://doi.org/10.1007/BF02536641

Kallio, H., Nylund, M., Boström, P., & Yang, B. (2017). Triacylglycerol regioisomers in human milk resolved with an algorithmic novel electrospray ionization tandem mass spectrometry method. *Food Chemistry*, *233*, 351–360. https://doi.org/10.1016/j.foodchem.2017.04.122

Kallio, H., & Rua, P. (1994). Distribution of the major fatty acids of human milk between sn-2 and sn-1,3 positions of triacylglycerols. *Journal of the American Oil Chemists' Society*, *71*(9), 985–992. https://doi.org/10.1007/BF02542266

Kalpio, M., Linderborg, K. M., Fabritius, M., Kallio, H., & Yang, B. (2021). Strategy for Stereospecific Characterization of Natural Triacylglycerols Using Multidimensional Chromatography and Mass Spectrometry. *Journal of Chromatography A*, 461992. https://doi.org/10.1016/j.chroma.2021.461992

Kalpio, M., Nylund, M., Linderborg, K. M., Yang, B., Kristinsson, B., Haraldsson, G. G., & Kallio, H. (2015). Enantioselective chromatography in analysis of triacylglycerols common in edible fats and oils. *Food Chemistry*, *172*, 718–724. https://doi.org/10.1016/j.foodchem.2014.09.135

Kim, H., Kang, S., Jung, B.-M., Yi, H., Jung, J. A., & Chang, N. (2017). Breast milk fatty acid composition and fatty acid intake of lactating mothers in South Korea. *British Journal of Nutrition*, *117*(4), 556–561. https://doi.org/10.1017/S0007114517000253

Kozlowski, R. L., Mitchell, T. W., & Blanksby, S. J. (2015a). A rapid ambient ionization-mass spectrometry approach to monitoring the relative

abundance of isomeric glycerophospholipids. *Scientific Reports*, *5*. https://doi.org/10.1038/srep09243

Kozlowski, R. L., Mitchell, T. W., & Blanksby, S. J. (2015b). Separation and Identification of Phosphatidylcholine Regioisomers by Combining Liquid Chromatography with a Fusion of Collision- and Ozone-Induced Dissociation. *European Journal of Mass Spectrometry*, *21*(3), 191–200. https://doi.org/10.1255/ejms.1300

Kuksis, A., Itabashi, Y., & Pruzanski, W. (2016). Chiral High-Performance Liquid Chromatography of Glycerophospholipids. In *Encyclopedia of Lipidomics* (pp. 1–16). Springer Netherlands. https://doi.org/10.1007/978-94-007-7864-1_163-1

Küllenberg, D., Taylor, L. A., Schneider, M., & Massing, U. (2012). Health effects of dietary phospholipids. *Lipids in Health and Disease*, *11*(1), 3. https://doi.org/10.1186/1476-511X-11-3

Kurvinen, J.-P., Rua, P., Sjövall, O., & Kallio, H. (2001). Software (MSPECTRA) for automatic interpretation of triacylglycerol molecular mass distribution spectra and collision induced dissociation product ion spectra obtained by ammonia negative ion chemical ionization mass spectrometry. *Rapid Communications in Mass Spectrometry*, *15*(13), 1084–1091. https://doi.org/10.1002/rcm.340

Kurvinen, J.-P., Sjövall, O., & Kallio, H. (2002). Molecular weight distribution and regioisomeric structure of triacylglycerols in some common human milk substitutes. *Journal of the American Oil Chemists' Society*, *79*(1), 13–22. https://doi.org/10.1007/s11746-002-0428-3

Kyle, J. E., Zhang, X., Weitz, K. K., Monroe, M. E., Ibrahim, Y. M., Moore, R. J., Cha, J., Sun, X., Lovelace, E. S., Wagoner, J., Polyak, S. J., Metz, T. O., Dey, S. K., Smith, R. D., Burnum-Johnson, K. E., & Baker, E. S. (2016). Uncovering biologically significant lipid isomers with liquid chromatography, ion mobility spectrometry and mass spectrometry. *Analyst*, *141*(5), 1649–1659. https://doi.org/10.1039/c5an02062j

Lagace, T. A., & Ridgway, N. D. (2013). The role of phospholipids in the biological activity and structure of the endoplasmic reticulum. *Biochimica et Biophysica Acta (BBA) - Molecular Cell Research*, *1833*(11), 2499–2510. https://doi.org/10.1016/j.bbamcr.2013.05.018

Lasekan, J. B., Hustead, D. S., Masor, M., & Murray, R. (2017). Impact of palm olein in infant formulas on stool consistency and frequency: a meta-analysis of randomized clinical trials. *Food & Nutrition Research*, *61*(1), 1330104. https://doi.org/10.1080/16546628.2017.1330104

Lee, J. W., Nagai, T., Gotoh, N., Fukusaki, E., & Bamba, T. (2014). Profiling of regioisomeric triacylglycerols in edible oils by supercritical fluid chromatography/tandem mass spectrometry. *Journal of Chromatography B*, *966*, 193–199. https://doi.org/10.1016/j.jchromb.2014.01.040

Leskinen, H., Suomela, J. P., & Kallio, H. P. (2009). Effect of latitude and weather conditions on the regioisomer compositions of α- and λ-linolenoyldilinoleoylglycerol in currant seed oils. In *Journal of Agricultural and Food Chemistry* (Vol. 57, Issue 9, pp. 3920–3926). https://doi.org/10.1021/jf900068b

Leskinen, H., Suomela, J.-P., & Kallio, H. P. (2010). Quantification of triacylglycerol regioisomers by ultra-high-performance liquid chromatography and ammonia negative ion atmospheric pressure chemical ionization tandem mass spectrometry. *Rapid Communications in Mass Spectrometry*, *24*(1), 1–5. https://doi.org/10.1002/rcm.4346

Leskinen, H., Suomela, J.-P., Pinta, J., & Kallio, H. (2008). Regioisomeric Structure Determination of α- and γ-Linolenoyldilinoleoylglycerol in Blackcurrant Seed Oil by Silver Ion High-Performance Liquid Chromatography and Mass Spectrometry. *Analytical Chemistry*, *80*(15), 5788–5793. https://doi.org/10.1021/ac8004132

Leskinen, H., Suomela, J.-P., Yang, B., & Kallio, H. P. (2010). Regioisomer Compositions of Vaccenic and Oleic Acid Containing Triacylglycerols in Sea Buckthorn (Hippophaë rhamnoides) Pulp Oils: Influence of Origin and Weather Conditions. *Journal of Agricultural and Food Chemistry*, *58*(1), 537–545. https://doi.org/10.1021/jf902679v

Leveque, N. L., Acheampong, A., Heron, S., & Tchapla, A. (2012). Determination of triacylglycerol regioisomers using electrospray ionization-quadrupole ion trap mass spectrometry with a kinetic method. *Analytica Chimica Acta*, *722*, 80–86. https://doi.org/10.1016/j.aca.2012.02.016

Lévêque, N. L., Héron, S., & Tchapla, A. (2010). Regioisomer characterization of triacylglycerols by non-aqueous reversed-phase liquid chromatography/electrospray ionization mass spectrometry using silver nitrate as a post column reagent. *Journal of Mass Spectrometry*, *45*(3), 284–296. https://doi.org/10.1002/jms.1713

Li, M., Li, Q., Kang, S., Cao, X., Zheng, Y., Wu, J., Wu, R., Shao, J., Yang, M., & Yue, X. (2020). Characterization and comparison of lipids in bovine colostrum and mature milk based on

UHPLC-QTOF-MS lipidomics. *Food Research International*, *136*(June), 109490. https://doi.org/10.1016/j.foodres.2020.109490

Li, X., Collins, E. J., & Evans, J. J. (2006). Examining the collision-induced decomposition spectra of ammoniated triglycerides as a function of fatty acid chain length and degree of unsaturation. II. The PXP/YPY series. *Rapid Communications in Mass Spectrometry*, *20*(2), 171–177. https://doi.org/10.1002/rcm.2270

Li, X., & Evans, J. J. (2005). Examining the collision-induced decomposition spectra of ammoniated triglycerides as a function of fatty acid chain length and degree of unsaturation. I. The OXO/YOY series. *Rapid Communications in Mass Spectrometry*, *19*(18), 2528–2538. https://doi.org/10.1002/rcm.2087

Liebisch, G., Fahy, E., Aoki, J., Dennis, E. A., Durand, T., Ejsing, C. S., Fedorova, M., Feussner, I., Griffiths, W. J., Köfeler, H., Merrill, A. H., Murphy, R. C., O'Donnell, V. B., Oskolkova, O., Subramaniam, S., Wakelam, M. J. O., & Spener, F. (2020). Update on LIPID MAPS classification, nomenclature, and shorthand notation for MS-derived lipid structures. *Journal of Lipid Research*, *61*(12), 1539–1555. https://doi.org/10.1194/jlr.S120001025

Lillja, J., & Lanekoff, I. (2022). Quantitative determination of sn-positional phospholipid isomers in MSn using silver cationization. *Analytical and Bioanalytical Chemistry*, *414*(25), 7473–7482. https://doi.org/10.1007/s00216-022-04173-6

Lin, J. T., & Arcinas, A. (2008). Analysis of regiospecific triacylglycerols by electrospray ionization-mass spectrometry3 of lithiated adducts. *Journal of Agricultural and Food Chemistry*, *56*(13), 4909–4915. https://doi.org/10.1021/jf072837k

Lin, J. T., & Chen, G. Q. (2010). Acylglycerols containing trihydroxy fatty acids in castor oil and the regiospecific quantification of triacylglycerols. *JAOCS, Journal of the American Oil Chemists' Society*, *87*(11), 1371–1379. https://doi.org/10.1007/s11746-010-1617-7

Linderborg, K. M., & Kallio, H. P. T. (2005). Triacylglycerol Fatty Acid Positional Distribution and Postprandial Lipid Metabolism. *Food Reviews International*, *21*(3), 331–355. https://doi.org/10.1080/FRI-200061623

Linderborg, K. M., Kalpio, M., Mäkelä, J., Niinikoski, H., Kallio, H. P., & Lagström, H. (2014). Tandem mass spectrometric analysis of human milk triacylglycerols from normal weight and overweight mothers on different diets. *Food Chemistry*, *146*, 583–590. https://doi.org/10.1016/j.foodchem.2013.09.092

Lísa, M., Denev, R., & Holčapek, M. (2013). Retention behavior of isomeric triacylglycerols in silver-ion HPLC: Effects of mobile phase composition and temperature. *Journal of Separation Science*, *36*(17), 2888–2900. https://doi.org/10.1002/jssc.201300550

Lísa, M., & Holčapek, M. (2013). Characterization of triacylglycerol enantiomers using chiral HPLC/APCI-MS and synthesis of enantiomeric triacylglycerols. *Analytical Chemistry*, *85*(3), 1852–1859. https://doi.org/10.1021/ac303237a

Lísa, M., & Holčapek, M. (2015). High-Throughput and Comprehensive Lipidomic Analysis Using Ultrahigh-Performance Supercritical Fluid Chromatography-Mass Spectrometry. *Analytical Chemistry*, *87*(14), 7187–7195. https://doi.org/10.1021/acs.analchem.5b01054

Lísa, M., Netušilová, K., Franěk, L., Dvořáková, H., Vrkoslav, V., & Holčapek, M. (2011). Characterization of fatty acid and triacylglycerol composition in animal fats using silver-ion and non-aqueous reversed-phase high-performance liquid chromatography/mass spectrometry and gas chromatography/flame ionization detection. *Journal of Chromatography A*, *1218*(42), 7499–7510. https://doi.org/10.1016/j.chroma.2011.07.032

Lísa, M., Velínská, H., & Holčapek, M. (2009). Regioisomeric Characterization of Triacylglycerols Using Silver-Ion HPLC/MS and Randomization Synthesis of Standards. *Analytical Chemistry*, *81*(10), 3903–3910. https://doi.org/10.1021/ac900150j

Liu, Z., Li, C., Pryce, J., & Rochfort, S. (2020). Comprehensive Characterization of Bovine Milk Lipids: Phospholipids, Sphingolipids, Glycolipids, and Ceramides. *Journal of Agricultural and Food Chemistry*, *68*(24), 6726–6738. https://doi.org/10.1021/acs.jafc.0c01604

Liu, Z., & Rochfort, S. (2021). Bovine Milk Triacylglycerol Regioisomer Ratio Shows Remarkable Inter-Breed and Inter-Cow Variation. *Molecules*, *26*(13), 3938. https://doi.org/10.3390/molecules26133938

Liu, Z., & Rochfort, S. (2022). Regio-distribution and double bond locations of unsaturated fatty acids in phospholipids of bovine milk. *Food Chemistry*, *373*. https://doi.org/10.1016/j.foodchem.2021.131515

López-López, A., Castellote-Bargalló, A. I., Campoy-Folgoso, C., Rivero-Urgel, M., Tormo-Carnicé, R., Infante-Pina, D., & López-Sabater, M. C.

(2001). The influence of dietary palmitic acid triacylglyceride position on the fatty acid, calcium and magnesium contents of at term newborn faeces. *Early Human Development*, *65*, S83–S94. https://doi.org/10.1016/S0378-3782(01)00210-9

Maccarone, A. T., Duldig, J., Mitchell, T. W., Blanksby, S. J., Duchoslav, E., & Campbell, J. L. (2014). Characterization of acyl chain position in unsaturated phosphatidylcholines using differential mobility-mass spectrometry. *Journal of Lipid Research*, *55*(8), 1668–1677. https://doi.org/10.1194/jlr.M046995

Makarov, P., Zheng, D., Le, D., & Evans, J. J. (2018). Impact of the complexing cation on the sensitivity of collision-induced dissociation spectra to fatty acid position for a set of YXY/YYX-type triglycerides. *Rapid Communications in Mass Spectrometry*, *32*(18), 1591–1598. https://doi.org/10.1002/rcm.8211

Mäkelä, J., Linderborg, K., Niinikoski, H., Yang, B., & Lagström, H. (2013). Breast milk fatty acid composition differs between overweight and normal weight women: the STEPS Study. *European Journal of Nutrition*, *52*(2), 727–735. https://doi.org/10.1007/s00394-012-0378-5

Malone, M., & Evans, J. J. (2004). Determining the relative amounts of positional isomers in complex mixtures of triglycerides using reversed-phase high-performance liquid chromatography-tandem mass spectrometry. *Lipids*, *39*(3), 273–284. https://doi.org/10.1007/s11745-004-1230-6

Marchand, J., Guitton, Y., Martineau, E., Royer, A.-L., Balgoma, D., le Bizec, B., Giraudeau, P., & Dervilly, G. (2021). Extending the Lipidome Coverage by Combining Different Mass Spectrometric Platforms: An Innovative Strategy to Answer Chemical Food Safety Issues. *Foods*, *10*(6), 1218. https://doi.org/10.3390/foods10061218

Marshall, D. L., Pham, H. T., Bhujel, M., Chin, J. S. R., Yew, J. Y., Mori, K., Mitchell, T. W., & Blanksby, S. J. (2016). Sequential Collision- and Ozone-Induced Dissociation Enables Assignment of Relative Acyl Chain Position in Triacylglycerols. *Analytical Chemistry*, *88*(5), 2685–2692. https://doi.org/10.1021/acs.analchem.5b04001

Masuda, K., Abe, K., & Murano, Y. (2021). A Practical Method for Analysis of Triacylglycerol Isomers Using Supercritical Fluid Chromatography. *Journal of the American Oil Chemists' Society*, *98*(1), 21–29. https://doi.org/10.1002/aocs.12432

Minato, A., Ueno, S., Smith, K., Amemiya, Y., & Sato, K. (1997). Thermodynamic and Kinetic Study on Phase Behavior of Binary Mixtures of POP and PPO Forming Molecular Compound Systems. *The Journal of Physical Chemistry B*, *101*(18), 3498–3505. https://doi.org/10.1021/jp962956v

Momchilova, S., Itabashi, Y., Nikolova-Damyanova, B., & Kuksis, A. (2006). Regioselective separation of isomeric triacylglycerols by reversed-phase high-performance liquid chromatography: Stationary phase and mobile phase effects. *Journal of Separation Science*, *29*(17), 2578–2583. https://doi.org/10.1002/jssc.200500504

Mondello, L., Tranchida, P. Q., Stanek, V., Jandera, P., Dugo, G., & Dugo, P. (2005). Silver-ion reversed-phase comprehensive two-dimensional liquid chromatography combined with mass spectrometric detection in lipidic food analysis. *Journal of Chromatography A*, *1086*(1–2), 91–98. https://doi.org/10.1016/j.chroma.2005.06.017

Much, D., Brunner, S., Vollhardt, C., Schmid, D., Sedlmeier, E.-M., Brüderl, M., Heimberg, E., Bartke, N., Boehm, G., Bader, B. L., Amann-Gassner, U., & Hauner, H. (2013). Breast milk fatty acid profile in relation to infant growth and body composition: results from the INFAT study. *Pediatric Research*, *74*(2), 230–237. https://doi.org/10.1038/pr.2013.82

Nagai, T., Gotoh, N., Mizobe, H., Yoshinaga, K., Kojima, K., Matsumoto, Y., & Wada, S. (2011). Rapid separation of triacylglycerol positional isomers binding two saturated fatty acids using octacocyl silylation column. *Journal of Oleo Science*, *60*(7), 345–350. https://doi.org/10.5650/jos.60.345

Nagai, T., Kinoshita, T., Kasamatsu, E., Yoshinaga, K., Mizobe, H., Yoshida, A., Itabashi, Y., & Gotoh, N. (2019). Simultaneous separation of triacylglycerol enantiomers and positional isomers by chiral high performance liquid chromatography coupled with mass spectrometry. *Journal of Oleo Science*, *68*(10), 1019–1026. https://doi.org/10.5650/jos.ess19122

Nagai, T., Kinoshita, T., Kasamatsu, E., Yoshinaga, K., Mizobe, H., Yoshida, A., Itabashi, Y., & Gotoh, N. (2020). Simultaneous quantification of mixed-acid triacylglycerol positional isomers and enantiomers in palm oil and lard by chiral high-performance liquid chromatography coupled with mass spectrometry. *Symmetry*, *12*(9), 1–7. https://doi.org/10.3390/SYM12091385

Nagai, T., Mizobe, H., Otake, I., Ichioka, K., Kojima, K., Matsumoto, Y., Gotoh, N., Kuroda, I., & Wada, S. (2011). Enantiomeric separation of asymmetric triacylglycerol by recycle high-performance liquid chromatography with chiral

column. *Journal of Chromatography A*, *1218*(20), 2880–2886. https://doi.org/10.1016/j.chroma.2011.02.067

Nagai, T., Watanabe, N., Yoshinaga, K., Mizobe, H., Kojima, K., Kuroda, I., Odanaka, Y., Saito, T., Beppu, F., & Gotoh, N. (2015). Abundances of triacylglycerol positional isomers and enantiomers comprised of a dipalmitoylglycerol backbone and short- or medium-chain fatty acids in bovine milk fat. *Journal of Oleo Science*, *64*(9), 943–952. https://doi.org/10.5650/jos.ess15040

Nakanishi, H., Iida, Y., Shimizu, T., & Taguchi, R. (2010). Separation and quantification of sn-1 and sn-2 fatty acid positional isomers in phosphatidylcholine by RPLC-ESIMS/MS. *The Journal of Biochemistry*, *147*(2), 245–256. https://doi.org/10.1093/jb/mvp171

Nguyen, T. L., Hlangothi, D., & Saleh, M. A. (2018). Characterization of Silybum marianum triacylglycerol regioisomers using accurate mass quadrupole time of flight mass spectrometry . *Cogent Chemistry*, *4*(1), 1477246. https://doi.org/10.1080/23312009.2018.1477246

Ovčačíková, M., Lísa, M., Cífková, E., & Holčapek, M. (2016). Retention behavior of lipids in reversed-phase ultrahigh-performance liquid chromatography-electrospray ionization mass spectrometry. *Journal of Chromatography A*, *1450*, 76–85. https://doi.org/10.1016/j.chroma.2016.04.082

Paine, M. R. L., Poad, B. L. J., Eijkel, G. B., Marshall, D. L., Blanksby, S. J., Heeren, R. M. A., & Ellis, S. R. (2018). Mass Spectrometry Imaging with Isomeric Resolution Enabled by Ozone-Induced Dissociation. *Angewandte Chemie*, *130*(33), 10690–10694. https://doi.org/10.1002/ange.201802937

Palyzová, A., & Řezanka, T. (2020a). Enantiomeric separation of triacylglycerols containing fatty acids with a ring (cyclofatty acids). *Journal of Chromatography A*, *1622*, 1–9. https://doi.org/10.1016/j.chroma.2020.461103

Palyzová, A., & Řezanka, T. (2020b). Separation of triacylglycerols containing allenic and acetylenic fatty acids by enantiomeric liquid chromatography-mass spectrometry. *Journal of Chromatography A*, *1623*. https://doi.org/10.1016/j.chroma.2020.461161

Peng, K.-Y., Salim, M., Pelle, J., Ramirez, G., & Boyd, B. J. (2021). TAILOR-MS, a Python Package that Deciphers Complex Triacylglycerol Fatty Acyl Structures: Applications for Bovine Milk and Infant Formulas. *Analytical Chemistry*, *93*(14), 5684–5690. https://doi.org/10.1021/acs.analchem.0c04373

Pham, H. T., Maccarone, A. T., Thomas, M. C., Campbell, J. L., Mitchell, T. W., & Blanksby, S. J. (2014). Structural characterization of glycerophospholipids by combinations of ozone- and collision-induced dissociation mass spectrometry: The next step towards "top-down" lipidomics. *Analyst*, *139*(1), 204–214. https://doi.org/10.1039/c3an01712e

Purdy, G. E., Pacheco, S., Turk, J., & Hsu, F.-F. (2013). Characterization of mycobacterial triacylglycerols and monomeromycolyl diacylglycerols from Mycobacterium smegmatis biofilm by electrospray ionization multiple-stage and high-resolution mass spectrometry. *Analytical and Bioanalytical Chemistry*, *405*(23), 7415–7426. https://doi.org/10.1007/s00216-013-7179-4

Ramaley, L., Cubero Herrera, L., & Melanson, J. E. (2015). Quantitative analysis of TAG in oils using lithium cationization and direct-infusion ESI tandem mass spectrometry. *JAOCS, Journal of the American Oil Chemists' Society*, *92*(3), 323–334. https://doi.org/10.1007/s11746-015-2604-9

Ramaley, L., Herrera, L. C., & Melanson, J. E. (2013). Applicability of non-linear versus linear fractional abundance calibration plots for the quantitative determination of triacylglycerol regioisomers by tandem mass spectrometry. *Rapid Communications in Mass Spectrometry*, *27*(11), 1251–1259. https://doi.org/10.1002/rcm.6569

Randolph, C. E., Blanksby, S. J., & McLuckey, S. A. (2020). Toward Complete Structure Elucidation of Glycerophospholipids in the Gas Phase through Charge Inversion Ion/Ion Chemistry. *Analytical Chemistry*, *92*(1), 1219–1227. https://doi.org/10.1021/acs.analchem.9b04376

Renaud, J. B., Overton, S., & Mayer, P. M. (2013). Energy and entropy at play in competitive dissociations: The case of uneven positional dissociation of ionized triacylglycerides. *International Journal of Mass Spectrometry*, *352*, 77–86. https://doi.org/10.1016/j.ijms.2013.06.027

Řezanka, T., Lukavský, J., Nedbalová, L., & Sigler, K. (2011). Effect of nitrogen and phosphorus starvation on the polyunsaturated triacylglycerol composition, including positional isomer distribution, in the alga Trachydiscus minutus. *Phytochemistry*, *72*(18), 2342–2351. https://doi.org/10.1016/j.phytochem.2011.08.017

Řezanka, T., Lukavský, J., Rozmoš, M., Nedbalová, L., & Jansa, J. (2022). Separation of triacylglycerols containing positional isomers of hexadecenoic acids by enantiomeric liquid

chromatography-mass spectrometry. *Journal of Chromatography B: Analytical Technologies in the Biomedical and Life Sciences*, *1208*(April), 123401. https://doi.org/10.1016/j.jchromb.2022.123401

Řezanka, T., Lukavský, J., Siristova, L., & Sigler, K. (2012). Regioisomer separation and identification of triacylglycerols containing vaccenic and oleic acids, and α- and γ-linolenic acids, in thermophilic cyanobacteria Mastigocladus laminosus and Tolypothrix sp. *Phytochemistry*, *78*, 147–155. https://doi.org/10.1016/j.phytochem.2012.02.028

Řezanka, T., Nedbalová, L., & Sigler, K. (2016). Enantiomeric separation of triacylglycerols containing polyunsaturated fatty acids with 18 carbon atoms. *Journal of Chromatography A*, *1467*, 261–269. https://doi.org/10.1016/j.chroma.2016.07.006

Řezanka, T., Schreiberová, O., Krulikovská, T., Masák, J., & Sigler, K. (2010). RP-HPLC/MS-APCI analysis of odd-chain TAGs from Rhodococcus erythropolis including some regioisomers. *Chemistry and Physics of Lipids*, *163*(4–5), 373–380. https://doi.org/10.1016/j.chemphyslip.2010.01.007

Řezanka, T., & Sigler, K. (2014). Separation of enantiomeric triacylglycerols by chiral-phase HPLC. *Lipids*, *49*(12), 1251–1260. https://doi.org/10.1007/s11745-014-3959-7

Šala, M., Lísa, M., Campbell, J. L., & Holčapek, M. (2016). Determination of triacylglycerol regioisomers using differential mobility spectrometry. *Rapid Communications in Mass Spectrometry*, *30*(2), 256–264. https://doi.org/10.1002/rcm.7430

Santoro, V., Dal Bello, F., Aigotti, R., Gastaldi, D., Romaniello, F., Forte, E., Magni, M., Baiocchi, C., & Medana, C. (2018). Characterization and determination of interesterification markers (triacylglycerol regioisomers) in confectionery oils by liquid chromatography-mass spectrometry. *Foods*, *7*(2), 23. https://doi.org/10.3390/foods7020023

Sazzad, M. A. Al, Fabritius, M., Boström, P., Tarvainen, M., Kalpio, M., Linderborg, K. M., Kallio, H., & Yang, B. (2022). A novel UHPLC-ESI-MS/MS method and automatic calculation software for regiospecific analysis of triacylglycerols in natural fats and oils. *Analytica Chimica Acta*, *1210*(March), 339887. https://doi.org/10.1016/j.aca.2022.339887

Segall, S. D., Artz, W. E., Raslan, D. S., Ferraz, V. P., & Takahashi, J. A. (2005). Analysis of triacylglycerol isomers in Malaysian cocoa butter using HPLC-mass spectrometry. *Food Research International*, *38*(2), 167–174. https://doi.org/10.1016/j.foodres.2004.09.008

Skórkowska-Telichowska, K., Kosińska, J., Chwojnicka, M., Tuchendler, D., Tabin, M., Tuchendler, R., Bobak, Ł., Trziszka, T., & Szuba, A. (2016). Positive effects of egg-derived phospholipids in patients with metabolic syndrome. *Advances in Medical Sciences*, *61*(1), 169–174. https://doi.org/10.1016/j.advms.2015.12.003

Sorensen, M. J., Miller, K. E., Jorgenson, J. W., & Kennedy, R. T. (2020). Ultrahigh-Performance capillary liquid chromatography-mass spectrometry at 35 kpsi for separation of lipids. *Journal of Chromatography A*, *1611*. https://doi.org/10.1016/j.chroma.2019.460575

Specker, J. T., van Orden, S. L., Ridgeway, M. E., & Prentice, B. M. (2020). Identification of Phosphatidylcholine Isomers in Imaging Mass Spectrometry Using Gas-Phase Charge Inversion Ion/Ion Reactions. *Analytical Chemistry*, *92*(19), 13192–13201. https://doi.org/10.1021/acs.analchem.0c02350

Straarup, E. M., & Høy, C.-E. (2000). Structured Lipids Improve Fat Absorption in Normal and Malabsorbing Rats. *The Journal of Nutrition*, *130*(11), 2802–2808. https://doi.org/10.1093/jn/130.11.2802

Sun, N., Chen, J., Wang, D., & Lin, S. (2018). Advance in food-derived phospholipids: Sources, molecular species and structure as well as their biological activities. *Trends in Food Science and Technology*, *80*(1), 199–211. https://doi.org/10.1016/j.tifs.2018.08.010

Sundaram, S., Žáček, P., Bukowski, M. R., Mehus, A. A., Yan, L., & Picklo, M. J. (2018). Lipidomic Impacts of an Obesogenic Diet Upon Lewis Lung Carcinoma in Mice. *Frontiers in Oncology*, *8*. https://doi.org/10.3389/fonc.2018.00134

Suomela, J. P., Leskinen, H., & Kallio, H. (2011). Analysis of isomeric forms of oxidized triacylglycerols using ultra-high-performance liquid chromatography and tandem mass spectrometry. *Journal of Agricultural and Food Chemistry*, *59*(15), 8095–8100. https://doi.org/10.1021/jf2011936

Takahashi, H., Shimabukuro, Y., Asakawa, D., Yamauchi, S., Sekiya, S., Iwamoto, S., Wada, M., & Tanaka, K. (2018). Structural Analysis of Phospholipid Using Hydrogen Abstraction Dissociation and Oxygen Attachment Dissociation in Tandem Mass Spectrometry.

Analytical Chemistry, *90*(12), 7230–7238. https://doi.org/10.1021/acs.analchem.8b00322

Takeda, H., Izumi, Y., Takahashi, M., Paxton, T., Tamura, S., Koike, T., Yu, Y., Kato, N., Nagase, K., Shiomi, M., & Bamba, T. (2018). Widely-targeted quantitative lipidomics method by supercritical fluid chromatography triple quadrupole mass spectrometry. *Journal of Lipid Research*, *59*(7), 1283–1293. https://doi.org/10.1194/jlr.D083014

Tamba Sompila, A. W. G., Héron, S., Hmida, D., & Tchapla, A. (2017). Fast non-aqueous reversed-phase liquid chromatography separation of triacylglycerol regioisomers with isocratic mobile phase. Application to different oils and fats. *Journal of Chromatography B: Analytical Technologies in the Biomedical and Life Sciences*, *1041–1042*, 151–157. https://doi.org/10.1016/j.jchromb.2016.12.030

Tang, S., Chen, X., Ke, Y., Wang, F., & Yan, X. (2022). Voltage-Controlled Divergent Cascade of Electrochemical Reactions for Characterization of Lipids at Multiple Isomer Levels Using Mass Spectrometry. *Analytical Chemistry*, *94*(37), 12750–12756. https://doi.org/10.1021/acs.analchem.2c02375

Tarvainen, M., Kallio, H., & Yang, B. (2019). Regiospecific Analysis of Triacylglycerols by Ultrahigh-Performance-Liquid Chromatography-Electrospray Ionization-Tandem Mass Spectrometry. *Analytical Chemistry*, *91*(21), 13695–13702. https://doi.org/10.1021/acs.analchem.9b02968

Tian, H.-M., Wu, Y.-X., Lin, Y.-Q., Chen, X.-Y., Yu, M., Lu, T., & Xie, L. (2019). Dietary patterns affect maternal macronutrient intake levels and the fatty acid profile of breast milk in lactating Chinese mothers. *Nutrition*, *58*, 83–88. https://doi.org/10.1016/j.nut.2018.06.009

Tu, A., Ma, Q., Bai, H., & Du, Z. (2017). A comparative study of triacylglycerol composition in Chinese human milk within different lactation stages and imported infant formula by SFC coupled with Q-TOF-MS. *Food Chemistry*, *221*, 555–567. https://doi.org/10.1016/j.foodchem.2016.11.139

Velasco, M., Balgoma, D., & Montero, O. (2022). Ammonia Concentration in the Eluent Influences Fragmentation Pattern of Triacylglycerols in Mass Spectrometry Analysis. *Metabolites*, *12*(5), 452. https://doi.org/10.3390/metabo12050452

Virtanen, P., Gommers, R., Oliphant, T. E., Haberland, M., Reddy, T., Cournapeau, D., Burovski, E., Peterson, P., Weckesser, W., Bright, J., van der Walt, S. J., Brett, M., Wilson, J., Millman, K. J., Mayorov, N., Nelson, A. R. J., Jones, E., Kern, R., Larson, E., … Vázquez-Baeza, Y. (2020). SciPy 1.0: fundamental algorithms for scientific computing in Python. *Nature Methods*, *17*(3), 261–272. https://doi.org/10.1038/s41592-019-0686-2

Wang, C., Wang, D., Xu, J., Yanagita, T., Xue, C., Zhang, T., & Wang, Y. (2018). DHA enriched phospholipids with different polar groups (PC and PS) had different improvements on MPTP-induced mice with Parkinson's disease. *Journal of Functional Foods*, *45*(November 2017), 417–426. https://doi.org/10.1016/j.jff.2018.04.017

Wang, H. Y. J., & Hsu, F.-F. (2022). Structural characterization of phospholipids and sphingolipids by in-source fragmentation MALDI/TOF mass spectrometry. *Analytical and Bioanalytical Chemistry*, *414*(6), 2089–2102. https://doi.org/10.1007/s00216-021-03843-1

Watanabe, S., Yoshikawa, S., Arishima, T., & Sato, K. (2018). Polymorphism and Mixing Phase Behavior in Ternary Mixture Systems of SOS-SSO-OSO: Formation of Molecular Compound Crystals. *Journal of the American Oil Chemists' Society*, *95*(4), 447–460. https://doi.org/10.1002/aocs.12054

Watanabe, S., Yoshikawa, S., & Sato, K. (2021). Formation and properties of dark chocolate prepared using fat mixtures of cocoa butter and symmetric/asymmetric stearic-oleic mixed-acid triacylglycerols: Impact of molecular compound crystals. *Food Chemistry*, *339*, 127808. https://doi.org/10.1016/j.foodchem.2020.127808

West, C. (2018). Current trends in supercritical fluid chromatography. *Analytical and Bioanalytical Chemistry*, *410*(25), 6441–6457. https://doi.org/10.1007/s00216-018-1267-4

Wijesundera, C., Ceccato, C., Watkins, P., Fagan, P., Fraser, B., Thienthong, N., & Perlmutter, P. (2008). Docosahexaenoic Acid is More Stable to Oxidation when Located at the sn-2 Position of Triacylglycerol Compared to sn-1(3). *Journal of the American Oil Chemists' Society*, *85*(6), 543–548. https://doi.org/10.1007/s11746-008-1224-z

Williams, P. E., Klein, D. R., Greer, S. M., & Brodbelt, J. S. (2017). Pinpointing Double Bond and sn-Positions in Glycerophospholipids via Hybrid 193 nm Ultraviolet Photodissociation (UVPD) Mass Spectrometry. *Journal of the American Chemical Society*, *139*(44), 15681–15690. https://doi.org/10.1021/jacs.7b06416

Wolrab, D., Chocholoušková, M., Jirásko, R., Peterka, O., & Holčapek, M. (2020). Validation of lipidomic analysis of human plasma and serum by supercritical fluid chromatography–mass

spectrometry and hydrophilic interaction liquid chromatography–mass spectrometry. *Analytical and Bioanalytical Chemistry*, *412*(10), 2375–2388. https://doi.org/10.1007/s00216-020-02473-3

Wozny, K., Lehmann, W. D., Wozny, M., Akbulut, B. S., & Brügger, B. (2019). A method for the quantitative determination of glycerophospholipid regioisomers by UPLC-ESI-MS/MS. *Analytical and Bioanalytical Chemistry*, *411*(4), 915–924. https://doi.org/10.1007/s00216-018-1517-5

Yang, Q., Shi, X., Gu, Q., Zhao, S., Shan, Y., & Xu, G. (2012). On-line two dimensional liquid chromatography/mass spectrometry for the analysis of triacylglycerides in peanut oil and mouse tissue. *Journal of Chromatography B: Analytical Technologies in the Biomedical and Life Sciences*, *895–896*, 48–55. https://doi.org/10.1016/j.jchromb.2012.03.013

Yao, Y., Zhao, G., Xiang, J., Zou, X., Jin, Q., & Wang, X. (2016). Lipid composition and structural characteristics of bovine, caprine and human milk fat globules. *International Dairy Journal*, *56*, 64–73. https://doi.org/10.1016/j.idairyj.2015.12.013

Young, R. S. E., Bowman, A. P., Tousignant, K. D., Poad, B. L. J., Gunter, J. H., Philp, L. K., Nelson, C. C., Ellis, S. R., Heeren, R. M. A., Sadowski, M. C., & Blanksby, S. J. (2022). Isomeric lipid signatures reveal compartmentalized fatty acid metabolism in cancer. *Journal of Lipid Research*, *63*(6). https://doi.org/10.1016/j.jlr.2022.100223

Zacek, P., Bukowski, M., Rosenberger, T. A., & Picklo, M. (2016). Quantitation of isobaric phosphatidylcholine species in human plasma using a hybrid quadrupole linear ion-trap mass spectrometer. *Journal of Lipid Research*, *57*(12), 2225–2234. https://doi.org/10.1194/jlr.D070656

Zhang, X., Qi, C., Zhang, Y., Wei, W., Jin, Q., Xu, Z., Tao, G., & Wang, X. (2019). Identification and quantification of triacylglycerols in human milk fat using ultra-performance convergence chromatography and quadrupole time-of-flight mass spectrometery with supercritical carbon dioxide as a mobile phase. *Food Chemistry*, *275*, 712–720. https://doi.org/10.1016/j.foodchem.2018.09.150

Zhang, X., Wei, W., Tao, G., Jin, Q., & Wang, X. (2021). Identification and Quantification of Triacylglycerols Using Ultraperformance Supercritical Fluid Chromatography and Quadrupole Time-of-Flight Mass Spectrometry: Comparison of Human Milk, Infant Formula, Other Mammalian Milk, and Plant Oil. *Journal of Agricultural and Food Chemistry*, *69*(32), 8991–9003. https://doi.org/10.1021/acs.jafc.0c07312

Zhang, X., Wei, W., Tao, G., Jin, Q., & Wang, X. (2022). Triacylglycerol regioisomers containing palmitic acid analyzed by ultra-performance supercritical fluid chromatography and quadrupole time-of-flight mass spectrometry: Comparison of standard curve calibration and calculation equation. *Food Chemistry*, *391*, 133280. https://doi.org/10.1016/j.foodchem.2022.133280

Zhao, L., Zhang, J., Ge, W., & Wang, J. (2022). Comparative Lipidomics Analysis of Human and Ruminant Milk Reveals Variation in Composition and Structural Characteristics. *Journal of Agricultural and Food Chemistry*, *70*(29), 8994–9006. https://doi.org/10.1021/acs.jafc.2c02122

Zhao, X., Zhang, W., Zhang, D., Liu, X., Cao, W., Chen, Q., Ouyang, Z., & Xia, Y. (2019). A lipidomic workflow capable of resolving: Sn - And CC location isomers of phosphatidylcholines. *Chemical Science*, *10*(46), 10740–10748. https://doi.org/10.1039/c9sc03521d

Zhu, H., Liang, A., Wang, X., Zhang, W., Zhang, Y., He, X., Liu, Y., Jiang, S., Lu, J., & Lv, J. (2021). Comparative Analysis of Triglycerides From Different Regions and Mature Lactation Periods in Chinese Human Milk Project (CHMP) Study. *Frontiers in Nutrition*, *8*(December), 1–10. https://doi.org/10.3389/fnut.2021.798821

Zou, X., Huang, J., Jin, Q., Guo, Z., Liu, Y., Cheong, L., Xu, X., & Wang, X. (2013). Lipid Composition Analysis of Milk Fats from Different Mammalian Species: Potential for Use as Human Milk Fat Substitutes. *Journal of Agricultural and Food Chemistry*, *61*(29), 7070–7080. https://doi.org/10.1021/jf401452y

Züllig, T., & Köfeler, H. C. (2021). High Resolution Mass Spectrometry in Lipidomics. *Mass Spectrometry Reviews*, *40*(3), 162–176. https://doi.org/10.1002/mas.21627

DOCTORAL THESES IN FOOD SCIENCES AT THE UNIVERSITY OF TURKU

1. **REINO R. LINKO (1967)** Fatty acids and other components of Baltic herring flesh lipids. (Organic chemistry).
2. **HEIKKI KALLIO (1975)** Identification of volatile aroma compounds in arctic bramble, *Rubus arcticus* L. and their development during ripening of the berry, with special reference to *Rubus stellatus* SM.
3. **JUKKA KAITARANTA (1981)** Fish roe lipids and lipid hydrolysis in processed roe of certain *Salmonidae* fish as studied by novel chromatographic techniques.
4. **TIMO HIRVI (1983)** Aromas of some strawberry and blueberry species and varieties studied by gas liquid chromatographic and selected ion monitoring techniques.
5. **RAINER HUOPALAHTI (1985)** Composition and content of aroma compounds in the dill herb, *Anethum graveolens* L., affected by different factors.
6. **MARKKU HONKAVAARA (1989)** Effect of porcine stress on the development of PSE meat, its characteristics and influence on the economics of meat products manufacture.
7. **PÄIVI LAAKSO (1992)** Triacylglycerols – approaching the molecular composition of natural mixtures.
8. **MERJA LEINO (1993)** Application of the headspace gas chromatography complemented with sensory evaluation to analysis of various foods.
9. **KAISLI KERROLA (1994)** Essential oils from herbs and spices: isolation by carbon dioxide extraction and characterization by gas chromatography and sensory evaluation.
10. **ANJA LAPVETELÄINEN (1994)** Barley and oat protein products from wet processes: food use potential.
11. **RAIJA TAHVONEN (1995)** Contents of lead and cadmium in foods in Finland.
12. **MAIJA SAXELIN (1995)** Development of dietary probiotics: estimation of optimal *Lactobacillus* GG concentrations.
13. **PIRJO-LIISA PENTTILÄ (1995)** Estimation of food additive and pesticide intakes by means of a stepwise method.
14. **SIRKKA PLAAMI (1996)** Contents of dietary fiber and inositol phosphates in some foods consumed in Finland.
15. **SUSANNA EEROLA (1997)** Biologically active amines: analytics, occurrence and formation in dry sausages.
16. **PEKKA MANNINEN (1997)** Utilization of supercritical carbon dioxide in the analysis of triacylglycerols and isolation of berry oils.
17. **TUULA VESA (1997)** Symptoms of lactose intolerance: influence of milk composition, gastric emptying, and irritable bowel syndrome.
18. **EILA JÄRVENPÄÄ (1998)** Strategies for supercritical fluid extraction of analytes in trace amounts from food matrices.
19. **ELINA TUOMOLA (1999)** *In vitro* adhesion of probiotic lactic acid bacteria.
20. **ANU JOHANSSON (1999)** Availability of seed oils from Finnish berries with special reference to compositional, geographical and nutritional aspects.
21. **ANNE PIHLANTO-LEPPÄLÄ (1999)** Isolation and characteristics of milk-derived bioactive peptides.
22. **MIKA TUOMOLA (2000)** New methods for the measurement of androstenone and skatole – compounds associated with boar taint problem. (Biotechnology).
23. **LEEA PELTO (2000)** Milk hypersensitivity in adults: studies on diagnosis, prevalence and nutritional management.
24. **ANNE NYKÄNEN (2001)** Use of nisin and lactic acid/lactate to improve the microbial and sensory quality of rainbow trout products.
25. **BAORU YANG (2001)** Lipophilic components of sea buckthorn (*Hippophaë rhamnoides*) seeds and berries and physiological effects of sea buckthorn oils.
26. **MINNA KAHALA (2001)** Lactobacillar S-layers: Use of *Lactobacillus brevis* S-layer signals for heterologous protein production.
27. **OLLI SJÖVALL (2002)** Chromatographic and mass spectrometric analysis of non-volatile oxidation products of triacylglycerols with emphasis on core aldehydes.
28. **JUHA-PEKKA KURVINEN (2002)** Automatic data processing as an aid to mass spectrometry of dietary triacylglycerols and tissue glycerophospholipids.
29. **MARI HAKALA (2002)** Factors affecting the internal quality of strawberry (*Fragaria x ananassa* Duch.) fruit.
30. **PIRKKA KIRJAVAINEN (2003)** The intestinal microbiota – a target for treatment in infant atopic eczema?
31. **TARJA ARO (2003)** Chemical composition of Baltic herring: effects of processing and storage on fatty acids, mineral elements and volatile compounds.
32. **SAMI NIKOSKELAINEN (2003)** Innate immunity of rainbow trout: effects of opsonins, temperature and probiotics on phagocytic and complement activity as well as on disease resistance.
33. **KAISA YLI-JOKIPII (2004)** Effect of triacylglycerol fatty acid positional distribution on postprandial lipid metabolism.
34. **MARIKA JESTOI (2005)** Emerging *Fusarium*-mycotoxins in Finland.
35. **KATJA TIITINEN (2006)** Factors contributing to sea buckthorn (*Hippophaë rhamnoides* L.) flavour.
36. **SATU VESTERLUND (2006)** Methods to determine the safety and influence of probiotics on the adherence and viability of pathogens.
37. **FANDI FAWAZ ALI IBRAHIM (2006)** Lactic acid bacteria: an approach for heavy metal detoxification.
38. **JUKKA-PEKKA SUOMELA (2006)** Effects of dietary fat oxidation products and flavonols on lipoprotein oxidation.
39. **SAMPO LAHTINEN (2007)** New insights into the viability of probiotic bacteria.

40. **SASKA TUOMASJUKKA (2007)** Strategies for reducing postprandial triacylglycerolemia.
41. **HARRI MÄKIVUOKKO (2007)** Simulating the human colon microbiota: studies on polydextrose, lactose and cocoa mass.
42. **RENATA ADAMI (2007)** Micronization of pharmaceuticals and food ingredients using supercritical fluid techniques.
43. **TEEMU HALTTUNEN (2008)** Removal of cadmium, lead and arsenic from water by lactic acid bacteria.
44. **SUSANNA ROKKA (2008)** Bovine colostral antibodies and selected lactobacilli as means to control gastrointestinal infections.
45. **ANU LÄHTEENMÄKI-UUTELA (2009)** Foodstuffs and medicines as legal categories in the EU and China. Functional foods as a borderline case. (Law).
46. **TARJA SUOMALAINEN (2009)** Characterizing *Propionibacterium freudenreichii* ssp. *shermanii* JS and *Lactobacillus rhamnosus* LC705 as a new probiotic combination: basic properties of JS and pilot *in vivo* assessment of the combination.
47. **HEIDI LESKINEN (2010)** Positional distribution of fatty acids in plant triacylglycerols: contributing factors and chromatographic/mass spectrometric analysis.
48. **TERHI POHJANHEIMO (2010)** Sensory and non-sensory factors behind the liking and choice of healthy food products.
49. **RIIKKA JÄRVINEN (2010)** Cuticular and suberin polymers of edible plants – analysis by gas chromatographic-mass spectrometric and solid state spectroscopic methods.
50. **HENNA-MARIA LEHTONEN (2010)** Berry polyphenol absorption and the effect of northern berries on metabolism, ectopic fat accumulation, and associated diseases.
51. **PASI KANKAANPÄÄ (2010)** Interactions between polyunsaturated fatty acids and probiotics.
52. **PETRA LARMO (2011)** The health effects of sea buckthorn berries and oil.
53. **HENNA RÖYTIÖ (2011)** Identifying and characterizing new ingredients *in vitro* for prebiotic and synbiotic use.
54. **RITVA REPO-CARRASCO-VALENCIA (2011)** Andean indigenous food crops: nutritional value and bioactive compounds.
55. **OSKAR LAAKSONEN (2011)** Astringent food compounds and their interactions with taste properties.
56. **ŁUKASZ MARCIN GRZEŚKOWIAK (2012)** Gut microbiota in early infancy: effect of environment, diet and probiotics.
57. **PENGZHAN LIU (2012)** Composition of hawthorn (*Crataegus* spp.) fruits and leaves and emblic leafflower (*Phyllanthus emblica*) fruits.
58. **HEIKKI ARO (2012)** Fractionation of hen egg and oat lipids with supercritical fluids. Chemical and functional properties of fractions.
59. **SOILI ALANNE (2012)** An infant with food allergy and eczema in the family – the mental and economic burden of caring.
60. **MARKO TARVAINEN (2013)** Analysis of lipid oxidation during digestion by liquid chromatography-mass spectrometric and nuclear magnetic resonance spectroscopic techniques.
61. **JIE ZHENG (2013)** Sugars, acids and phenolic compounds in currants and sea buckthorn in relation to the effects of environmental factors.
62. **SARI MÄKINEN (2014)** Production, isolation and characterization of bioactive peptides with antihypertensive properties from potato and rapeseed proteins.
63. **MIKA KAIMAINEN (2014)** Stability of natural colorants of plant origin.
64. **LOTTA NYLUND (2015)** Early life intestinal microbiota in health and in atopic eczema.
65. **JAAKKO HIIDENHOVI (2015)** Isolation and characterization of ovomucin – a bioactive agent of egg white.
66. **HANNA-LEENA HIETARANTA-LUOMA (2016)** Promoting healthy lifestyles with personalized, *APOE* genotype based health information: The effects on psychological-, health behavioral and clinical factors.
67. **VELI HIETANIEMI (2016)** The *Fusarium* mycotoxins in Finnish cereal grains: How to control and manage the risk.
68. **MAARIA KORTESNIEMI (2016)** NMR metabolomics of foods – Investigating the influence of origin on sea buckthorn berries, *Brassica* oilseeds and honey.
69. **JUHANI AAKKO (2016)** New insights into human gut microbiota development in early infancy: influence of diet, environment and mother's microbiota.
70. **WEI YANG (2017)** Effects of genetic and environmental factors on proanthocyanidins in sea buckthorn (*Hippophaë rhamnoides*) and flavonol glycosides in leaves of currants (*Ribes* spp.).
71. **LEENAMAIJA MÄKILÄ (2017)** Effect of processing technologies on phenolic compounds in berry products.
72. **JUHA-MATTI PIHLAVA (2017)** Selected bioactive compounds in cereals and cereal products – their role and analysis by chromatographic methods.
73. **TOMMI KUMPULAINEN (2018)** The complexity of freshness and locality in a food consumption context
74. **XUEYING MA (2018)** Non-volatile bioactive and sensory compounds in berries and leaves of sea buckthorn (*Hippophaë rhamnoides*)
75. **ANU NUORA (2018)** Postprandial lipid metabolism resulting from heated beef, homogenized milk and interesterified palm oil.
76. **HEIKKI AISALA (2019)** Sensory properties and underlying chemistry of Finnish edible wild mushrooms.
77. **YE TIAN (2019)** Phenolic compounds from Finnish berry species to enhance food safety.
78. **MAIJA PAAKKI (2020)** The importance of natural colors in food for the visual attractiveness of everyday lunch.

79. **SHUXUN LIU (2020**) Fermentation with non-*Saccharomyces* yeasts as a novel biotechnology for berry wine production.
80. **MARIKA KALPIO (2020)** Strategies for analyzing the regio- and stereospecific structures of individual triacylglycerols in natural fats and oils.
81. **JOHANNA JOKIOJA (2020)** Postprandial effects and metabolism of acylated anthocyanins originating from purple potatoes.
82. **NIINA KELANNE (2021)** Novel bioprocessing for increasing consumption of Nordic berries.
83. **NIKO MARKKINEN (2021)** Bioprocessing of berry materials with malolactic fermentation.
84. **GABRIELE BELTRAME (2021)** Polysaccharides from Finnish fungal resources.
85. **SALLA LAITO (2022)** Bioactive compounds in oats and gut health.
86. **KANG CHEN (2022)** Multi-omics study on the effects of anthocyanin extracts from bilberries and purple potatoes on type 2 diabetes in Zucker diabetic fatty rats.
87. **WENJIA HE (2022)** Bioprocessing of alcoholic beverages from apples and pears: Effects of raw materials and processes on quality.
88. **TANJA KAKKO (2023)** Alternative approaches to improve the processing and quality of under-utilized fish.
89. **MIKAEL FABRITIUS (2023)** Mass spectrometric methodologies for analysis of triacylglycerol and phospholipid regioisomers in natural fats and oils.

TURUN
YLIOPISTO
UNIVERSITY
OF TURKU